Electronic structure of extended systems, within density functional theory and beyond

---

eingericht an der **Bayreuther Graduiertenschule für Mathematik und Naturwissenenschaften (BayNAT)** unter Berücksichtigung der Vereinbarung einer gemeinsamen Doktorarbeit zwischen der **Universität Bayreuth** und der **Hebrew University of Jerusalem**

submitted to the **Bayreuth Graduate School of Mathematics and Natural Sciences (BayNAT)** under consideration of the Specific Agreement for a Joint Doctoral Thesis between the **University of Bayreuth** and the **Hebrew University of Jerusalem**

zur Erlangung des gemeinsam verliehenen akademischen Grades

Doktors der Naturwissenschaften
(Dr. rer. nat.)

דוקטור לפילוסופיה
(Ph.D.)

Dissertation

Vorgelegt durch
Vojtěch Vlček, aus Prag (Tschechische Republik)

Bayreuth, 2016

This work was performed at Bayerisches Geoinstitut, University of Bayreuth and the Fritz-Haber Center for Molecular Dynamics, Institute of Chemistry, The Hebrew University of Jerusalem under the supervision of Dr. Gerd Steinle-Neumann (University of Bayreuth) and Prof. Dr. Roi Baer (The Hebrew University of Jerusalem). This thesis is subject to a "Specific Agreement for a co-tuelle Arrangement of a Joint Doctoral Thesis" between the University of Bayreuth and the Hebrew University of Jerusalem, signed on October 14, 2015.

Abstract

A first-principles description of the electronic structure of systems, ranging from individual atoms and small molecules to infinite periodic solids, firmly based in theoretical physics, provides substantial insight into physical and chemical processes on the nanoscale. Over the past decades, density functional theory (DFT) has become the prevalent theoretical approach to study physical properties of molecules and solids as it shows an excellent balance between computational demand and accuracy. However, a description of quasiparticles, which form the fundamental charge carriers in materials, responsible for their electrical and optical properties, cannot be accurately inferred from DFT due to a fundamental limitation of the theory. The only exception is the lowest energy of a quasi-hole, corresponding to the ionization potential of the system, which is provided exactly, in principle. However, practical approximate forms of DFT often fail to describe even this quantity correctly. Many-body perturbation theory, on the other hand, provides a route to such properties, but implementations pose significant computational demands. As a consequence, they can only be applied to small finite systems or periodic solids characterized by unit cells with a small number of electrons.

In this thesis we develop theories, computational tools and present new applications that allow us to study various aspects of quasiparticles in large finite systems, effectively bridging some of the gaps separating the finite and the infinite domains. The main aspect of the work is the theoretical description of charge removal and addition energies, which correspond to the energies of quasi-holes and quasi-electrons. Well-documented errors associated with the description of the ionization potentials within the Kohn-Sham approach to DFT include the incorrect behavior of the total energies with respect to the number of particles and related missing discontinuous behavior of the effective potential, issues that have been addressed for finite systems. In the first part of the thesis, these approaches are reviewed from the perspective of application to extended and infinite systems. First, we apply a new exchange energy functional (AK13), which corrects some of the deficiencies in isolated systems, and this improved description also translates to enhanced fundamental band gaps and dielectric constants for periodic infinite crystals. Second, we show the nature of the error associated with charge removal and addition energies in 1-D molecular chains and nanocrystals and develop its analytical form to describe and interpret this behavior. This finding explains why and how some of the correction schemes for charge removal in DFT deteriorate as the system size increases. In addition, by examining total energies for fractionally charged systems we establish a criterion for a behavior that DFT should satisfy when the system size increases to infinity.

The electronic structure of systems based on molecular chains with increasing size is further explored using DFT functionals which include non-local exchange interaction and which enforce exact behavior for the total energies of systems when fractional charge is removed (optimally tuned range-separated hybrid functionals). These studies on chains of transpolyacetlyene and polythiophene reveal a novel phenomenon in which the quasi-hole spontaneously localizes on length scales of several nanometers. Upon further increase in chain length, the hole size and energy become independent of system size. Similarly, optical absorption peaks and excitonic binding energies cease to depend on length. We find this localization phenomenon to be driven by the presence of non-local exchange. Furthermore, the spontaneous localization of quasi-holes explains the formation of polarons without need for self trapping mechanism, contrary to the traditional view. Computations with many-body perturbation theory in the GW approximation further support the notion of spontaneous charge localization. For the GW computations we employ a recently developed stochastic formulation. We review the theory in detail, and reformulate and implement some adjustments to it. The favorable scaling of this approach allows us to perform calculations on extremely large systems (containing up to 1446 valence electrons), the largest system for which GW computations have been reported to date.

Zusammenfassung

Eine Beschreibung der Elektronenstruktur von physikalischen Systemen auf der Basis der theoretischen Physik erlaubt tiefe Einblicke in physikalische und chemische Prozesse auf der Nano-Skala, von einzelne Atome über Moleküle bis zu periodischen Festkörpern. In diesem Feld hat sich im Lauf der letzten Jahrzehnte die Dichtefunktionaltheorie (DFT) zur führenden Methode in der Berechnung von physikalischen Eigenschaften sowohl von Molekülen als auch von Festkörpern entwickelt, da DFT einen hervorragenden Kompromiss zwischen Anforderungen an Computer-Ressourcen und Genauigkeit zeigt. Quasiteilchen, die typischerweise als Ladungsträger in Materialien für elektrische und optische Eigenschaften verantwortlich sind, können infolge theoretischer Beschränkungen mit Hilfe der DFT prinzipiell nicht bestimmt werden. Die Elektronenfehlstelle (Ladungsloch) mit der niedrigsten Anregungsenergie stellt eine Ausnahme dar; dieses Ionisationspotential entspricht dem des gebundenen Elektrons, das energetisch am höchsten gelegen ist (HOMO Niveau). Praktische Näherungen der DFT beschreiben diesen Elektronenzustand jedoch oft unzureichend. Im Gegensatz zur DFT kann man mit Vielteilchen-Störungstheorie die Ladungsträger berechnen, ihre praktische Durchführung erfordert jedoch erhebliche Computer-Ressourcen. Als Folge daraus können solche Methoden nur für kleine Moleküle oder Nanokristalle sowie Festkörper genutzt werde, die wenige Elektronen in der Einheitszelle haben.

In der vorliegenden Doktorarbeit entwickeln wir neue theoretische Ansätze und Werkzeuge, die es uns erlauben, verschiedene Aspekte von Quasiteilchen in großen endlichen Systemen zu untersuchen. Die Anwendung dieser Methoden erlaubt es uns, einige Fragen zu beantworten, die bisher an der Schnittstelle zwischen endlichen (Moleküle oder Nano-Kristalle) und unendlichen (periodische Festkörper) Systemen bestanden. Der Schwerpunkt der Arbeit liegt darin, die Energien von Ladungsaddition (Affinität) und Ladungssubtraktion (Ionisation) zu beschreiben, die den Anregungen von Elektronen und Defektelektronen (Löchern) entsprechen. Typische Näherungen innerhalb des Kohn-Sham (KS) Formalismus der DFT führen zu einem gut dokumentierten Fehler bei der Berechnung der Ionisationsenergie. Der Fehler lässt sich unter anderem zurückführen auf ein falsches Verhalten der Gesamtenergie in Bezug auf die Teilchenzahl und dem Fehlen eines nicht stetigen Sprungs im effektiven Potential in der direkten Umgebung von ganzen Teilchenzahlen (derivative discontinuity). Im ersten Teil dieser Dissertation untersuchen wir dieses Verhalten für große endliche Systeme sowie Festkörper. Wir wenden ein neuentwickeltes Austausch-Funktional (AK13) für die Berechnung der Elektronenstruktur von Festkörpern an. Dieses Funktional korrigiert einige der Schwächen in der Beschreibung der Elektronenstruktur endlicher Systeme in typischen Näherungen in der KS-DFT, und

diese Korrektur spiegelt sich in einer verbesserten Beschreibung der Bandlücken sowie der Dielektrizitätskonstanten der kristallinen Festkörper wider. Des Weiteren analysieren wir den Fehler, der bei der Berechnung der Energie bei Ladungsaddition und Ladungssubtraktion in eindimensionalen Molekülen sowie Nano-Kristallen auftritt. Wir zeigen mit Hilfe von analytischen Ergebnissen, dass dieses Verhalten von elektrostatischen Effekten dominiert wird. Die Ergebnisse können erklären, warum und wie bestimmte Näherungen in der Dichtefunktionaltheorie das Verhalten des Systems schlechter beschreiben, wenn Moleküle oder Nano-Kristalle vergrößert werden. Ergebnisse für die Energieänderung beim Laden mit einem Bruchteil eines Elektrons in solchen Systemen erlaubt es uns, eine Bedingung aufzustellen, die eine korrekte Formulierung der DFT erfüllen muss.

Im zweiten Teil der Dissertation untersuchen wir die Elektronenstruktur von quasi-eindimensionalen Molekülen, indem wir DFT-Funktionale anwenden, die nicht-lokale Austausch-Wechselwirkungen beinhalten und die das theoretisch beschriebene genaue Verhalten der Energie beim Entfernen eines Bruchteils von elektronischer Ladung erfüllen (piecewise linearity condition), die optimal abgestimmte Hybrid-Funktionale mit getrenntem Aufteilungsbereich (optimally tuned range-separated hybrid functionals). Diese Untersuchungen an Ketten von trans-Polyethin und poly-Thiophen zeigen ein neues Phänomen, bei dem sich Ladungslöcher spontan auf wenige Nanometer lokalisieren. Bei einer weiteren Verlängerung der Molekülketten ändern sich die Größe und Energie von Defektelektronen nicht weiter. In ähnlicher Weise hängen optische Absorptionsspitzen und die Bindungsenergie von Exzitonen nicht länger von der Kettenlänge ab. Diese Eingrenzung von Ladung wird von nicht-lokalem Austausch bestimmt. Im Gegensatz zum klassischen Erklärungsansatz kann diese spontane Lokalisierung von Defektelektronen die Bildung von Polaronen ohne self-trapping Mechanismus erklären. Ergebnisse aus Berechnungen mit Vielteilchen Methoden in der GW-Näherung unterstützen die Interpretation der spontanen Ladungseingrenzung. Für die GW-Rechnungen nutzen wir eine kürzlich entwickelte stochastische Formulierung. In der vorliegenden Arbeit präsentieren wir die Theorie im Detail und formulieren und implementieren einige Änderungen an der Methode. Die vorteilhafte lineare Skalierung der stochastischen GW-Näherung mit der Anzahl der Elektronen im System erlaubt es uns, Rechnungen für sehr große Systeme durchzuführen (bis zu 1466 Valenzelektronen), die größte Anzahl von Elektronen für die GW-Berechnungen bisher durchgeführt wurden.

תקציר

תיאוריה המבוססת על עקרונות-יסוד פיזיקליים של המבנה האלקטרוני של חומרים מאפשרת הבנה מעמקיה של התהליכים הפיסיקליים והכימיים במערכות כימיות החל מאטומים בודדים עבור במולקולות קטנות ועד מוצקים אינסופיים. במהלך העשורים האחרונים, תורת פונקציונל הצפיפות (DFT) הפכה גישה תיאורטית מקובלת לתיאור תכונות פיסיקליות של מולקולות ומוצקים, תוך שהיא מציגה איזון מצוין בין נגישות חישובית ודיוק שימושי. עם זאת, תיאור של קוואזי-חלקיקים במערכות כאלה, המהווים את נושאי המטען הבסיסיים ולכן קובעים את התכונות החשמליות והאופטיות שלהן, אינם מתוארים היטב על-ידי DFT בשל מגבלה מהותית של התיאוריה. אנרגית היסוד של קוואזי-חור, אנרגיה השווה לפוטנציאל היינון של המערכת כן נגישה על-ידי DFT אבל הקירובים הכרוכים ביישום התיאוריה מונעים תיאור מדוייק גם של גודל זה. מצד שני, תורת ההפרעות הרב-גופית מספקת אמנם נתיב מתאים לתיאור קוואזי-חלקיקים אבל מימושה דורש משאבי חישוב גבוהים ועד כה לא היתה ישימה למערכות גדולות: שיטות אלה ניתנות ליישום רק במערכות סופיות קטנות או במוצקים אינסופיים בעלי תאי יחידה עם מספר קטן של אלקטרונים. בעבודה זו אדווח על התקדמות בתיאור התיאורטי של אנרגיות קוואזי חלקיקים באופן שניתו ליישום במערכות גדולות, ובכך לאפשר גישור בין מערכות סופיות ואינסופיות. ההיבט העיקרי של העבודה הוא התיאור התיאורטי של אנרגיות הגריעה או ההוספה של אלקטרונים, הן האנרגיות הקוואזי חורים ואלקטרונים. פוטנציאלי היינון המבוססות על קירובים לתיאוריית קוהן-שאם של DFT סוטים ביחס לניסוי כתוצאה מהתנהגות איכותית שגוייה של האנרגיה הכוללת ביחס למספר החלקיקים, ומהעדר תכונת ה"אי-רציפות של הנגזרת" הנדרשת של פונקציונל השיחלוף-קורלציה (derivative discontinuity). בעיות אלה נפתרו במערכות סופיות אבל לא במערכות מאד גדולות או אינסופיות. בחלקה הראשון של התיזה פיתחנו גישות הנבחנות מנקודת מבט של יישום למערכות מורחבות ואינסופיות. ראשית, פיתחנו פונקציונל שיחלוף חדש (AK13) אשר מתקן חלק מהליקויים של DFT במערכות מבודדות. תיאור כזה גם משפר את ההתאמה של הפער האלקטרוני היסודי (fundamental energy gap) וגם את הקבוע הדיאלקטרי של גבישים אינסופיים. שנית, אנו חוקרים את מהות השגיאה הקשורה בתיאור של DFT של אנרגיות היינון והאפיניות בשרשרות מולקולריות חד-מימדיות ובננוגבישים ומפרשים את ההתנהגות שנצפית. ממצא זה מסביר מדוע וכיצד קורה שחלק מהשיטות לתיקון אנרגיית היינון מפסיקות להיות אפקטיביות ככל שגודל המערכת עולה. בנוסף, בבחינת האנרגיות של מערכות טעונות בשיעור זעום (fractionally charged systems) אנו קובעים קריטריון כיצד קירובי ה-DFT צריכים להתנהג כאשר המערכות גודלות.

מצאנו כי שימוש באינטראקציית שיחלוף (exchange) לא-מקומית חשובה לתיאור נכון של אנרגיות הקוואזי חלקיקים בשרשרות מולקולריות. אנו מדגימים זאת על שרשרות של transpolyacetlyene ו polythiophene וגילינו תופעת לוקליזציה ספונטנית של קוואזי חלקיקים בסקאלת אורך של מספר ננומטרים. אנו מראים שגודל החור והאנרגיה של הקוואזי חלקיקים הופכים בלתי תלויים בגודל המערכת החל מגודל מסויים והלאה. באופן דומה, גם אנרגיות הבליעה ואנרגית הקשר של אקסיטונים הופכים בלתי תלויים בגודל המערכת. אנו מוצאים שתופעת הלוקליזציה הזו מונעת מנוכחות של אינטראקציית שיחלוף לא מקומית. יתר על כן, הלוקליזציה הספונטנית של קוואזי חורים מסבירה את ההיווצרות המהירה של

פולארונים ללא צורך במעברים לא אדיאבטים בניגוד לתפיסה המסורתית. השתמשנו בחישובי תורת הפרעות רב-גופית תחת קירוב GW ומצאנו שאלה תומכים ברעיון של לוקליזציה ספונטנית. בנוסף פיתחנו שיטות סטוכסטיות המאפשרות יישום של שיטות הפרעה רב גופית לחישובי אנרגיות קוואזי חלקיקים במערכות גדולות מאוד, עד כדי 1446 אלקטרוני ערכיות - המערכת הגדולה, ביותר שבה התאפשרו חישובי GW עד כה.

Contents

Chapter 1

Introduction

Modern society has an ever growing need for technological development, which is inherently intertwined with the optimization of functionality of known materials, their design or the discovery of novel compounds altogether[1]. Aside from perfecting manufacturing processes, the design and production of high-tech purpose-tailored materials requires a detailed understanding of their stability, structure, and more importantly physical processes that determine their applicability and govern their behavior. Over the last decades significant progress has been made using *ab initio* calculations which address the physics of materials on the nanoscale and complement experiments. Provided that the theoretical description is entirely from the first-principles, the calculations have immense predictive power which is used to design compounds *in silico* but also to yield insight into physical properties at conditions which are not accessible experimentally.

The computational approach seeks to describe the electronic structure of matter, which governs its properties. Since the beginning of quantum theory it was clear that calculations for realistic systems represent a serious challenge and are ultimately intractable. The most accurate theoretical approaches are used to describe only small molecules (or even atoms), since their computational cost for larger systems is prohibitive. First-principles investigation is however needed for the description of molecules and compounds of appreciable sizes in which new phenomena may arise, and the ultimate goal is to describe the nanoscale systems, for which experiments can be performed.

The practical workhorse of *ab initio* calculations thus became density functional theory (DFT – [1–6]) which maps exactly the many-body system into a non-interacting single particle problem. Although DFT has to use approximations in practice, it yields excellent agreement for predictions of equations of state of solids, liquids or individual molecules, their stabilities and vibrational characteristics [7–12]. Furthermore, owing to advances in computer architecture and numerical algorithms DFT has been successfully applied even to problems dealing with very large systems containing ∼100,000 electrons [13–17].

Besides the behavior related to the total energies of particular systems, which are mentioned in the preceding paragraph, the microscopic description of the optical and electrical properties requires knowledge of the fundamental

[1]This has been recently strongly supported by a joint project of "Material Genome Initiative" - https://www.mgi.gov/

charge carriers: quasielectrons and quasiholes [18, 19]. Aside from the fundamental interest in understanding the spectral and exictonic properties of matter [20–26] the ability to predict them is crucial for further development of new (opto)electronic devices [27–31], sensors and data storage materials [32–35] or (nano)materials used, e.g. in chemical catalysis [36]. Despite being commonly used to qualitatively infer the nature of excitations [37], DFT by design does not provide access to quasiparticle states. The only exception is the lowest energy to remove an electron, corresponding to the ionization potential of the system, which should be provided exactly. Practical implementations however often fail to describe even this quantity correctly [38, 39].

Some improvement in prediction of the quasiparticle energies associated with charge removal and addition can be obtained indirectly by considering systems with $N \pm 1$ and N particles, where N is the number of electrons in the neutral system. While simple, in principle, the procedure is cumbersome, especially for extended systems and it is not straightforward to apply it to infinite systems. Furthermore as the system grows in size, the performance of such method deteriorates [40]. The most important caviot is the fact that this approach leads only to the estimate of a single excitation energy and thus cannot be used to characterize the complete electronic structure. Recent theoretical developments in the description of finite systems aim to obtain improvement by finding new approximations that more closely reproduce the exact behavior for charge additon or removal [41], or through first-principles adjustment for each system independently such that this exact behavior is enforced [42, 43]. However, the path to demonstrating and exploring this exact behavior for infinite systems is unknown, and in the case of the first-principles adjustment method the current results indicate that the correction will ultimately fail even for sufficiently large finite systems [43, 44] and schemes beyond DFT need to be sought.

Such a route is provided through many-body perturbation theory [18, 19, 45], which (unlike DFT) aims at describing quasiparticles. Here, DFT results are considered as the zeroth order quasiparticle energies and states, and the method seeks correction to them. In practice, one needs to resort to approximations that were found to yield a substantial improvement over the (approximate) DFT predictions [46–48]. The downside of such calculations is their cost; common implementations show scaling with number of particles as N^4 or even N^5 (Refs. [49, 50]). Even with currently available computational resources, this unfavorable scaling limits the applicability to small molecular systems or unit cells of periodic solids having a limited number of electrons.

The goal of the present work is to discover and explore new theories and computational procedures that will lead to reliable predictions of quasiparticle energies in large nanoscale systems, providing a connection between finite and infinite systems and correspondingly unifying these two domains of active research, which have been advanced (to some extent) independently. Novel methods will ultimately enable scientist to understand, control and design the electrical and optical properties of materials. Furthermore, they will allow to quantitatively address the mechanisms of interplay between charge carriers in actual materials: the most prominent examples of practical relevance are quantum confinement, localization, charging, screening, excitonic effects or correlation. Such theories potentially have significant impact on nanotechnology. In order to make quantitative predictions for large systems, it is required that the methods must rely on first principles approaches and be of low algorithmic complexity not much

greater than that of DFT.

Bibliography

[1] P. Hohenberg and W. Kohn, Phys. Rev. **136**, 864 (1964).

[2] W. Kohn and L. J. Sham, Phys. Rev. **140**, A1133 (1965).

[3] A. Seidl, A. Görling, P. Vogl, J. A. Majewski, and M. Levy, Phys. Rev. B **53**, 3764 (1996).

[4] R. G. Parr and W. Yang, *Density Functional Theory of Atoms and Molecules* (Oxford Science Publications, Oxford, 1989).

[5] R. M. Dreizler and E. K. U. Gross, *Density Functional Theory: An Approach to the Quantum Many-Body Problem* (Springer Science & Business Media, 1990).

[6] R. M. Martin, *Electronic Structure: Basic Theory and Practical Methods* (Cambridge University Press, 2004).

[7] S. Kurth, J. P. Perdew, and P. Blaha, Int. J. Quantum Chem. **75**, 889 (1999).

[8] V. N. Staroverov, G. E. Scuseria, J. Tao, and J. P. Perdew, Phys. Rev. B **69**, 075102 (2004).

[9] P. Haas, F. Tran, and P. Blaha, Phys. Rev. B **79**, 085104 (2009).

[10] L. Goerigk and S. Grimme, Phys. Chem. Chem. Phys. **13**, 6670 (2011).

[11] K. Lejaeghere, V. Van Speybroeck, G. Van Oost, and S. Cottenier, Crit. Rev. Solid State Mater. Sci. **39**, 1 (2014).

[12] K. Lejaeghere, G. Bihlmayer, T. Björkman, P. Blaha, S. Blügel, V. Blum, D. Caliste, I. E. Castelli, S. J. Clark, A. Dal Corso, et al., Science **351**, aad3000 (2016).

[13] S. Tomov, W. Lu, J. Bernholc, S. Moore, and J. Dongarra, Proceedings of CUG09 (2009).

[14] J. VandeVondele, U. Borstnik, and J. Hutter, J. Chem. Theory Comput. **8**, 3565 (2012).

[15] R. Baer, D. Neuhauser, and E. Rabani, Phys. Rev. Lett. **111**, 106402 (2013).

[16] D. Neuhauser, R. Baer, and E. Rabani, J. Chem. Phys. **141**, 041102 (2014).

[17] W. Hu, L. Lin, and C. Yang, J. Chem. Phys. **143**, 124110 (2015).

[18] A. L. Fetter and J. D. Walecka, *Quantum Theory of Many-Particle Systems* (Dover Publications, 2003).

[19] E. K. U. Gross, E. Runge, and O. Heinonen, *Many-Particle Theory* (Hilger, Bristol, 1991).

[20] A. Damascelli, Z. Hussain, and Z.-X. Shen, Rev. Mod. Phys. **75**, 473 (2003).

[21] F. Reinert and S. Hüfner, New J. Phys. **7**, 97 (2005).

[22] G. D. Scholes and G. Rumbles, Nat. Mater. **5**, 683 (2006).

[23] Y. Ping, D. Rocca, and G. Galli, Chem. Soc. Rev. **42**, 2437 (2013).

[24] S. Hüfner, *Photoelectron Spectroscopy: Principles and Applications* (Springer Science & Business Media, 2013).

[25] C. Di Valentin, S. Botti, and M. Cococcioni, *First Principles Approaches to Spectroscopic Properties of Complex Materials*, vol. 347 (Springer, 2014).

[26] G. Grancini, M. Maiuri, D. Fazzi, A. Petrozza, H. Egelhaaf, D. Brida, G. Cerullo, and G. Lanzani, Nat. Mater. **12**, 29 (2013).

[27] D. J. Norris, A. L. Efros, and S. C. Erwin, Science **319**, 1776 (2008).

[28] R. Ghosh Chaudhuri and S. Paria, Chem. Rev. **112**, 2373 (2011).

[29] H. S. Jung and N.-G. Park, Small **11**, 10 (2015).

[30] A. Lauchner, A. E. Schlather, A. Manjavacas, Y. Cui, M. J. McClain, G. J. Stec, F. J. Garci a de Abajo, P. Nordlander, and N. J. Halas, Nano Lett. **15**, 6208 (2015).

[31] P. Docampo and T. Bein, Acc. Chem. Res. **49**, 339 (2016).

[32] H. Paulsen and A. X. Trautwein, in *Spin Crossover in Transition Metal Compounds III* (Springer, 2004), pp. 197–219.

[33] J.-F. Létard, P. Guionneau, and L. Goux-Capes, in *Spin Crossover in Transition Metal Compounds III* (Springer, 2004), pp. 221–249.

[34] A. Bousseksou, G. Molnár, L. Salmon, and W. Nicolazzi, Chem. Soc. Rev. **40**, 3313 (2011).

[35] M. Montalti, A. Cantelli, and G. Battistelli, Chem. Soc. Rev. **44**, 4853 (2015).

[36] M. B. Gawande, A. Goswami, T. Asefa, H. Guo, A. V. Biradar, D.-L. Peng, R. Zboril, and R. S. Varma, Chem. Soc. Rev. **44**, 7540 (2015).

[37] D. Chong, O. Gritsenko, E. Baerends, et al., J. Chem. Phys. **116**, 1760 (2002).

[38] A. J. Cohen, P. Mori-Sánchez, and W. Yang, Science **321**, 792 (2008).

[39] P. Mori-Sánchez, A. J. Cohen, and W. Yang, Phys. Rev. Lett. **100** (2008).

[40] R. W. Godby and I. D. White, Phys. Rev. Lett. **80**, 3161 (1998).

[41] R. Armiento and S. Kümmel, Phys. Rev. Lett. **111**, 36402 (2013).

[42] R. Baer, E. Livshits, and U. Salzner, Annu. Rev. Phys. Chem. **61**, 85 (2010).

[43] L. Kronik, T. Stein, S. Refaely-Abramson, and R. Baer, J. Chem. Theory Comput. **8**, 1515 (2012).

[44] T. Stein, H. Eisenberg, L. Kronik, and R. Baer, Phys. Rev. Lett. **105**, 266802 (2010).

[45] L. Hedin, Phys. Rev. **139**, A796 (1965).

[46] F. Aryasetiawan and O. Gunnarsson, Reports Prog. Phys. **61**, 237 (1998).

[47] L. Hedin, J. Phys.: Condens. Matter **11**, R489 (1999).

[48] C. Friedrich and A. Schindlmayr, NIC Series **31**, 335 (2006).

[49] H.-V. Nguyen, T. A. Pham, D. Rocca, and G. Galli, Phys. Rev. B **85**, 081101 (2012).

[50] J. Deslippe, G. Samsonidze, D. A. Strubbe, M. Jain, M. L. Cohen, and S. G. Louie, Comput. Phys. Commun. **183**, 1269 (2012).

Chapter 2

Theory

In this chapter, we review in a condesed form the theoretical concepts of density functional theory, its approximations, and many-body perturbation theory. We will, however, omit detailed derivations of the individual results, and rather focus on the most important relations that are applied in the following chapters. Section 2.1 provides an overview of density functional theory and the conditions that are further used to characterize the behavior and possible failure of its implementations. This is followed by two sections in which we provide the two main practical approaches to the theory and illustrate their bottlenecks and shortcomings. Finally, in Section 2.4 the quasiparticle equations used in many-body perturbation theory are briefly reviewed with focus on the GW approximation.

For clarity, we use atomic units throughout the chapter and we consider only non-relativistic cases.

2.1 General Overview of the Density Functional Theory

The solution of the full many-body problem is provided by the Schrödinger equation

$$\hat{H}\Psi = E\Psi, \tag{2.1}$$

where E is the energy of the system of electrons, Ψ the many body wave function and the Hamiltonian

$$\hat{H} = \hat{T} + \hat{V}_{e-e} + \hat{V}_{ext}. \tag{2.2}$$

The individual terms in the Hamiltonian are the kinetic energy, electron-electron interaction potential and the external potential operator. In atomic units the can be witten as:

$$\hat{T} = -\frac{1}{2}\sum_{i}^{N} \nabla_i^2, \tag{2.3}$$

where the sum goes over all particles N,

$$\hat{V}_{e-e} = \frac{1}{2}\sum_{i,j\neq i}^{N} \frac{1}{|\mathbf{r_i} - \mathbf{r_j}|}, \tag{2.4}$$

where the electron positions are denoted by $\mathbf{r_i}$, and

$$\hat{V}_{ext} = \sum_i V_{ext}\left(\mathbf{r}_i\right), \tag{2.5}$$

where $V_{ext}\left(\mathbf{r}_i\right)$ is the potential at point $\mathbf{r}_i$. The external potential contains the contributions from the (Coulombic) potential of atomic nuclei and other external fields.

While the Schrödinger equation represents an exact expression for the interacting electrons and nuclei, it is intractable. *Density functional theory* (DFT) provides a rigorous and exact route to solving the many-body problem by mapping the physical system of N interacting particles onto a tractable system consisting of N fermionic particles. The mapping ensures that both systems have the same single particle ground-state density. The most developed and used approach is Kohn-Sham (KS) DFT (discussed in Section 2.2) in which the system is composed of non-interacting Fermions. Other approaches include the so-called "Generalized Kohn-Sham" (GKS) DFTs are discussed in Section 2.3.

As explained below, DFT shows that all observables can be considered functionals of the one electron density. Hence the approach allows solution of the many-body problem solely in terms of the electronic density

$$n\left(\mathbf{r_1}\right) = N \iint ... \int \left|\Psi\left(\mathbf{r_1}, \mathbf{r_2}, \mathbf{r_3}...\mathbf{r_N}\right)\right|^2 \mathrm{d}\mathbf{r_2}\mathrm{d}\mathbf{r_3}...\mathrm{d}\mathbf{r_N}. \tag{2.6}$$

instead of the full N-particle wave function $\Psi\left(\mathbf{r_1}, \mathbf{r_2}, \mathbf{r_3}...\mathbf{r_N}\right)$.

The Schrödinger equation provides a map between the external potential and the many body wave function $\mathcal{M} : V_{ext}\left(\mathbf{r}\right) \rightarrow \Psi$ and through Eq. (2.6) we obtain the density $n\left(\mathbf{r}\right)$ from the wave function Ψ. This, however, does not guarantee that the many-body problem can be solved by means of the density alone. In their seminal paper [1], Hohenberg and Kohn proved two fundamental theorems of DFT to address this issue:

1. For any system of particles in an external potential $V_{ext}\left(\mathbf{r}\right)$, this potential is uniquely determined (up to a constant term) by the ground state density $n\left(\mathbf{r}\right)$. In other words, for such densities there is a map $\mathcal{M}' : n\left(\mathbf{r}\right) \rightarrow V_{ext}\left(\mathbf{r}\right)$, and hence we can also map the density to the ground state wave function, $n\left(\mathbf{r}\right) \rightarrow \Psi$. We denote such wave function as $\Psi\left[n\right]$.

2. For any external potential $V_{ext}\left(\mathbf{r}\right)$, a universal energy functional $E_{HK}\left[n\right]$ of the density $n\left(\mathbf{r}\right)$ can be defined as

$$E_{HK}\left[n\right] = \left\langle \Psi\left[n\right] \middle| \hat{T} + \hat{V}_{e-e} \middle| \Psi\left[n\right] \right\rangle + \int V_{ext}\left(\mathbf{r}\right) n\left(\mathbf{r}\right) \mathrm{d}\mathbf{r}. \tag{2.7}$$

   The ground state density then yields the global minimum of the functional E_{HK}.

Though the theorems of Hohenberg and Kohn represent a rigorous foundation for density functional theory, we are left with the so-called v-representable problem: The search for the minimum of the total energy (and thus for the ground state density) is strictly valid only for densities that correspond to some $V_{ext}\left(\mathbf{r}\right)$. For a practical implementation of DFT, however, it is desirable to seek the minimum of the total energy by employing the variational principle, which

requires that the energy functional is differentiable with respect to any density n. A solution was provided by Levy and Lieb [2, 3] who defined an energy functional as

$$E_{\mathrm{LL}}[n] = \inf_{\Psi \to n} \left\langle \Psi \middle| \hat{T} + \hat{V}_{e-e} + \hat{V}_{ext} \middle| \Psi \right\rangle, \tag{2.8}$$

where the search is performed through all the states Ψ that yield the density $n(\mathbf{r})$. Using the definitions in Eqs. (2.3), (2.4) and (2.5), we can rewrite Eq. (2.8):

$$E_{\mathrm{LL}}[n] = F_{\mathrm{LL}}[n] + \int V_{ext}(\mathbf{r})\, n(\mathbf{r})\, \mathrm{d}\mathbf{r}, \tag{2.9}$$

where F_{LL} is a universal functional of density defined as

$$F_{\mathrm{LL}}[n] = \inf_{\Psi \to n} \left\langle \Psi \middle| \hat{T} + \hat{V}_{e-e} \middle| \Psi \right\rangle. \tag{2.10}$$

For any given external potential V_{ext}, the Levy-Lieb functional E_{LL} has its minimum for the ground state density of N electrons and provides the ground state energy of the system

$$E_{GS}(N; V_{ext}) = \inf_{n \to N} E_{LL}[n]. \tag{2.11}$$

This corresponds to the minimum of the E_{HK} functional for given V_{ext}. This is an important restatement of the second theorem of Hohenberg and Kohn, since the domain of search is extended to all N-representable densities. We can now denote the density that minimizes E_{LL} for the given external potential as $n[V_{ext}]$, and the minimization of E_{LL} under the constraint yields the Euler equation

$$\frac{\delta}{\delta n(\mathbf{r})} \left[E_{\mathrm{LL}}[n] - \mu \left(\int n(\mathbf{r})\, d^3 r - N \right) \right]_{n[V_{ext}]} = 0, \tag{2.12}$$

where

$$\left. \frac{\delta E_{LL}[n]}{\delta n(\mathbf{r})} \right|_{n[V_{ext}]} = \mu. \tag{2.13}$$

Analogously, if the constraint N in Eq. (2.12) changes by an infinitesimal amount $N \to N + \delta N$, the corresponding minimum of E_{LL} changes by the Lagrange multiplier (μ) and we can write

$$\left. \frac{\mathrm{d}E_{GS}(N)}{\mathrm{d}N} \right|_{n[V_{ext}]} = \mu. \tag{2.14}$$

To take the derivative of the ground state energy of N particles with respect to N, however, we need to extend our domain of definition such that N is a real number: For a system in equilibrium with a bath of electrons (with which particles can be exchanged), the particle number can be considered to be a time averaged quantity $N = M + \omega$, where M is an integer and $0 \leq \omega < 1$. It has to be noted that in this case the state of the system is non-pure, i.e. it is a mixture of Ψ^M and Ψ^{M+1} for M and $M+1$ particles, respectively. Following the derivation in Refs. [4, 5], the total particle number is thus

$$N = \int \mathrm{tr}\left[\hat{P} \hat{n}(\mathbf{r}) \right] \mathrm{d}\mathbf{r}, \tag{2.15}$$

where $\hat{n}$ is the number operator and $\hat{P}$ is the ensemble density matrix given as

$$\hat{P} = \alpha^M \left|\Psi^M\right\rangle\left\langle\Psi^M\right| + \alpha^{M+1}\left|\Psi^{M+1}\right\rangle\left\langle\Psi^{M+1}\right|. \tag{2.16}$$

The projectors on the M and $M+1$ particle states are multiplied by positive weights α^M and α^{M+1}, with the condition that $\alpha^M + \alpha^{M+1} = 1$. For the total number of particles we thus obtain

$$N = M + \omega = \alpha^M \left\langle\Psi^M\right|\hat{n}\left|\Psi^M\right\rangle + \alpha^{M+1}\left\langle\Psi^{M+1}\right|\hat{n}\left|\Psi^{M+1}\right\rangle, \tag{2.17}$$

and $\alpha^{M+1} = \omega$ and $\alpha^M = (1-\omega)$.

In order to find the total energy we first replace the Levy-Lieb functional by its ensemble analogue:

$$E_{LL}[n] = \inf_{\hat{P}\to n} \operatorname{tr}\left[\hat{P}\left(\hat{T} + \hat{V}_{ee} + \hat{V}_{ext}\right)\right]. \tag{2.18}$$

The ground state energy of the ensemble is then given by Eq. (2.11):

$$E_{GS}(M+\omega) = \omega E_{GS}(M+1) + (1-\omega) E_{GS}(M). \tag{2.19}$$

While this equation represent a seemingly trivial relation for the total energies, its consequences are far-reaching.

First, this finding has a significant bearing on the estimates of the charge removal and addition energies and related quantities, which are of immense importance for the description of the electronic structure of the system. One of the most prominent examples is the *fundamental band gap* of a system, E_g, which characterizes the properties of materials such as the ability to conduct electrons and also (indirectly) determines its optical properties. Similarly, the charge removal and addition energies are crucial for the description of the transfer of charge carriers (electrons and holes), which is widely applied in (opto)electronic devices [6–10].

The fundamental band gap of a system is defined as

$$E_g = I - A, \tag{2.20}$$

where the *ionization potential* I

$$I = E_{GS}(M-1) - E_{GS}(M) \tag{2.21}$$

is the lowest energy needed to remove an electron and the *electron affinity* A

$$A = E_{GS}(M) - E_{GS}(M+1) \tag{2.22}$$

denotes the highest energy gained by inserting an electron into the system. It should be noted that it is commonly assumed that for a series of integer values for M, the total energies are convex, i.e. the energy for any intermediate number of electrons M lies below the tie-line of energies with $M+1$ and $M-1$ electrons. This assumption is known as the ionization conjecture and is seemingly valid, although it has not been proven to date [11, 12].

The piecewise linearity condition for the energy (Eq. 2.19) implies that if we take $\omega \to 0^+$ the total energy differences can be obtained from the derivatives of E_{GS} as

$$\left.\frac{\mathrm{d}E_{GS}(N)}{\mathrm{d}N}\right|_{N=M^-} = E_{GS}(M) - E_{GS}(M-1) \tag{2.23}$$

and

$$\left.\frac{\mathrm{d}E_{GS}\left(N\right)}{\mathrm{d}N}\right|_{N=M^{+}} = E_{GS}\left(M+1\right) - E_{GS}\left(M\right), \tag{2.24}$$

where the subscripts M^{-} and M^{+} denote that the derivatives are evaluated from the electron deficient and the excess electron side of integer point M, respectively. By comparing this with Eq. (2.14) we find that

$$E_{GS}\left(M\right) - E_{GS}\left(M-1\right) = \mu_{M^{-}} \tag{2.25}$$

and

$$E_{GS}\left(M+1\right) - E_{GS}\left(M\right) = \mu_{M^{+}}, \tag{2.26}$$

where $\mu_{M^{-}}$ and $\mu_{M^{+}}$ denote the chemical potential for a system with excess positive and negative charge, respectively. The fundamental band gap can thus be written as

$$E_g = \mu_{M^{+}} - \mu_{M^{-}}. \tag{2.27}$$

The discontinuous change in the chemical potential is thus exactly the fundamental band gap of a system. We shall see in the next section, that such behavior has nontrivial consequences for the potentials when dealing with non (or partially) interacting particles.

A simple demonstration of the significance of the fact that the chemical potential changes discontinuously can be illustrated by the following example [4, 5]:

We consider two systems with integer number of particles, which have distinct chemical potentials and are well separated; for instance two neutral atoms A and B in an otherwise empty universe. Their separation is such that they do not interact. Moreover, the two atoms have distinct chemical potentials $\mu^{A}_{M_A} < \mu^{B}_{M_B}$, where M_A and M_B denote the number of electrons for neutral atoms A and B, respectively. Since the atoms do not interact with each other, the total energy is $E_{GS} = E^{A}_{GS} + E^{B}_{GS}$, where E^{A}_{GS} and E^{B}_{GS} are the total energies of atoms A and B, respectively.

If we now assume that the chemical potential does not change discontinuously, i.e. $\mu^{A}_{M^{-}_{A}} = \mu^{A}_{M^{+}_{A}}$, it follows from Eqs. (2.21)-(2.26) that the ionization potential I^{A} and electron affinity A^{A} would be equal (and the same would hold for atom B). In such case, E_{GS} would be lowered by amount of $\omega\left(I^{B} - I^{A}\right)$ when a fractional number of an electron ω is transferred from atom B to A and, ultimately, the minimum of the total energy would thus be achieved when there is a net negative and positive charge on atoms A and B, respectively.

In fact, however, the chemical potential changes discontinuously $\mu^{A}_{M^{-}_{A}} \neq \mu^{A}_{M^{+}_{A}}$ and hence $I^{A} \neq A^{A}$. Upon transferring fractional charge ω from atom B ta A, the change in total energy is $\omega\left(I^{B} - A^{A}\right)$. Provided that the ionization conjecture holds, which seems reasonable since even the the smallest known ionization potential in nature (for Cs atom) is greater than the largest electron affinity (for Cl atom) [5], we find that in this example the total energy E_{GS} will be minimal if both atoms remain neutral, as can be expected.

2.2 Kohn-Sham approach to DFT

Here we will describe one of the most commonly used theoretical approaches applied in electronic structure calculation, Kohn-Sham theory [13]. After defining the theoretical concepts behind it, we will demonstrate its practical implementations with special focus on their limitations. Furthermore, the energies of individual charge carriers, especially the ionization potentials and electron affinities are discussed in detail.

2.2.1 Overview of the Kohn-Sham theory

While in DFT the full many-body problem is reduced to finding the ground state charge density of the system, the interactions are embodied in an intractable electron-electron interaction term $\hat{V}_{e-e}$ in Eq. (2.2). Kohn and Sham [13] provided a route that allowed DFT to become the practical workhorse for *ab-inito* computations: The problem of the interacting many particle system is mapped onto a system of non-interacting particles subject to a common local potential, termed the Kohn-Sham potential $V^{\mathrm{KS}}(\mathbf{r})$, and with the charge density identical to the fully interacting many-body problem system.

For the non-interacting electrons the Levy-Lieb energy functional (Eq. 2.8) becomes

$$E_{LL}^{\mathrm{KS}}[n] = \inf_{\Phi \to n} \left\langle \Phi \middle| \hat{T} + \hat{V}^{KS} \middle| \Phi \right\rangle, \tag{2.28}$$

where the search of the infimum is limited to the ground states of non-interacting electrons, namely wave functions Φ expressed through a Slater determinant composed of single particle states $\{\phi\}$

$$\Phi(\mathbf{r_1}, \mathbf{r_2}, \mathbf{r_3}, \ldots \mathbf{r_N}) = \begin{vmatrix} \phi_1(\mathbf{r_1}) & \phi_2(\mathbf{r_1}) & \cdots & \phi_N(\mathbf{r_1}) \\ \phi_1(\mathbf{r_2}) & \phi_2(\mathbf{r_2}) & \cdots & \phi_N(\mathbf{r_2}) \\ \vdots & \vdots & \ddots & \vdots \\ \phi_1(\mathbf{r_N}) & \phi_2(\mathbf{r_N}) & \cdots & \phi_N(\mathbf{r_N}) \end{vmatrix}. \tag{2.29}$$

Conveniently, we rewrite Eq. (2.28) as

$$E_{LL}^{\mathrm{KS}}[n] = T_S[n] + \int V^{\mathrm{KS}}(\mathbf{r})\, n(\mathbf{r})\, \mathrm{d}\mathbf{r}, \tag{2.30}$$

where the first term represents the density functional of the kinetic energy of non-interacting particles

$$T_S[n] = \inf_{\Phi \to n} \left\langle \Phi \middle| \hat{T} \middle| \Phi \right\rangle. \tag{2.31}$$

It follows that the Euler equation (Eq. 2.13) yields

$$\frac{\delta T_S}{\delta n(\mathbf{r})} = \mu^{\mathrm{KS}} - V^{\mathrm{KS}}, \tag{2.32}$$

where μ^{KS} is the chemical potential of the non-interacting electrons.

The kinetic energy of the non-interacting electrons, together with the classical Coulomb (Hartree) energy

$$E_H[n] = \frac{1}{2} \iint \frac{n(\mathbf{r})\, n(\mathbf{r}')}{|\mathbf{r}' - \mathbf{r}|} \mathrm{d}\mathbf{r}\mathrm{d}\mathbf{r}', \tag{2.33}$$

and the *exchange and correlation* density functional $E_{XC}[n]$ which embodies all the many-body interactions, constitute the Levy-Lieb functional:

$$F_{LL}[n] = T_S[n] + E_H[n] + E_{XC}[n]. \tag{2.34}$$

For a given density, we can (formally) define the XC term as

$$E_{XC}[n] = (T[n] - T_S[n]) + (V_{e-e}[n] - E_H[n]), \tag{2.35}$$

which is composed of two contributions (bracketed): (i) The difference between the kinetic energy of interacting and non-interacting particles. (ii) The difference between the energy of the electron-electron interaction energy $V_{e-e}[n]$ and the Hartree energy functional. It should be noted that while the KS approach may merely appear as a transformation of the original problem of accounting for the many-body interactions, its strength lies in the fact that the XC energy is usually only a small contribution to the total energy and that it can be suitably approximated as we will see in Section 2.2.2.

Since the density of the non-interacting electrons in the Kohn-Sham system is identical to the physical system, we can combine the Euler equation (Eq. 2.13) with the result of Eq. (2.32), and obtain

$$\mu = \frac{\delta E_{LL}}{\delta n(\mathbf{r})} = \mu_{KS} - V^{\mathrm{KS}}(\mathbf{r}) + V_H(\mathbf{r}) + V_{XC}(\mathbf{r}) + V_{ext}(\mathbf{r}). \tag{2.36}$$

Here, the Hartree potential term is given as

$$V_H(\mathbf{r}) = \frac{\delta E_H}{\delta n(\mathbf{r})} = \int \frac{n(\mathbf{r}')}{|\mathbf{r} - \mathbf{r}'|} \mathrm{d}\mathbf{r}', \tag{2.37}$$

and the exchange-correlation potential is

$$V_{XC}(\mathbf{r}) = \frac{\delta E_{XC}}{\delta n(\mathbf{r})}. \tag{2.38}$$

From Eq. (2.36) we can determine the Kohn-Sham potential (up to a constant) as

$$V^{\mathrm{KS}}(\mathbf{r}) = V_H(\mathbf{r}) + V_{ext}(\mathbf{r}) + V_{XC}(\mathbf{r}). \tag{2.39}$$

It follows that for each non-interacting particle we can write a Schrödinger-like equation

$$\left[-\frac{1}{2}\nabla^2 + V^{\mathrm{KS}}(\mathbf{r})\right] \phi_n(\mathbf{r}) = \varepsilon_n^{\mathrm{KS}} \phi_n(\mathbf{r}), \tag{2.40}$$

and the total charge density is given as

$$n(\mathbf{r}) = \sum_i^{N_{occ}} |\phi_i(\mathbf{r})|^2. \tag{2.41}$$

The sum is taken over all occupied KS eigenstates ϕ, i.e. the states with energy $\varepsilon_i^{\mathrm{KS}}$ lower or equal to the chemical potential μ in Eq. (2.36).

Although the structure of Eq. (2.40) strongly resembles the Schrödinger equation, the eigenvalues $\varepsilon_i^{\mathrm{KS}}$ cannot be interpreted as energies of the quasi-particles (holes or electrons) in the original (fully interacting) system. The

only exception is the eigenvalue of the highest occupied eigenstate $\varepsilon_H^{\mathrm{KS}}$ which is (in principle) associated with the lowest energy needed to remove charge from the system, i.e. the lowest energy to create a hole. This is a consequence of the asymptotic behavior of the charge density. Katriel and Davidson [14] and Almbladh and von Barth [15] demonstrated that the asymptotic form of the bound wave function decays exponentially and leads to the charge density

$$\lim_{r\to\infty} n(r) = \exp\left[-2r\sqrt{2I}\right], \tag{2.42}$$

where I is the ionization potential (or equivalently the chemical potential μ_-, described in the previous section). At the same time, it is straightforward to show that the wavefunction of a state i (cf. Eq. (2.40)) decays asymptotically in an exponential way as

$$\phi_i(r\to\infty) \propto \exp\left[-r\sqrt{2\varepsilon_i^{\mathrm{KS}}}\right], \tag{2.43}$$

and at large distances r from the system the dominant contribution stems from the highest occupied eigenstate ϕ_H. Since the density of the non-interacting system is identical to the real system, Eq. (2.43) implies that $\varepsilon_H^{\mathrm{KS}}$ equals the ionization potential in Eq. (2.42) and we can write the so-called *ionization potential theorem*:

$$E_{GS}(M) - E_{GS}(M-1) = \varepsilon_H^{KS}. \tag{2.44}$$

This finding has a very important consequence for practical calculations and their possible interpretation. While the ionization potential is predicted exactly in principle and is given directly by the negative of the KS eigenvalue $\varepsilon_H^{\mathrm{KS}}$, the energy of the first unoccupied eigenstate of the KS Hamiltonian $\varepsilon_{H+1}^{\mathrm{KS}}$ is not guaranteed to have any physical meaning, i.e. it cannot serve as estimate of the electron affinity. Indeed we will see below that further consideration is required in order to calculate A. This leads to a well known *band gap problem* of DFT: The energy difference between the energies of the first unoccupied state and the last occupied state of non-interacting fermions of the KS system yields an eigenvalue gap

$$\Delta_T = \varepsilon_{H+1}^{\mathrm{KS}} - \varepsilon_H^{\mathrm{KS}}, \tag{2.45}$$

which is however distinct from the fundamental band gap E_g (Eq. 2.20).

In a less stringent interpretation, the KS eigenvalues can be taken at least as an approximation to the quasiparticle energies [16]: With commonly used approximations to V_{xc}, Eq. (2.45) yields qualitatively correct descriptions in the vast majority of cases, i.e. $\Delta_T > 0$ for most insulators and semiconductors, though values are consistently smaller than the corresponding E_g (taken from experiments or higher order calculations) [17, 18]. Moreover, many-body perturbation theory employs the KS eigenvalues and eigenstates, assuming that they are approximations to the corresponding quasiparticle couterparts (see Section 2.4).

In order to gain additional insight into this issue, we investigate in more detail the piecewise linearity condition given by Eq. (2.19) and the related expression for the fundamental band gap (Eq. 2.27). From Eq. (2.36) it follows that by evaluating the derivative of the total energy ($\delta E_{LL}/\delta n(\mathbf{r})$) at the integer

point of electrons M from the sides of excess and deficient electronic charge, denoted M^+ and M^- respectively, we obtain

$$\left(\frac{\delta T_S}{\delta n\left(\mathbf{r}\right)} + V^{\mathrm{KS}}\left(\mathbf{r}\right)\right)_{M^\pm} = \mu_\pm. \tag{2.46}$$

Moreover from the previous discussion (Eq. (2.43) and Refs. [14, 15]) we know that $\mu_- = \varepsilon_H^{\mathrm{KS}}$.

Following Eq. (2.27) we now require that the chemical potential changes discontinuously when an infinitesimal amount of charge is added to the system, i.e. the M^+ side of the derivative. Such a discontinuity is trivially found in the kinetic energy term (Eq. 2.31) which explicitly contains sum over all occupied states (Eq. 2.3): By considering a system with M^+ particles a new eigenstate (ϕ_{H+1}) needs to be occupied and hence it contributes to the total energy. If we now assume that the KS potential V^{KS} does not change when the particle number crosses the integer point M (i.e. we are neglecting the interactions of the excess infinitesimal charge with the other M particles) then

$$\left(V^{\mathrm{KS}}\left(\mathbf{r}\right)\right)_{M^-} = \left(V^{\mathrm{KS}}\left(\mathbf{r}\right)\right)_{M^+}, \tag{2.47}$$

and we find [19–21]:

$$\left.\frac{\delta T_S}{\delta n\left(\mathbf{r}\right)}\right|_{M^+} - \left.\frac{\delta T_S}{\delta n\left(\mathbf{r}\right)}\right|_{M^-} = \Delta_T. \tag{2.48}$$

The fundamental gap of non-interacting particles, which are considered in the KS approach, then naturally coincides with the eigenvalue gap Δ_T.

Due to the Hohenberg-Kohn theorems, the exact map between the ground state density and potential is guaranteed; the potential, however, is determined only up to a constant. In other words, an infinitesimal change in the charge density can be related to an infinitesimal change in the effective potential *plus a constant term* Δ_L [20–22]. Following Eq. (2.27), the fundamental band gap is then given as

$$E_g = \left.\frac{\delta E_{LL}}{\delta n\left(\mathbf{r}\right)}\right|_{M^+} - \left.\frac{\delta E_{LL}}{\delta n\left(\mathbf{r}\right)}\right|_{M^-} = \Delta_T + \Delta_L, \tag{2.49}$$

where the subscript on Δ_L denotes the fact that it is provided by a jump in the *local* KS potential, i.e. the assumption made in Eq. (2.47) is generally not valid. By investigating the behavior of the potential terms appearing in Eq. (2.39) we see that both V_H and V_{ext} vary smoothly with $n\left(\mathbf{r}\right)$ and thus cannot contribute to Δ_L. The jump Δ_L, usually termed the *derivative discontinuity*, should thus be provided by the XC potential and we can write

$$\Delta_L = \left.\frac{\delta E_{XC}}{\delta n\left(\mathbf{r}\right)}\right|_{M^+} - \left.\frac{\delta E_{XC}}{\delta n\left(\mathbf{r}\right)}\right|_{M^-}. \tag{2.50}$$

From this consideration it is clear that for systems where Δ_L is small, E_g can be effectively approximated by Eq. (2.45). However, the size of the derivative discontinuity for a given system is unknown *a priori*. It should be noted that even insulators for which $\Delta_T = 0$ exist: Highly correlated systems (Mott-Hubbard insulators), systems with local magnetic order (Mott-Heisenberg insulators) and charge transfer insulators are typical examples [23–25]. In these

cases the finite fundamental band gap arises from the electron-electron interactions and is given by Δ_L. The theoretical description of the electronic states in insulators remains one of the most challenging questions in electronic structure theory.

2.2.2 Application of the Kohn-Sham approach

In Eq. (2.30), the energy contribution stemming from the many body interaction are described by an XC energy functional. Moreover, we require that the associated XC potential (Eq. 2.38) exhibits discontinuous jumps when the particle number crosses an integer. Such a functional is not known, however, and has to be approximated in practice. The construction of XC functionals is constrained by a number of conditions that the functional has to satisfy (e.g. Refs. [26, 27]) and is an area of ongoing research which now predominantly focuses on the improvement of the description of the eigenstate energies $\varepsilon^{\mathrm{KS}}$, such that they approximate the quasiparticle energies well (as it was indicated earlier, e.g. Refs. [16, 28–30]). Here we will only consider the ionization potentials and affinities, since looking at these two quantities is at the center of the thesis research presented in Chapters 4 - 7.

The conceptually simplest approximation is based on the exact behavior of the homogeneous electron gas (HEG), termed the *local density approximation* (LDA) which was introduced together with the foundations of DFT [1, 13] and turned out to be a very successful XC functional given its simplicity. Important steps in constructing LDA, provided by Dirac [31] and Slater [32], included a simplified version of the Hartree-Fock equations in which an averaged exchange energy per particle in HEG with density $\overline{n}$ was evaluated:

$$\epsilon_X^{\mathrm{Slater}}\left(\overline{n}\right) = -\frac{3}{4}\left(\frac{3}{\pi}\right)^{\frac{1}{3}}\overline{n}^{\frac{4}{3}}. \tag{2.51}$$

The remaining contribution, i.e. the correlation energy, is given by parametrizations [33, 34] based on accurate Quantum Monte Carlo calculations for HEG [35]. The crucial idea was to consider the XC energy to depend only on the local charge density at point $\mathbf{r}$, i.e. to approximate it at each point by HEG with $\overline{n} \to n\left(\mathbf{r}\right)$. The resulting expression can be written in a short form as

$$E_{XC}^{\mathrm{LDA}} = \int \epsilon_{XC}^{\mathrm{LDA}}\left(n\left(\mathbf{r}\right)\right) n\left(\mathbf{r}\right) \mathrm{d}\mathbf{r}, \tag{2.52}$$

where $\epsilon_{XC}^{\mathrm{LDA}}\left(n\left(\mathbf{r}\right)\right)$ is the XC energy per particle for a homogeneous gas of density n. Additional improvement is found through the class of semi-local functionals in which the XC energy also depends on the local gradient of the density, for example in the *generalized gradient approximation* [36] (GGA - for instance Refs. [37–39]), but even higher order derivatives can be included [40–45].

Though the approximations involved in constructing (semi)local functionals (SLF) are crude, SLF were found to be extremely successful in predicting properties depending on the total energies of the system (relative stability, compressibility, vibrational frequencies, etc.) [46]. This can be understood as a consequence of the fact that they fulfil some of the fundamental sum rules [36, 47]. However, it stands to reason that the eigenvalues $\left\{\varepsilon_i^{\mathrm{KS}}\right\}$ are more sensitive to

the precise form of the XC functional, since the sum rules are based on integration over the whole system and all (occupied) states, which may lead to error cancellation.

If we look at an eigenstate ϕ_i (where $i \leq H$), which is occupied by a single electron and construct a charge density corresponding to this state $n_i(\mathbf{r}) = |\phi_i(\mathbf{r})|^2$, the following should hold [48, 49]:

$$E_H[n_i] + E_{XC}[n_i] = 0. \tag{2.53}$$

This is a simple consequence of the fact that the XC part should exactly cancel the interaction of the electron with itself (*self-interaction*), incorporated naturally in the Hartree functional E_H. However, the approximate forms of the SLF fail to fulfil this condition and Eq. (2.53) is grossly disobeyed [29] which influence the values of $\left\{\varepsilon_i^{\mathrm{KS}}\right\}$ and ultimately lead to inaccurate predictions of the ionization potential that should be given by $-\epsilon_H^{\mathrm{KS}}$.

In order to investigate the influence of approximate SLF on the prediction of ϵ_H^{KS}, we first consider the change of energy upon variation in the number of particles. It was shown by Janak [50] that for $E_{GS}(N)$ the ground state energy of a KS system with N non-interacting particles

$$\left.\frac{\mathrm{d}E_{GS}(N)}{\mathrm{d}N}\right|_{N=M^-} = \varepsilon_H^{KS} \tag{2.54}$$

holds, irrespective of the functional used. This is a simple consequence of the fact that infinitesimal charge removed from the system is taken from the highest occupied eigenstate. Due to the ionization potential theorem (Eq. 2.44) and Eq. (2.25), it follows that the derivative $\mathrm{d}E_{GS}(N)/\mathrm{d}N$ is constant and the energy ε_H^{KS} is independent of the occupation of the state ϕ_H. In actual calculations using a SLF, the ionization potential theorem is grossly disobeyed and a pronounced negative deviation from the piecewise linearity behavior of E_{GS} is observed (Figure 2.1) [28, 30, 51, 52].

We can estimate this deviation through *energy curvature*, defined as [53]

$$C_- = \left.\frac{\mathrm{d}^2E_{GS}}{\mathrm{d}N^2}\right|_{N=M^-} = \left.\frac{\mathrm{d}\varepsilon_H^{KS}}{\mathrm{d}N}\right|_{N=M^-}, \tag{2.55}$$

where the minus sign in the subscript indicates that it is the energy curvature related to charge removal. It is worth noting that higher order terms (i.e. higher order derivatives of the total energy) can also be evaluated, but energies obtained with SLF follow a convex curve with the deviation strongly dominated by C [53]. The second equality in Eq. (2.55) holds due to the Janak's theorem (Eq. 2.54) and nonzero curvature indicates that the energy of the highest occupied eigenstate changes with the number of particles (cf. Figure 2.1). Such a behavior is clearly spurious: As mentioned in Section 2.1, the fractional number of electrons arises as a time average when the system is allowed to exchange particles with a bath of electrons. Although the occupation of the highest occupied eigenstate is fractional in the time-average, the corresponding eigenvalue $\varepsilon_H^{\mathrm{KS}}$ cannot depend on the occupation number itself. This is violated for $C_- \neq 0$.

The nonzero curvature can be interpreted as one of the consequences of the self-interaction error (cf. Chapter 5). In addition to poor predictions of the ionization potentials, it also overstabilizes fractional occupation (with respect

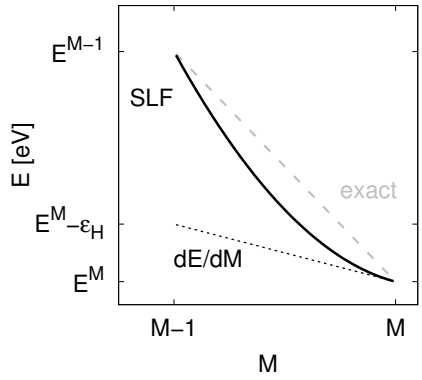

Figure 2.1: Schematic illustration of the total energy curve calculated with a (semi)local density functional of XC (SLF - full black line). The exact behavior dictated by the piecewise linearity condition given by Eq. (2.19) is shown by the dashed gray line. The dotted line represents the derivative of the total energy from the electron deficient side evaluated at M point, which coincides with Eq. (2.54).

to the exact behavior). As a result of this, the excess charge tends to *delocalize* over the whole system [51] and SLF yield incorrect description of charge transfer [51, 54, 55] or even the prediction of fractional charge loss in finite systems [56].

The unsatisfactory behavior of SLF functionals is amplified when electron affinities and KS band gaps are investigated. Upon addition of charge, we require that the XC functional provides a derivative discontinuity Δ_L (Eq. 2.50). To date the only energy functional with such a property is that of Armiento and Kümmel [57] for exchange interaction (discussed further in Chapter 4), which is GGA in nature and yields a discontinuous jump in the XC potential for finite systems when charge is added to a new eigenstate. By contrast, the commonly used XC functionals [34, 39] are smoothly varying with density $n(\mathbf{r})$ and thus cannot provide Δ_L when the particle number crosses an integer point. Instead, we observe a convex energy curve with curvature C_+ when adding charge to a system.

Finally, the presence of curvature in SLF was directly linked to the missing derivative discontinuity [53], i.e. the lack of Δ_L is compensated by the presence of curvature. Assuming that the total energy as a function of particle number deviates from the exact behavior by the quadratic term at most, we can write Eq. (2.19) for charge removal as

$$E_{GS}(M-\omega) = E_{GS}(M) + \omega\varepsilon_H^{\mathrm{KS}} + \frac{1}{2}C_-\omega^2,\ 0 \le \omega \le 1. \tag{2.56}$$

Similarly, we can write for C_+:

$$E_{GS}(M+\omega) = E_{GS}(M) + \omega\varepsilon_{H+1}^{\mathrm{KS}} + \frac{1}{2}C_+\omega^2,\ 0 < \omega \le 1. \tag{2.57}$$

It follows that the fundamental band gap can be approximated as [53]

$$E_g \approx \Delta_T + \frac{1}{2}\left(C_- + C_+\right). \tag{2.58}$$

With increasing system size, however, both C_- and C_+ of SLFs approach zero and do not provide any correction to the eigenvalue gap for extended finite and infinite systems. The origin and behavior of energy curvature is discussed in detail in Chapter 5.

A significant improvement was recently found through ensemble DFT [58]: This approach considers Slater determinants of M and $M \pm 1$ particle systems simultaneously and the total energy of a system with fractional number of particles is described as an ensemble average, following the fundamental considerations leading to Eq. (2.19). For finite systems, it was found that even if simple LDA is used in ensemble DFT, the approach yields derivative discontinuity and improves the predictions of I, A and E_g. Yet again, with increasing system size the results for the eigenvalues approach the "standard" KS results and provide no improvement for infinite systems. This can be viewed as a consequence of vanishing curvature for very large systems: For $C \to 0$ the ground state energy in Eq. (2.56) naturally follows a straight line, though with an incorrect slope dictated by $\varepsilon_H^{\mathrm{KS}}$, which is a poor estimate of I (a similar argument applies to $\varepsilon_{H+1}^{\mathrm{KS}}$ and A). This suggests that for extended and infinite systems, the improvement should be sought in an improved descriptions of the electron-electron interactions, e.g. by employing the generalized Kohn-Sham approach.

2.3 Generalized Kohn-Sham approach to DFT

2.3.1 Overview of the Generalized Kohn-Sham approach

The Kohn-Sham approach is based on mapping the many-body problem onto a system of non-interacting particles. Along a similar line we can now consider a *generalized* Kohn-Sham theory (GKS) formalized by Seidl and co-workers [59] in which the particle-particle interaction can be partially included. As a first step, we formally rewrite the Levy-Lieb functional (Eq. 2.9) as

$$E_{\mathrm{LL}}[n] = \inf_{\Psi \to n} S\left[\Psi\right] + R\left[n\right] + \int V_{ext}\left(\mathbf{r}\right) n\left(\mathbf{r}\right) \mathrm{d}\mathbf{r}. \tag{2.59}$$

In addition to the last term which represents the contribution from the external potential, two quantities are introduced. The first term, S, represents all the energy contributions that explicitly depend on the many-body state Ψ. The second term R is the "remainder", which includes all other terms necessary for the LL functional to yield the exact ground state energy and density upon minimization of $E_{\mathrm{LL}}\left[n\right]$ with respect to all densities n that integrate to N ($n \to N$). It has to be noted that we will again consider a single Slater determinant Φ constructed from states $\{\phi_i\}$ and the search in Eq. (2.59) is performed over all determinants that yield density $n\left(\mathbf{r}\right)$. The term R in Eq. (2.59) represents all contributions that are functionals of the charge density $n\left(\mathbf{r}\right) = \sum_i \left|\phi_i\left(\mathbf{r}\right)\right|^2$, where the summation goes over all occupied states.

In this approach, we can recover the KS theory by choosing

$$S^{\mathrm{KS}}\left[\Phi\right] =: \left\langle \Phi \middle| \hat{T} \middle| \Phi \right\rangle, \tag{2.60}$$

and we obtain T_S in Eq. (2.31) as

$$T_S\left[n\right] = \inf_{\Phi \to n} S^{\mathrm{KS}}\left[\Phi\right]. \tag{2.61}$$

It follows that

$$R^{\mathrm{KS}}\left[n\right] = E_H\left[n\right] + E_{XC}\left[n\right], \tag{2.62}$$

where the Hartree and exchange-correlation potentials are both functionals of density n. The form of Eq. (2.59), however, allows us to equally well define a more general form

$$S^{\mathrm{GKS}}\left[\Phi\right] =: \left\langle \Phi \middle| \hat{T} + \hat{V}_{e-e} \middle| \Phi \right\rangle, \tag{2.63}$$

where the electron-electron interaction potential $\hat{V}_{e-e}$ describes the effects embodied in the single Slater determinant Φ. In this case, our reference system includes part of the particle-particle interaction and differs from the KS picture.

We can now define the functional S such that it explicitly contains the Hartree and exchange term

$$S^{\mathrm{GKS-X}}\left[\Phi\right] = \left\langle \Phi \middle| \hat{T} \middle| \Phi \right\rangle + E_H\left[\Phi\right] + E_X\left[\Phi\right], \tag{2.64}$$

where

$$E_H\left[\Phi\right] = \frac{1}{2} \sum_{i,j} \iint \frac{\phi_i^*\left(\mathbf{r}'\right) \phi_i\left(\mathbf{r}'\right) \phi_j^*\left(\mathbf{r}\right) \phi_j\left(\mathbf{r}\right)}{\left|\mathbf{r} - \mathbf{r}'\right|} \mathrm{d}\mathbf{r}\mathrm{d}\mathbf{r}' \tag{2.65}$$

and

$$E_X\left[\Phi\right] = -\frac{1}{2}\sum_{i,j}\iint \frac{\phi_i^*\left(\mathbf{r}'\right)\phi_j\left(\mathbf{r}'\right)\phi_j^*\left(\mathbf{r}\right)\phi_i\left(\mathbf{r}\right)}{\left|\mathbf{r}-\mathbf{r}'\right|}\mathrm{d}\mathbf{r}\mathrm{d}\mathbf{r}'. \tag{2.66}$$

In both Eqs. (2.65) and (2.66), the summation goes over all occupied states with subscripts i and j. Such a definition of the S functional is strongly reminiscent of the Hartree-Fock approach [60, 61] and contains non-local exchange interaction. In addition, the total energy contains contribution from R, which represents electron correlation. We shall see later that the non-locality of the exchange functional plays a significant role in the description of the individual states ϕ_i and their energies ε_i. The main reason is that the exchange interaction exactly cancels the one electron self-interaction [29] and Eq. (2.53) is thus fulfilled.

Moreover, the explicit dependence on the occupied states $\{\phi_i\}$ yields the discontinuous energy behavior discussed in the preceding section (c.f. Eq. 2.27 and related discussion), in a similar fashion as we found for the KS kinetic term T^{KS} in Eq. (2.48). It is important to note here that such discontinuous behavior is already incorporated into the eigenvalues themselves, bringing them closer to the quasiparticle energies [52]. On the other hand, it will be shown in the next section that simple incorporation of the Hartree-Fock like exchange energy functional does not guarantee that the piecewise linearity condition (Eq. 2.19) is satisfied.

It should also be noted that there are approaches which employ $\{\phi_i\}$ but remain well *within* the KS formalism. This represents a conceptually interesting class of functionals which in general yield eigenvalues ε_i in better agreement with experiments and higher level calculations for quasiparticles [29, 52]. We are not going to pursue this route further here, but for completeness we mention the fact that such approaches directly employ densities n_i of individual eigenstates (e.g., Ref. [49]) or explicitly use the states ϕ_i (extensively reviewed in Ref. [29]). For the latter case, one can find an optimized effective potentials (OEP) approach [62–64] in which a local potential is sought that yields the minimum of the total energy of the Slater determinant Φ, constructed from $\{\phi_i\}$. This can serve as a starting point for further approximations: Becke and Johnson [65] have found a simple semi-local exchange *potential* functional that closely reproduces the OEP result. Such a potential functional provides the basis for the derivation of the exchange *energy* functional by Armiento and Kümmel [57] mentioned in the previous section and further discussed in Chapter 4.

However, here we will focus on employing the GKS formalism presented in Eq. (2.59) which includes an exchange energy functional (Eq. 2.66). We shall see that this flavor of DFT provides an important step towards improving the description of the eigenstate energies, more importantly the energy of the highest occupied eigenstate ε_H (cf. Eq. (2.43) and related discussion).

An important route in constructing an exchange energy functional is the *adiabatic connection theorem* (ACT). To arrive at the ACT we consider the following Levy-Lieb functional F_{LL} given by Eq. (2.10):

$$F_{\mathrm{LL}}\left[n,\lambda\right] = \inf_{\Psi\to n}\left\langle\Psi\middle|\hat{T}+\lambda\hat{V}_{e-e}\middle|\Psi\right\rangle, \tag{2.67}$$

where the parameter $\lambda \in [0,1]$ yields a continuous parametrization of the electron-electron interaction strength and Ψ is a many-body wave function that yields given density n. In the following we denote the many-body wave function

which provides the total energy minimum as Ψ_λ. For $\lambda = 0$ the functional F_{LL} reduces to the non-interacting case; for $\lambda = 1$ we solve the fully interacting system. For a system with given charge density n we can now construct the exchange-correlation energy functional:

$$E_{XC}[n] = F_{\mathrm{LL}}[n,1] - F_{\mathrm{LL}}[n,0] - E_H[n]. \tag{2.68}$$

This form can be conveniently rewritten as

$$E_{XC}[n] = \int_0^1 \mathcal{F}(\lambda)\,\mathrm{d}\lambda, \tag{2.69}$$

where $\mathcal{F}(\lambda) = \partial F_{\mathrm{LL}}[n,\lambda]/\partial\lambda$ and by using the Hellmann-Feynman theorem

$$\mathcal{F}(\lambda) = \left\langle \Psi_\lambda \middle| \hat{V}_{e-e} \middle| \Psi_\lambda \right\rangle - E_H[n]. \tag{2.70}$$

The adiabatic connection theorem presented in Eq. (2.69) provides a general definition of the XC energy functional as a path integral of $\mathcal{F}(\lambda)$ which has to be evaluated for all interaction strengths λ. Yet again, this result is a restatement of the original many-body problem and itself does not reduce its complexity (in general all many body states Ψ_λ need to be found).

2.3.2 Application of the Generalized Kohn-Sham approach

In order to employ the ACT (Eq. 2.69) for the practical construction of exchange-correlation functionals and to avoid calculations of $\mathcal{F}$ for all λ parameters along the path integral, we have to resort to approximations. The limiting cases can be inferred from Eq. (2.67): For $\lambda = 0$ we obtain the Slater determinant composed of the Kohn-Sham orbitals of the ground state Φ and for $\lambda = 1$ we obtain the fully correlated case, which can be in turn approximated by a suitable SLF. A natural approach is thus to suitably mix the non-local (Hartree-Fock like) part of the exchange energy functional with SLF expressions resulting in a class of *hybrid exchange-correlation functionals*.

This approach has been pioneered by Becke [66] who approximated the integrand by linear interpolation, where LDA (Eq. 2.52) was considered to represent the $\lambda = 1$ end point. The resulting functional is simply termed *half-half* hybrid and is expressed as

$$E_{XC}^{\mathrm{H-H}}[n] = \frac{1}{2}E_{XC}^{\mathrm{LDA}}[n] + \frac{1}{2}E_X[\Phi], \tag{2.71}$$

where the last term represents the Hartree-Fock like exchange functional applied on the determinant Φ which yields the density n. Another choice, denoted as PBE0 [39], suggested to use fraction of 0.25 of the Hartree-Fock like exchange and 0.75 of the GGA functional, based on assumed quartic polynomial dependence of the integrand.

As an example of widely popular, though semi-empirical, approaches we can further mention the B3LYP functional (employed in Chapter 6) developed by Becke [66] which can be written as

$$E_{XC}^{\mathrm{B3LYP}} = E_{XC}^{\mathrm{LDA}} + a_0\left(E_X - E_{XC}^{\mathrm{LDA}}\right) + a_x\left(E_X^{\mathrm{GGA}} - E_X^{\mathrm{LDA}}\right) + a_c\left(E_C^{\mathrm{GGA}} - E_C^{\mathrm{LDA}}\right), \tag{2.72}$$

where we used a simplified notation for clarity and E_X is the Hartree-Fock like exchange term (Eq. 2.66). All the remaining terms are functionals of n. The functional takes into account two distinct types of SLF: namely LDA [34] and GGA [38]. The parameters a_0, a_x and a_c were obtained to reproduce the experimental atomization energies. It should be noted that other parametrizations of the hybrid functionals can be devised with adjustable fractions of SLF.

We will now look in more detail at a class of *range-separated* exchange-correlation hybrid functionals [67], and in particular at their derivation based on ACT provided by Baer and Neuhauser [68]. The F_{LL} functional which appears in Eq. (2.67) is modified:

$$F_{\mathrm{LL}}^{RS}[n,\gamma] =: \inf_{\Psi\to n}\left\langle \Psi\middle|\hat{T}+\hat{V}_{e-e}^{\gamma}\middle|\Psi\right\rangle, \tag{2.73}$$

where the second term corresponds to a potential explicitly dependent on the interaction strength γ ($\gamma\in[0,\infty)$),

$$\hat{V}_{e-e}^{\gamma} =: \frac{1}{2}\sum_{i,j}\frac{1-e^{-\gamma|\mathbf{r_i}-\mathbf{r_j}|}}{|\mathbf{r_i}-\mathbf{r_j}|}. \tag{2.74}$$

We see that Eq. (2.74) represents an electron-electron potential which is non-divergent for $r\to 0$. The many-body wave function that yields density n and provides the minimum of F_{LL}^{RS} is denoted as Ψ_λ. Yet again, for $\gamma=0$ the functional F_{LL} in Eq. (2.73) reduces to the non-interacting case, and for $\gamma\to\infty$ Eq. (2.74) yields the bare Coulomb interaction $\hat{v}=\frac{1}{2}\sum_{i,j}|\mathbf{r_i}-\mathbf{r_j}|^{-1}$.

We will see in the next section, focused on many-body perturbation theory, that the presence of some form of screening is of crucial importance for the description of the quasiparticle energies and the fact that *some* form of screened interaction is included already at the DFT level spurs hopes that such a treatment will yield eigenvalues $\{\varepsilon_i\}$ that approximate the quasiparticle energies well. We can symbollically rewrite Eq. (2.74) as $V_{e-e}^{\gamma}=\epsilon_\gamma^{-1}v$, where ϵ_γ^{-1} can be interpreted as the inverse of a/some microscopic frequency-independent dielectric function and v is the bare Coulomb potential.

The two-body interaction given by Eq. (2.74) can now be used to derive an exchange-correlation functional:

$$E_{XC}[n]=\int_0^\infty \mathcal{F}(\gamma)\,\mathrm{d}\gamma, \tag{2.75}$$

where $\mathcal{F}(\gamma)=\partial F_{\mathrm{LL}}^{RS}[n,\gamma]/\partial\gamma$ which is merely a modification of the original Eq. (2.69) such that the integration range goes from 0 to ∞. The integrand is readily obtained from Eq. (2.73) as

$$\mathcal{F}(\gamma)=\frac{1}{2}\left\langle\Psi_\gamma\middle|\sum_{ij}e^{-\gamma|\hat{\mathbf{r}}_\mathbf{i}-\hat{\mathbf{r}}_\mathbf{j}|}\middle|\Psi_\gamma\right\rangle - E_H[n]. \tag{2.76}$$

Furthermore, we assume that the Ψ_γ can be approximated by the the two limiting cases for $\gamma=0$ and $\gamma=\infty$, i.e. for the Hartree-Fock and Kohn-Sham systems, respectively. We can now rewrite Eq. (2.75):

$$E_{XC}[n]\approx\int_0^{\gamma^*}\mathcal{F}^0(\gamma)\,\mathrm{d}\gamma+\int_{\gamma^*}^\infty\mathcal{F}^\infty(\gamma)\,\mathrm{d}\gamma. \tag{2.77}$$

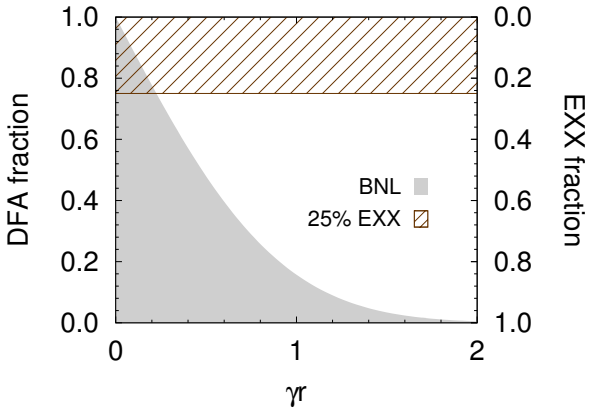

Figure 2.2: Fraction of a semi-local functional for the exchange and correlation energy (SLF), taken as the enumerator of the first term in Eq. (2.78), is shown as a function of distance γr, where γ is the range separation parameter and r is the distance (gray). The complementary part of the functional is given by E_X (Eq. 2.66) applied to a Slater determinant Φ that yields density n (white). A functional which combines a fixed (γr-independent) fraction (25%) of E_X with SLF is illustrated by a hatched area

Here the superscript in the integrand $\mathcal{F}$ denotes whether Ψ_0 or Ψ_∞ was used in Eq. (2.76) and the parameter γ^* indicates the interaction strength at which the two reference points interchange. It is worth noting that for a given system a parameter γ^* can be found such that the resulting XC energy obtained with Eq. (2.77) is exact [68].

Given the structure of the screened potential (Eq. 2.74), i.e. the fact that the parameter γ modifies the strength of V_{e-e} for a given length r, we see that the approximation in Eq. (2.77) leads to effective *range separation* of the electron-electron interaction. The short range (SR) part of the XC functional is approximated by the KS system, characterized by Φ, and is treated by a SLF. The long range part (LR), on the other hand, is treated with Hartree-Fock like exchange constructed from the single particle eigenstates $\{\phi_i\}$. The parameter γ^* provides the characteristic inverse length at which the transition between SR and LR occurs.

In practice, the separation is performed by error-functions [69]:

$$\frac{1}{\mathbf{r}-\mathbf{r}'} = \left[\frac{1-\mathrm{erf}\left(\gamma\left(\mathbf{r}-\mathbf{r}'\right)\right)}{\mathbf{r}-\mathbf{r}'}\right]_{\mathrm{SLF}} + \left[\frac{\mathrm{erf}\left(\gamma\left(\mathbf{r}-\mathbf{r}'\right)\right)}{\mathbf{r}-\mathbf{r}'}\right]_{\mathrm{X}}. \tag{2.78}$$

This separation is illustrated in Figure 2.2 in which the countour of the filled gray area shows the fraction of SLF at each distance point γr (and the complementary part supplied by the Hartree-Fock like exchange). For comparison, the behavior of a hybrid functional with constant (distance independent) fraction of E_X is also shown (if SLF is GGA, this particular example would correspond to the PBE0 functional mentioned above).

The Hartree-Fock like exchange potential has the correct $1/r$ asymptotic behavior by construction [27, 29] and the same holds for the range separated

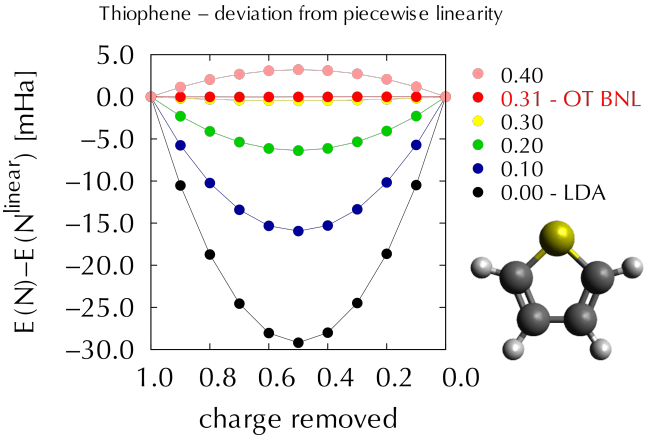

Figure 2.3: Deviation of the total energy from the piecewise linear behavior shown as a function of fractional charge removed from a single thiophene molecule (shown in the right panel of the figure; sulphur, carbon and hydrogen atoms are shown by yellow, black and white spheres). Results for BNL functional with different values of γ (in a_0^{-1} units) are shown by colored lines, where $\gamma = 0.00$ corresponds to the LDA result. For the optimally tuned BNL ($\gamma = 0.31\ a_0^{-1}$) the energy follows a straight line between the two endpoints, given by the total energies of neutral and positively charged thiophene molecule.

hybrid functionals which employ E_X in its LR part. This can be expected to significantly improve the description of charge transfer and removal in comparison to KS DFT approaches. The approximate XC treatment employed in the KS approach leads to potentials which can be expressed as a functional of charge density n, and since the density decays exponentially (Eq. 2.41) the resulting asymptotic behavior of SLF is faster than $1/r$ for $r \to \infty$.

In this context it has to be mentioned that despite of the correct asymptotic potential, the Hatree-Fock method does not correct for the major deficiencies related to charge removal, namely the energy curvature (C) discussed in the context of KS DFT (Eq. 2.55). Nevertheless, while the approximate XC semilocal density functionals suffer form $C > 0$ (Figure 2.1), i.e. spurious negative energy devitation from the piecewise linearity for systems with fractional number of electrons, the Hartree-Fock method shows positive curvature. In other words, the systems with fractional charge shows concave energy curve and suffers from over-localization of the charge [51]. The mixing of both approaches, based on approximations to the integrand (Eq. 2.70), thus naturally arises as a way to mitigate this spurious behavior and can be interpreted as a reason for the general success of the hybrid functionals [28, 30].

A very successful approach for finite systems, which we will pursue further in Chapter 6, is provided by *optimal tuning* of the BNL range separated hybrid functional [68, 70–73]. In this method, the range separation parameter γ^* (Eq. 2.77) is chosen such that the piecewise linearity for the total energy is restored (Figure 2.3). This range separated functional employs a combination of the LDA functional for exchange and correlation with E_X. Four points should be noted here:

1. The optimal tuning approach has a solid theoretical basis.

2. The optimal tuning process is fully *ab-initio*. It relies only on the first principles calculations of the total energies and no prior knowledge or experimental data are required.

3. The range separation parameter γ^* is system dependent and can vary significantly with composition, geometry and size.

4. Total energies of neutral and charged systems change with the value of the range separation parameter. For the optimally tuned functional, the difference between the energy of the cation and neutral system is exactly equal to the highest occupied eigenvalue. This leads to a tremendous improvement in the prediction of charge removal energies [70–73]. Similar tuning procedure can be applied to negatively charged system to obtain electron affinity.

The determination of γ^* is a non-trivial task. For finite systems, we can avoid the calculation of the full set of energy curves by estimating the deviation from the the ionization potential theorem (Eq. 2.44). For infinite systems, however, the charged calculations are not easily performed as discussed in detail in Chapter 5. Moreover, given that $C \to 0$ in calculations employing SLF for an infinite system, it appears that the tuning will ultimately collapse to the SLF solution. A similar conclusion can be conjectured based on the fact that with increasing system size the value of γ^* has been shown to progressively decrease [71].

In Chapter 6 we describe a new phenomenon which shows that for sufficiently large systems, the quasiparticles (holes in $M-1$ particle systems) become independent of the system size, due to many-body interaction that are captured by non-local exchange. This has significant bearing on the applicability of optimal tuning, but also for the fundamental understanding of electronic structure of extended systems.

2.4 Beyond the Density Functional Theory

2.4.1 Quasiparticle Equation

We can now address the behavior of the quasiparticles directly from the many-body perspective. We write the many body Hamiltonian in Eq. (2.2) in the second quantization form as [60, 74]

$$\hat{H} = \int \hat{\psi}\left(\mathbf{r}\right)^{\dagger} h\hat{\psi}\left(\mathbf{r}\right) \mathrm{d}\mathbf{r} + \frac{1}{2} \iint \hat{\psi}\left(\mathbf{r}\right)^{\dagger} \hat{\psi}\left(\mathbf{r}'\right)^{\dagger} v\left(\mathbf{r},\mathbf{r}'\right) \hat{\psi}\left(\mathbf{r}'\right) \hat{\psi}\left(\mathbf{r}\right) \mathrm{d}\mathbf{r}\mathrm{d}\mathbf{r}', \quad (2.79)$$

where $\hat{\psi}\left(\mathbf{r}\right)$ and $\hat{\psi}\left(\mathbf{r}\right)^{\dagger}$ are field annihilation and creation operators respectively, $v\left(\mathbf{r},\mathbf{r}'\right)$ is the Coulomb interaction

$$v\left(\mathbf{r},\mathbf{r}'\right) = \frac{1}{|\mathbf{r}-\mathbf{r}'|}, \quad (2.80)$$

and h is the one particle term

$$h = -\frac{1}{2}\nabla^2 + V_{ext}\left(\mathbf{r}\right). \quad (2.81)$$

We will now focus on finding the energy of a quasiparticle, i.e. a quasihole or quasielectron in case we remove or add en electron to the many body system. First, we note that the single quasiparticle equation can be obtained through the Heisenberg equation of motion for the annihilation operator [60, 74, 75]

$$i\frac{\partial}{\partial t}\hat{\psi}\left(\mathbf{r},t\right) = \left[\hat{\psi}\left(\mathbf{r},t\right), \hat{H}\right] = h\hat{\psi}\left(\mathbf{r}\right) + \int \hat{\psi}\left(\mathbf{r}'\right)^{\dagger} v\left(\mathbf{r},\mathbf{r}'\right) \hat{\psi}\left(\mathbf{r}'\right) \hat{\psi}\left(\mathbf{r}\right) \mathrm{d}\mathbf{r}'. \quad (2.82)$$

To proceed further, we define the Dyson orbital of the quasiparticle as

$$\psi_i^{N-1}(\mathbf{r}) = \left\langle \Psi_i^{N-1} \middle| \hat{\psi}\left(\mathbf{r}\right) \middle| \Psi_0^N \right\rangle \quad (2.83)$$

and

$$\psi_i^{N+1}(\mathbf{r}) = \left\langle \Psi_i^{N+1} \middle| \hat{\psi}^{\dagger}\left(\mathbf{r}\right) \middle| \Psi_0^N \right\rangle, \quad (2.84)$$

where Ψ_i^N eigenstate of the many-body Hamiltonian for N electrons and the superscripts $N \mp 1$ are used to distinguish whether the orbital is for a quasihole or quasielectron. The subscript indicates the i^{th} eigenstate of the many-body system, from/to which the electron has been removed/added. Finally, we can write the equation for the quasiparticle [76–79]:

$$h\psi_i^{\mathrm{N}\pm1}\left(\mathbf{r}\right) + V_H\left(\mathbf{r}\right)\psi_i^{\mathrm{N}\pm1}\left(\mathbf{r}\right) + \int \Sigma\left(\mathbf{r},\mathbf{r}',\varepsilon_i^{N\pm1}\right)\psi_i^{\mathrm{N}\pm1}\left(\mathbf{r}'\right)\mathrm{d}\mathbf{r}' = \varepsilon_i^{N\pm1}\psi_i^{\mathrm{N}\pm1}\left(\mathbf{r}\right). \quad (2.85)$$

This expression is strongly reminiscent of the Schrödinger equation with the single particle terms h (Eq. 2.81) on the left. We can recognize that (similar to the approaches introduced in the preceding sections) the crucial part of Eq. (2.85) is the factorization of the intractable electron-electron interaction in two main contributions:
(i) The Hartree potential, in which the ground-state density of the N electron system can be obtained through the Dyson orbitals as

$$n\left(\mathbf{r}\right) = \sum_i \left|\psi_i^{\mathrm{N}-1}\left(\mathbf{r}\right)\right|^2 = \sum_i \left\langle \Psi_0^N \middle| \hat{\psi}^{\dagger}\left(\mathbf{r}\right) \middle| \Psi_i^{N-1} \right\rangle \left\langle \Psi_i^{N-1} \middle| \hat{\psi}\left(\mathbf{r}\right) \middle| \Psi_0^N \right\rangle, \quad (2.86)$$

where the sum goes over all eigenstates of the many body system with $N-1$ particles.
(ii) The non-local energy-dependent *self-energy* term $\Sigma(\mathbf{r},\mathbf{r}',\omega)$ which describes the many-body exchange and correlation effects.

Formally, this separation is done using expressions for the time propagation of the particles (which will be introduced later in this section) and factorization of the two-particle propagators, which (for simplicity) we will completely avoid here. This approach was pioneered by Dyson [80] and Schwinger [76] in the context of quantum field theory, and later it was applied to the electron gas by Hedin [79], who derived a full set of equations which in principle provide a route to obtain the self-energy exactly and which we will outline in the next subsections.

2.4.2 Green's Function and Quasiparticle Energies

In order to investigate further the expression for the self-energy introduced (heuristically) in Eq. (2.85) we will consider the dynamics of the quasiparticles. We first define the quasiparticle propagators, i.e. Green's functions as the probability amplitude to propagate from point $\mathbf{r}'$ at t to point $\mathbf{r}'$ at time t', where $t > t'$ for quasielectrons and $t < t'$ for quasiholes [60, 74]:

$$G(\mathbf{r},t,\mathbf{r}',t') = -i\left\langle \Psi_0^N \middle| \mathcal{T}\hat{\psi}^\dagger(\mathbf{r}',t')\,\hat{\psi}(\mathbf{r},t) \middle| \Psi_0^N \right\rangle, \tag{2.87}$$

where $\mathcal{T}$ is the time-ordering operator and the field operator now explicitly include the time coordinate. As indicated earlier (Eq. 2.82), we consider the field operators to follow the Heisenberg picture and we can thus write

$$\hat{\psi}(\mathbf{r},t) = e^{i\hat{H}t}\hat{\psi}(\mathbf{r})\,e^{-i\hat{H}t}. \tag{2.88}$$

By inserting the complete set of $\Psi_i^{N\pm1}$ states between the two field operators we finally obtain:

$$\begin{aligned} &G(\mathbf{r},t,\mathbf{r}',t') = \\ &\quad -i\sum_i \psi_i^{N\pm1*}(\mathbf{r}')\,\psi_i^{\mathrm{N}\pm1}(\mathbf{r})\left[e^{-i\varepsilon_i^{N+1}(t-t')}\theta(t-t') - e^{-i\varepsilon_i^{N-1}(t'-t)}\theta(t'-t)\right], \end{aligned} \tag{2.89}$$

where we used the definition of the Dyson orbitals in Eqs. (2.83) and (2.84) and the presence of Heaviside functions θ is a result of the time ordering.

Using the definition of a propagator, we can now deduce the following expression for the dynamics of a quasiparticle

$$\begin{aligned} \left(i\frac{\partial}{\partial t} + \frac{1}{2}\nabla^2 - V_{ext}(\mathbf{r}) - V_H(\mathbf{r})\right) G(\mathbf{r},t,\mathbf{r}',t') &= \delta(\mathbf{r},\mathbf{r}') \\ &+ \int \Sigma(\mathbf{r},\mathbf{r}'',t)\,G(\mathbf{r}'',t',\mathbf{r}',t)\,\mathrm{d}\mathbf{r}''. \end{aligned} \tag{2.90}$$

As an auxiliary quantity, we also define a propagator G_f for a particle which is subjected to an external and Hartree potential:

$$\left(i\frac{\partial}{\partial t} + \frac{1}{2}\nabla^2 - V_{ext}(\mathbf{r}) - V_H(\mathbf{r})\right) G_f(\mathbf{r},t,\mathbf{r}',t') = \delta(\mathbf{r},\mathbf{r}'). \tag{2.91}$$

By combining Eqs. (2.90) and (2.91) we obtain the celebrated form of the Dyson equation describing the propagator of the fully interacting many-body system in terms of the propagator G_f and the self-energy:

$$G(\mathbf{r},t,\mathbf{r}',t') = G_f(\mathbf{r},t,\mathbf{r}',t') + \iint G_f(\mathbf{r},t,\mathbf{r}'',t'')\,\Sigma(\mathbf{r},t,\mathbf{r}',t')\,G(\mathbf{r},t,\mathbf{r}',t')\,. \tag{2.92}$$

One conceptually accessible way of interpreting the Dyson equation is to consider the self-energy as an "event" that modifies the G_f propagator, in a way similar to the propagators considered in scattering theory. If the self-energy is small in some sense we may recast the Dyson equation to a geometric series of $G_f + G_f\Sigma G_f + G_f\Sigma G_f\Sigma G_f + \ldots$ which can summed over (the arguments have been dropped for simplicity), though the number of successive events goes to infinity, in principle. This is the basis for the development of *many-body perturbation theory*. The full propagator is then (formally) written as:

$$G(\mathbf{r},t,\mathbf{r}',t') = \frac{1}{G_f^{-1}(\mathbf{r},t,\mathbf{r}',t') - \Sigma(\mathbf{r},t,\mathbf{r}',t')}. \tag{2.93}$$

In the following we will consider the results of the (generalized) Kohn-Sham approach as a suitable starting point in which the many-body interactions are approximated by the exchange-correlation potential, $V_{XC}(\mathbf{r})$. In this case we employ the eigenstates ϕ_i and eigenvalues ε_i of the Kohn-Sham system obtained through Eq. (2.40) and we consider the XC potential to be a zeroth order approximation to the self-energy. Using ϕ_i and ε_i we construct the Green's function G_0, similar to Eq. (2.89) which is a solution to the following equation:

$$\left(i\frac{\partial}{\partial t} + \frac{1}{2}\nabla^2 - V_{ext}(\mathbf{r}) - V_H(\mathbf{r}) - V_{XC}(\mathbf{r})\right) G_0(\mathbf{r},t,\mathbf{r}',t') = \delta(\mathbf{r},\mathbf{r}')\,. \tag{2.94}$$

To proceed further, we switch from time representation of the Green's function to expression in frequency domain. In order to perform a Fourier transform of G_0 and G we employ the identity

$$ie^{-i\varepsilon_i^{N\pm1}\tau}\theta(\pm\tau) = \mp\int_{-\infty}^{\infty}\frac{e^{-i\omega\tau}}{\omega - \epsilon_i^{N\pm1} \pm i\eta}\frac{d\omega}{2\pi}, \tag{2.95}$$

where $\tau = t - t'$ and the frequency ω is continuous on the whole complex plane. We can now express the free propagator in the so-called *Lehmann representation*

$$G_0(\mathbf{r},\mathbf{r}',\omega) = \lim_{\eta\to0^+}\sum_i \phi_i^*(\mathbf{r}')\,\phi_i(\mathbf{r})\left[\frac{f_i}{\omega - \varepsilon_i - i\eta} + \frac{1-f_i}{\omega - \varepsilon_i + i\eta}\right]., \tag{2.96}$$

where f_i is the occupation of the KS state, i.e. $f_i = 1$ for $\varepsilon_i \le \mu$, and $f_i = 0$ otherwise. We note that the Green's function of a system of non-interacting particles has poles at frequencies corresponding to the energies of the Kohn-Sham system $\omega = \varepsilon_i$ which are infinitesimally shifted by $\pm\eta$ along the imaginary axis. In the same vein, the Green's function of the fully interacting many-body system is given as:

$$G(\mathbf{r},\mathbf{r}',\omega) = \lim_{\eta\to0^+}\sum_i \frac{\psi_i^{N\pm1*}(\mathbf{r}')\,\psi_i^{\mathrm{N}\pm1}(\mathbf{r})}{\omega - \varepsilon_i^{N\pm1} \pm i\eta}, \tag{2.97}$$

where $\varepsilon_i^{N\pm1}$ are the quasiparticle energies that obey Eq. (2.85).

Our goal is to find the quasiparticle energies and we seek them as the poles of the Green's function G (Eq. 2.97), which can be constructed from G_0 employing the Dyson equation (Eq. 2.92). For this we also require knowledge of the self-energy, which will be discussed in the next subsection and in more detail in Chapter 7. Due to the formal similarity of the quasiparticle equation (Eq. 2.81) to the Kohn-Sham equation (Eq. 2.40), we interpret the exchange-correlation potential $V_{XC}(\mathbf{r})$ as a local mean-field approximation to the self-energy Σ. Finally, the expansion in the perturbation series is justified as we expect the difference between the self-energy and the exchange-correlation potential to be small such that $\phi_i \approx \psi_i^{\mathrm{N}\pm1}$ and $\varepsilon_i \approx \varepsilon_i^{N\pm1}$. By means of perturbation theory we thus seek the quasiparticle energy through calculation of an energy shift of the KS eigenvalue, termed *quasiparticle correction*. In the next section we will clarify that the self-energy Σ is in-principle found through a self-consistent procedure, the KS result is thus considered a zeroth step of this cycle.

2.4.3 Self-energy within the GW approximation

A very instructive approach to evaluating the self-energy is to use the diagrammatic technique, largely developed by Feynman [60, 74, 81]. For simplicity, details of this method are not introduced here, and we merely provide its flavor: The self-energy is approximated by an infinite sum over *selected* types of interactions, which are considered to be crucial for description of the physical system of interest. Each such type of interactions is associated with a type of Feynmann diagram and the summation is performed over them.

We now follow the elementary aspects of the many-body perturbation theory which are based on the the famous work of Hedin [79], who showed that the self-energy can be obtained successively through a set of five equations, which are (in principle) solved iteratively. In the language of many-body theory, such an approach is usually termed *self-consistent renormalization* as the set of bare interactions are due to self-consistency renormalized to represent the fully interacting case.

In the following we simplify the notation and represent a space-time point by numbers: $(\mathbf{r}_1, t_1, \mathbf{r}_2, t_2) \to (1, 2)$. The self-energy related to the Green's function G in Eq. (2.90) is given as

$$\Sigma(1,2) = i \iint G(1,3)\, W\left(1^+, 4\right) \Gamma(3,4,2)\, \mathrm{d}3\mathrm{d}4, \tag{2.98}$$

where the time associated with space-time point 1^+ is infinitesimally later then the time associated with 1. The need for an iterative treatment is already obvious at this stage: Σ is expressed by means of the full propagator G, which itself requires the knowledge of the self-energy, the *screened* Coulomb interaction W and the *vertex* function Γ.

The vertex function is a quantity that is difficult to track and contains all the terms in which multiple quasiparticles interact with each other and can be expressed through:

$$\begin{aligned}\Gamma(1,2,3) =& \delta(1,2)\,\delta(1,3) \\ &+ \iiiint \frac{\delta\Sigma(1,2)}{\delta G(4,5)} G(4,6)\, G(7,5)\, \Gamma(6,7,3)\, \mathrm{d}4\, \mathrm{d}5\, \mathrm{d}6\, \mathrm{d}7.\end{aligned} \tag{2.99}$$

This term is derived from the two-particle propagator needed to describe the two-particle interactions, represented by the second term of the many-body Hamiltonian in Eq. (2.79). The two-particle Green's function is expressed through two quasiparticle propagators independent of each other and the remaining interactions are embodied in the vertex function Γ (after some algebra [17, 75, 79, 82]). This is a crucial point for the description of electron-hole interactions in Section 2.4.5.

The screened Coulomb potential is of key importance for us in the later discussion and is defined as

$$W(\mathbf{r},\mathbf{r}',t) = \int \epsilon^{-1}(\mathbf{r},\mathbf{r}'',t)\, v(\mathbf{r}'',\mathbf{r}',t)\,\mathrm{d}\mathbf{r}'', \tag{2.100}$$

where ϵ^{-1} is the inverse dielectric function. W thus describes the Coulombic interaction in the presence of other particles of the system. It is straightforward that if the dielectric function is a constant of unity, W effectively reduces to the bare Hartree potential V_H which is equivalent to the particle-particle interaction potential in vacuum (cf. discussion in Chapter 7).

In order to obtain a practical expression for screening, we first consider a charged point particle and its corresponding potential δV_{ext}; presence of such potential leads to a change in the electronic density of the system and creates an *induced charge density* δn. Finally, the combined potential of the charged point particle and induced density is the change in the *total* potential δV_{tot},

$$\delta V_{tot}(\mathbf{r},t) = \delta V_{ext}(\mathbf{r},t) + \int \frac{\delta n(\mathbf{r}',t)}{|\mathbf{r}-\mathbf{r}'|}\mathrm{d}\mathbf{r}', \tag{2.101}$$

and within linear response theory we define the *irreducible* polarizability P:

$$P(1,2) = \frac{\delta n(1)}{\delta V_{tot}(2)}. \tag{2.102}$$

The term irreducible polarizability is related to the diagrammatic approach, namely to the topology of the diagrams related to P. For further application it can be simply understood as resulting from the change of the total potential. From the perspective of the self-consistent renormalization it is important that P can be expressed as:

$$P(1,2) = -i \iint G(1,3)\,\Gamma(3,4,2)\,G(4,1)\,\mathrm{d}3\mathrm{d}4. \tag{2.103}$$

In other words, the irreducible polarizability is represented by two Green's functions (corresponding to a particle-hole pair) and their mutual interaction is given via the vertex function. This expression will be of crucial importance when describing neutral exctations. The dielectric function can now be written in terms of P:

$$\epsilon(\mathbf{r},\mathbf{r}',\omega) = 1 - v(\mathbf{r},\mathbf{r}')\,P(\mathbf{r},\mathbf{r}',\omega). \tag{2.104}$$

Though the equations given above can be combined to a self-consistent loop, it is clear that their evaluation is highly non-trivial. In order to simplify the problem, we will choose to set the vertex function to

$$\Gamma^{GW}(1,2,3) = \delta(1,2)\,\delta(1,3), \tag{2.105}$$

which effectively removes all the mutual quasiparticle-quasiparticle interactions. The self-energy given in Eq. (2.98) reduces to

$$\Sigma^{GW}(1,2) = iG(1,3)\,W\left(1^{+},3\right), \tag{2.106}$$

and this expression is usually termed the GW approximation. The related vertex function and self-energy are labeled accordingly in their superscript.

Two things need to be mentioned here:

1. The vertex function (Eq. 2.99) is usually approximated by Γ^{GW} (Eq. 2.105), also in the calculation of the dielectric function (Eq. 2.103). The resulting ϵ is consequently obtained in the *random phase approximation* (RPA). In RPA the induced density δn is assumed to be represented by change in the density of non-interacting particles due to a variation of the potential. Similar to the GW approximation introduced earlier, RPA corresponds to neglect of the mutual quasiparticle interactions and will be discussed in the next section in relation to neutral excitations.

2. At each frequency the dielectric function obtained by Eq. (2.104) yields a matrix with elements labelled by the two spatial coordinates $\mathbf{r}$ and $\mathbf{r}'$. In order to evaluated W (Eq. 2.100) we need ϵ^{-1}, and we have to invert ϵ at each ω.

The latter point is a significant bottleneck of this approach and effectively limits the size of systems that can be calculated; this is further discussed in Chapter 7 where the evaluation of ϵ is avoided.

The set of Hedin equations can now be combined to an iterative cycle, repeated to self-consistency:

1. We use a starting point for the construction of the G_0 propagator (Eq. 2.96).

2. The propagators are used to calculate the irreducible polarizability P by aplying Γ^{GW} to Eq. (2.103).

3. We calculate the dielectric function ϵ by Eq. (2.104) and invert it to obtain ϵ^{-1}.

4. Using ϵ^{-1} we now calculate W through Eq. (2.100).

5. By combining G_0 in the first cycle (or the G obtained in the previous iteration) with the screened potential W we calculate the self-energy in the GW approximation (Eq. 2.106).

6. Using the self-energy we can now solve the quasiparticle equation (Eq. 2.85). The resulting Dyson orbitals and quasiparticle energies are used to form a new propagator G_j, where j is the iteration number, and we continue with step 2. The whole cycle is repeated until self-consistency in the quasiparticle energies (and Dyson orbitals) is reached.

The fully self-consistent GW calculations are computationally very demanding [83–86] and the usual approach is to use only a "single shot" algorithm in which steps 1-5 described above are used once and self-consistency is not sought [87]. In this case the quasiparticle equation (Eq. 2.85) is usually not solved and

only a first-order correction to the Kohn-Sham result is considered instead: We take the self-energy operator $\hat{\Sigma}(\omega)$ in the frequency domain as

$$\Sigma(\mathbf{r}, \mathbf{r}', \omega) = \left\langle \mathbf{r}' \middle| \hat{\Sigma}(\omega) \middle| \mathbf{r} \right\rangle \tag{2.107}$$

and approximate the quasiparticle energies as

$$\varepsilon_i^{N-1} \approx \varepsilon_i + \left\langle \phi_i \middle| \hat{\Sigma}\left(\varepsilon_i^{N-1}\right) - \hat{V}_{XC} \middle| \phi_i \right\rangle \ , \ i \leq \mu, \tag{2.108}$$

and

$$\varepsilon_i^{N+1} \approx \varepsilon_i + \left\langle \phi_i \middle| \hat{\Sigma}\left(\varepsilon_i^{N+1}\right) - \hat{V}_{XC} \middle| \phi_i \right\rangle \ , \ i > \mu, \tag{2.109}$$

where μ is the chemical potential and the first/second equation thus describes the energies of the quasiholes/quasielectrons. It has to be noted that the self-energy is evaluated at the frequency corresponding to the quasiparticle energy, i.e. we obtain a fixed point equation. This non-self-consistent approach is usually termed G_0W approximation.

It stands to reason that if the G_0W method is applied, the question of a starting point for G_0 emerges. Hedin's original work [79] used G_0 constructed from the solution of the Hartree-Fock equations, which do not include any type of correlation and self-consistency is required. It was argued, however, that since DFT already contains all many-body effects (on some approximate level), it represents an improved starting point and as such the single perturbative correction may be sufficient [87]. The particular flavor of DFT (e.g. the choice of the E_{XC}) which should be used is a vividly discussed research topic [88–93].

2.4.4 Screened Potential calculated with Time-Dependent DFT

In Chapters 6 and 7, we employ the "single shot" GW approach in which we avoid computationally demanding points 2, 3 and 4 of the algorithm above. Instead, we evaluate the expectation value of the self-energy directly, by considering the linear response of the system to weak *external* perturbation using real time propagation. In order to do so, we employ time-dependent DFT (TD DFT) calculations. Such treatment requires extending the validity of the Hohenberg-Kohn theorems to time-dependent densities.

The initial point of such a consideration is the time-dependent Schrödinger equation for the many-body wave function Ψ,

$$i\frac{\partial}{\partial t}\Psi(t) = \hat{H}(t)\,\Psi(t), \tag{2.110}$$

where the Hamiltonian is time-dependent and is given as

$$\hat{H}(t) = \hat{T} + \hat{V}_{e-e} + \hat{V}_{ext}(t). \tag{2.111}$$

The kinetic energy operator and the electron-electron interaction term remain the same as in the time-independent case (Eqs. 2.3 and 2.4), but the external potential operator is time-dependent and is given as

$$\hat{V}_{ext} = \sum_i V_{ext}(\mathbf{r}_i, t). \tag{2.112}$$

We assume that the initial condition for Eq. (2.110) is that $\Psi(t=0)$ is the ground state of the time-independent Hamiltonian (Eq. 2.2) and the time-dependent density $n(\mathbf{r},t)$ is obtained from the wave function Ψ in the same way as in the time-independent case (Eq. 2.6). Analogously to the Hohenberg-Kohn theorem, Runge and Gross [94] showed that the map $\Psi \rightarrow n(\mathbf{r},t)$ is invertible (up to a time-dependent function) and provides a rigorous foundation for TD DFT.

This conceptual development allows us to write the time-dependent Kohn-Sham equations for of non-interacting particles in analogy to Eq. (2.40) as

$$i\frac{\partial}{\partial t}\phi_n(\mathbf{r},t) = \left[-\frac{1}{2}\nabla^2 + V^{\mathrm{KS}}(\mathbf{r},t)\right]\phi_n(\mathbf{r},t), \tag{2.113}$$

where the time-dependent Kohn-Sham potential is decomposed:

$$V^{\mathrm{KS}}(\mathbf{r},t) = V_H(\mathbf{r},t) + V_{XC}(\mathbf{r},t) + V_{ext}(\mathbf{r},t). \tag{2.114}$$

The Hartree potential term depends directly on the time-dependent density $n(\mathbf{r},t)$ at time t:

$$V_H(\mathbf{r},t) = \int \frac{n(\mathbf{r},t)}{|\mathbf{r}-\mathbf{r}'|}\mathrm{d}\mathbf{r}. \tag{2.115}$$

The expression for the time-dependent exchange-correlation potential $V_{XC}(\mathbf{r},t)$ is however nontrivial and is given as a functional derivative of the exchange-correlation action A_{XC} [94–97],

$$V_{XC}(\mathbf{r},t) = \frac{\delta A_{XC}}{\delta n(\mathbf{r},\tau)}, \tag{2.116}$$

where τ is the so-called "pseudotime" that parametrizes the physical time $t(\tau)$ defined on a Keldysh contour [98]. Such treatment is necessary to fulfil simultaneous requirements on time-symmetry and causality [97]. In practical calculations, we will resort to the *adiabatic approximation*, in which V_{XC} depends only on the instantaneous density of the system; we thus employ the standard XC functionals for the time-independent Kohn-Sham approach.

After this brief introduction to TD DFT we now describe the polarizability in the time domain. We consider the response of the system to the change in the external potential δV_{ext}, and the corresponding *reducible* polarizability is given as

$$\chi(1,2) = \frac{\delta n(1)}{\delta V_{ext}(2)}, \tag{2.117}$$

where the space-time coordinates have been used. δV_{ext} represent only part of the change in the total potential used in definition of P in Eq. (2.102). In this case however, the charge density fluctuation (δn) leads to change in the Kohn-Sham potential, introduced in Eq. (2.30) and Eq. (2.117) becomes

$$\chi(1,2) = \int \frac{\delta n(1)}{\delta V^{\mathrm{KS}}(3)}\frac{\delta V^{\mathrm{KS}}(3)}{\delta V_{ext}(2)}\mathrm{d}3, \tag{2.118}$$

where we employ the chain rule. Here, the Kohn-Sham potential is explicitly time-dependent.

We can now use the decomposition of V^{KS} into individual terms introduced in Eq. (2.114) and after some algebra we obtain a Dyson-like equation

$$\chi(1,2) = \chi^{\mathrm{KS}}(1,2) + \int\int\int \chi^{\mathrm{KS}}(1,3)\left[v(3,4) + f_{XC}(3,4)\right]\chi(4,2)\,\mathrm{d3d4}, \tag{2.119}$$

where we defined the Kohn-Sham polarizability

$$\chi^{\mathrm{KS}}(1,2) = \frac{\delta n(1)}{\delta V^{\mathrm{KS}}(2)}, \tag{2.120}$$

which corresponds to a response of non-interacting particles to a change in the KS potential. In the brackets of the integrand, the first term represents the Coulomb kernel

$$v(\mathbf{r}_1, t_1, \mathbf{r}_2, t_2,) = \frac{\delta V_H(\mathbf{r}_1, t_1)}{\delta n(\mathbf{r}_2, t_2)} = \delta(t_1 - t_2)\frac{1}{|\mathbf{r}_1 - \mathbf{r}_2|}, \tag{2.121}$$

which is instantaneous in time (through the presence of the δ-function on the right side of the equation) and thus depends only on the *spatial* distance between the space-time points. The second term is the time-dependent exchange-correlation kernel

$$f_{XC}(1,2) = \frac{\delta V_{XC}(1)}{\delta n(2)}. \tag{2.122}$$

From this equation it is obvious that the extension to TD DFT has a tradeoff as the the XC kernel at time t has now to be a functional of the charge density of all the times $t' \leq t$. We continue the discussionwith this formal expression in the next equations, but in practical calculations we resort to the adiabatic approximation in which f_{XC} is time-independent.

It is now convenient to take the Fourier transform of Eq. (2.119) and drop the shortened space-time notation. We obtain the reducible frequency-dependent polarizability as [99]:

$$\begin{aligned}\chi(\mathbf{r}, \mathbf{r}', \omega) &= \chi^{\mathrm{KS}}(\mathbf{r}, \mathbf{r}', \omega) \\ &+ \int\int \chi^{\mathrm{KS}}(\mathbf{r}, \mathbf{r}'', \omega)\left(\frac{1}{|\mathbf{r}'' - \mathbf{r}'''|} + f_{XC}(\mathbf{r}'', \mathbf{r}''', \omega)\right)\chi(\mathbf{r}''', \mathbf{r}', \omega)\,\mathrm{d}\mathbf{r}''\mathrm{d}\mathbf{r}'''.\end{aligned} \tag{2.123}$$

In the frequency domain Adler and Wiser [100, 101] provided a practical expression for χ^{KS} given as

$$\begin{aligned}\chi^{\mathrm{KS}}(\mathbf{r}, \mathbf{r}', \omega) &= \lim_{\eta \to 0} \sum_{i,j} f(\epsilon_i)\left(1 - f(\epsilon_j)\right) \\ &\times \left[\frac{\phi_i^*(\mathbf{r}')\,\phi_j(\mathbf{r}')\,\phi_j^*(\mathbf{r})\,\phi_i(\mathbf{r})}{\varepsilon_i^{\mathrm{KS}} - \varepsilon_j^{\mathrm{KS}} - \omega + i\eta} + \frac{\phi_j^*(\mathbf{r}')\,\phi_i(\mathbf{r}')\,\phi_i^*(\mathbf{r})\,\phi_j(\mathbf{r})}{\varepsilon_i^{\mathrm{KS}} - \varepsilon_j^{\mathrm{KS}} + \omega - i\eta}\right],\end{aligned} \tag{2.124}$$

where $f(\epsilon_i)$ is the occupation of the KS eigenstate with energy ϵ_i. In the above equation, η is used only to guarantee the convergence of the Fourier transform.

Finally, we can now provide directly the expression for the *inverse dielectric function*

$$\epsilon^{-1}(\mathbf{r}, \mathbf{r}', \omega) = 1 + v(\mathbf{r}, \mathbf{r}')\,\chi(\mathbf{r}, \mathbf{r}', \omega), \tag{2.125}$$

which is needed to evaluate the screened potential Eq. (2.100). The reducible poarizability χ is a causal quantity, in order to pair it with the propagator, which is time ordered (Eq. 2.87), an appropriate transformation discussed in Chapter 7 has to be applied.

As a last remark, we note that in practical calculations f_{XC} in Eq. (2.123) needs to be approximated and this is achieved in two ways:

1. As mentioned earlier, in practical calculations we only consider V_{XC} in the *adiabatic approximation*, f_{XC} thus depends only on the density $n(\mathbf{r}, t)$ at given time t, i.e. the standard time-independent XC kernel is used. In addition, if adiabatic LDA is used, the kernel becomes local in space [102].

2. f_{XC} is neglected completely which is equivalent to RPA introduced earlier - this is the approach applied in Chapters 6 and 7.

2.4.5 Description of neutral excitations

Bound electron-hole pairs (termed excitons) are produced upon perturbation of the system by an external field (e.g. laser pulse) which does not ionize the system, but excites the system to a higher energy state.

We can describe the excited state of a system by considering propagation of two quasiparticles simultaneously: quasielectron and quasihole. In the preceding section, we used the KS system of non-interacting particles as a starting point and accounted for their many-body interactions through a perturbation technique. In the same vein, we take two independent quasiparticles as a starting point of considerations here and assume that the electron-hole interaction is a small perturbation. We note that we seek a two-particle propagator, i.e. a four-point function $\mathcal{L}(1,2,3,4)$ where the numbers are used to denote space-time points. For two non-interacting quasiparticles we can write

$$\mathcal{L}_0(1,2,3,4) = -iG(1,3)\,G(4,2)\,, \tag{2.126}$$

where the second Green's function on the right describes a quasihole, i.e. it corresponds to propagation back in time following the definition of the quasiparticle propagator in Eq. (2.87). If we now associate the time $t_1 = t_2 = 0$ and $t_3 = t_4 = t$, it follows that

$$\begin{aligned}\mathcal{L}_0(1,2,3,4) = &-i\sum_{i}^{N}\sum_{j>N}\psi_j^{N+1,*}(\mathbf{r}_1)\,\psi_j^{N+1}(\mathbf{r}_3)\,\psi_i^{N-1,*}(\mathbf{r}_4)\,\psi_i^{N-1}(\mathbf{r}_2)\\ &\times e^{-i\left(\varepsilon_j^{N+1}-\varepsilon_i^{N-1}\right)t},\end{aligned} \tag{2.127}$$

which can be conveniently rewritten in the frequency domain as

$$\mathcal{L}_0(\mathbf{r}_1,\mathbf{r}_2,\mathbf{r}_3,\mathbf{r}_4,\omega) = \lim_{\eta\to 0}\sum_{i}^{N}\sum_{j>N}\frac{\psi_j^{N+1,*}(\mathbf{r}_1)\,\psi_j^{N+1}(\mathbf{r}_3)\,\psi_i^{N-1,*}(\mathbf{r}_4)\,\psi_i^{N-1}(\mathbf{r}_2)}{\varepsilon_j^{N+1}-\varepsilon_i^{N-1}-\omega+i\eta}. \tag{2.128}$$

The first sum goes over all Dyson orbitals corresponding to the quasiholes ψ_i^{N-1} and the second sum goes over all quasielectron Dyson orbitals ψ_j^{N+1}. It is important to note that $\mathcal{L}_0$ in the form of Eq. (2.128) has poles at real frequencies

$$\omega_{ex}^0 = \varepsilon_j^{N+1} - \varepsilon_i^{N-1} \tag{2.129}$$

which correspond to the energies of isolated (i.e. non-interacting) quasiparticles.

We can regard the independent-quasiparticle propagator $\mathcal{L}_0$ in Eq. (2.126) as a generalization of the irreducible polarizability P given in Eq. (2.103) if Γ^{GW} (Eq. 2.105) is employed; a detailed discussion can be found e.g. in Ref. [99]. This is consistent with our interpretation of Γ as a quantity which contains all the quasiparticle-quasiparticle interactions (Eq. (2.99) and related discussion). In this interpretation, the irreducible polarizability, which is a two-point function, can be obtained from the two-particle propagator by contracting the space-time points, i.e. setting $1 = 2$ and $3 = 4$.

In order to account for the excitonic effects in the polarizability, we include the vertex function in the form:

$$\Gamma'(1,2,3) = \delta(1,2)\,\delta(1,3) - W(1,2) \iint G(1,4)\,G(5,2)\,\Gamma(4,5,3)\,\mathrm{d}4\,\mathrm{d}5, \tag{2.130}$$

where we apply the approximation [103, 104]

$$\frac{\delta\Sigma(1,2)}{\delta G(3,4)} \approx -W(1,2)\,\delta(1,3)\,\delta(2,4)\,. \tag{2.131}$$

This implies that while Γ^{GW} contracts all space-time points $(1,2,3)$ into a single point, Γ' contains an additional interaction term. By generalizing the polarizability P (Eq. 2.103) into a four-point function [99, 103] and including Γ' from Eq. (2.130), we arrive at the following Dyson-like expression for the irreducible two-particle propagator $\tilde{\mathcal{L}}$ [99]:

$$\tilde{\mathcal{L}}(1,2,3,4) \approx \mathcal{L}_0(1,2,3,4) - \iint \mathcal{L}_0(1,2,5,6)\,W(5,6)\,\tilde{\mathcal{L}}(5,6,3,4)\,\mathrm{d}5\,\mathrm{d}6. \tag{2.132}$$

This is only an approximate expression since we employ Eq. (2.131). Nevertheless, inclusion of Γ' even in the present form introduces excitonic interaction. One of the space time points in W correspond to the propagation of a quasielectron, the second one to a quasihole, and the mutual excitonic effect is described by the screened Coulomb interaction.

As mentioned above, Eq. (2.132) represents the irreducible propagator and can be connected to the irreducible polarizability that goes beyond RPA. It is our goal to describe the response of a many-body system to external perturbation and we thus seek the reducible propagator $\mathcal{L}$. The relation between those two can be written symbolically as $\mathcal{L} = \tilde{\mathcal{L}} + \tilde{\mathcal{L}}\,{}^4v\,\mathcal{L}$, where ${}^4v$ is the Coulomb kernel defined in the context of four-point quantities as [99]:

$${}^4v(1,2,3,4) = v(1,3)\,\delta(1,2)\,\delta(3,4)\,, \tag{2.133}$$

and $v(1,2)$ is the Coulomb kernel from Eq. (2.121). Finally we thus write the *Bethe-Salpeter equation* (BSE - Ref. [105]):

$$\begin{aligned}\mathcal{L}(1,2,3,4) =& \mathcal{L}_0(1,2,3,4) \\ &- \iiiint \mathcal{L}_0(1,2,5,6)\,\mathcal{K}(5,6,7,8)\,\mathcal{L}(7,8,3,4)\,\mathrm{d}5\,\mathrm{d}6\,\mathrm{d}7\,\mathrm{d}8,\end{aligned} \tag{2.134}$$

where $\mathcal{K}$ is the Bethe-Salpeter kernel given as

$$\mathcal{K}(1,2,3,4) \approx v(1,3)\,\delta(1,2)\,\delta(3,4) - W(1,2)\,\delta(1,3)\,\delta(2,4) \tag{2.135}$$

in our approximation. We recognize that the two types of Colomb interactions are different in strength since the excitonic term is screened as discussed above. Moreover, the first term on the right hand side does not describe the mutual interactions of the quasiparticles, but applies (instantaneously) on each particle independently. It thus corresponds to the exchange interaction term given by unscreened Coulomb interaction.

The four-point two-particle propagator given by BSE contains information on the excitations in the system. At the level of $\mathcal{L}_0$ we saw that the excitations are given directly by the difference between two quasiparticle energies ω^0_{ex} (Eq. 2.129). If we consider a system of interacting quasiparticles, the excitation energies are renormalized. Leaving out the details, which can be found in Ref. [74], we now transform the problem into the frequency domain (as we did for $\mathcal{L}_0$ in Eq. (2.128)) and represent the propagators by their matrix form

$$: \mathcal{L}^{1,2,3,4}(\omega) = \mathcal{L}_0^{1,2,3,4}(\omega) + \sum_{5,6,7,8} \mathcal{L}_0^{1,2,5,6}(\omega)\, \mathcal{K}^{5,6,7,8}(\omega)\, \mathcal{L}^{7,8,3,4}(\omega), \quad (2.136)$$

where the upper indeces label the position coordinates $(\mathbf{r}_1, \mathbf{r}_2, \mathbf{r}_3, \mathbf{r}_4) \rightarrow^{(1,2,3,4)}$. The matrix of the full propagator $\mathcal{L}$ can be diagonalized and so can be its inverse $\mathcal{L}^{-1}$ which directly provides access to the excitation energies. The solution is then found through [74]

$$\sum_{3,4} \left[\left(\mathcal{L}_0^{1,2,3,4}(\omega) \right)^{-1} - \mathcal{K}^{1,2,3,4}(\omega) \right] \mathbf{X}^{3,4} = 0, \quad (2.137)$$

which yields the eigenvectors $\mathbf{X}$ and eigenvalues ω_{ex} corresponding to the energies of the excitations

$$\omega_{ex} = \omega^0_{ex} + \omega^{int}_{ex}, \quad (2.138)$$

which are now shifted from ω^0_{ex} (poles of $\mathcal{L}_0$ given by Eq. (2.129)) by the electron-hole interaction energy ω^{int}_{ex}.

If we contract the space-time points and transform the propagator $\mathcal{L}$ into a two-point function (see Appendix of Ref. [99]), we obtain the reducible polarizability function $\chi(\mathbf{r}, \mathbf{r}', \omega)$ which we have introduced in Eq. (2.123). This is an important step, since we can connect the (transformed) propagator to an observable: we can now calculate the *absorption spectra* for the many-body system considered, obtained as the imaginary art of χ. Given the computational complexity of BSE and its connection to χ, an approximate solution to BSE is often sought through applying TD DFT. In principle, the poles of the BSE Hamiltonian should thus coincide with the position of absorption spectra, that are obtained as the imaginary part of χ [104, 106, 107]. In the following, we discuss this analogy further.

First, we note that the independent two-particle propagator $\mathcal{L}_0$ (Eq. 2.126) is reduced (upon contraction to the two-point function) to the form of χ^{KS} if we assume that the (generalized) KS eigenstates are Dyson orbitals and the (generalized) KS eigenvalues correspond to quasiparticle energies. In the previous sections we clarified that such association is not rigorous, but it is often made in practice. Moreover, using the generalized Kohn-Sham approach with range-separated hybrid functionals is known to provide eigenvalues that are comparable to those obtained with experiments or higher order methods. The range-separation of the electron-electron interaction can also be viewed as

a result of (some form of) screening, as suggested by Eq. (2.74) and related discussion. In the following we thus assume that

$$^2\mathcal{L}_0\left(\mathbf{r},\mathbf{r}',\omega\right) \approx \chi^{\mathrm{KS}}\left(\mathbf{r},\mathbf{r}',\omega\right), \tag{2.139}$$

where $^2\mathcal{L}_0\left(\mathbf{r},\mathbf{r}',\omega\right)$ is the contracted two-particle propagator.

Comparing Eq. (2.136) with Eq. (2.123) we see that the two equations yield the same result if the (contracted) Bethe-Salpeter kernel $^2\mathcal{K}$ can be approximated as

$$^2\mathcal{K}\left(\mathbf{r},\mathbf{r}',\omega\right) \approx \frac{1}{|\mathbf{r}-\mathbf{r}'|} + f_{XC}\left(\mathbf{r},\mathbf{r}',\omega\right) \tag{2.140}$$

Such an approximation will never strictly be valid, as the two quantities differ in dimensionality [99, 103], as the contracted kernel contains all the information of the four-point function. However, the formal similarity between the right side of the above equation and Eq. (2.135) used in actual BSE calculations is evident. Moreover, it was shown that TD DFT can capture the same effects as the approximate Bethe-Salpeter kernel in principle [104].

During the last decade, research in the area of TD DFT was thus strongly motivated towards finding XC kernels that would provide a good approximation to BSE. The key point was to realize that excitonic effects are driven mostly by the divergent long-wave length terms, i.e. $|\mathbf{r}-\mathbf{r}'| \to \infty$ [108]. This suggests that the non-locality of the XC kernel is of crucial importance and is missing for (semi)local functionals in the Kohn-Sham DFT. This is also the reason why for very large and infinite systems the excitonic effects are not observed if TD DFT is applied with standard LDA or GGA. A solution was found by including long-range corrections for the f_{XC} and new approaches, in which the kernel is derived linear response obtained with (semi)local functional [103, 107, 109–113]. Alternatively, non-local XC kernels based on hybrid functional are used and allow for calculation of ground and excited state properties on the same footing [112, 114, 115]. The latter approach was also employed for calculation of excitonic effects in Chapter 6.

Bibliography

[1] P. Hohenberg and W. Kohn, Phys. Rev. **136**, 864 (1964).

[2] M. Levy, Phys. Rev. A **26**, 1200 (1982).

[3] E. H. Lieb, Int. J. Quantum Chem. **24**, 243 (1983).

[4] J. P. Perdew, R. G. Parr, M. Levy, and J. L. Balduz, Phys. Rev. Lett. **49**, 1691 (1982).

[5] R. M. Dreizler and E. K. U. Gross, *Density Functional Theory: An Approach to the Quantum Many-Body Problem* (Springer Science & Business Media, 1990).

[6] M. C. Scharber, D. Mühlbacher, M. Koppe, P. Denk, C. Waldauf, A. J. Heeger, and C. J. Brabec, Adv. Mater. **18**, 789 (2006).

[7] G. D. Scholes and G. Rumbles, Nat. Mater. **5**, 683 (2006).

[8] J.-L. Brédas, J. E. Norton, J. Cornil, and V. Coropceanu, Acc. Chem. Res. **42**, 1691 (2009).

[9] T. M. Clarke and J. R. Durrant, Chem. Rev. **110**, 6736 (2010).

[10] A. Mishra and P. Bäuerle, Angew. Chem. Int. Ed. **51**, 2020 (2012).

[11] J. P. Solovej, Ann. Mat. **158**, 509 (2003).

[12] P. T. Nam, *XVIIth International Congress on Mathematical Physics* (World Scientific, 2013).

[13] W. Kohn and L. J. Sham, Phys. Rev. **140**, A1133 (1965).

[14] J. Katriel and E. R. Davidson, Proc. Natl. Acad. Sci. USA **77**, 4403 (1980).

[15] C.-O. Almbladh and U. Von Barth, Phys. Rev. B **31**, 3231 (1985).

[16] D. Chong, O. Gritsenko, E. Baerends, et al., J. Chem. Phys. **116**, 1760 (2002).

[17] L. Hedin, J. Phys.: Condens. Matter **11**, R489 (1999).

[18] K. Lejaeghere, V. Van Speybroeck, G. Van Oost, and S. Cottenier, Crit. Rev. Solid State Mater. Sci. **39**, 1 (2014).

[19] J. P. Perdew and M. Levy, Phys. Rev. Lett. **51**, 1884 (1983).

[20] L. J. Sham and M. Schlüter, Phys. Rev. Lett. **51**, 1888 (1983).

[21] E. Sagvolden and J. P. Perdew, Phys. Rev. A **77**, 012517 (2008).

[22] J. P. Perdew and M. Levy, Phys. Rev. Lett. **51**, 1884 (1983).

[23] W. Jones and N. H. March, *Theoretical Solid State Physics: Perfect Lattices in Equilibrium*, vol. 1 (Dover Publications Inc., 1986).

[24] W. A. Harrison, *Solid State Theory* (Dover Publications Inc., 2011).

[25] J. Zaanen, G. Sawatzky, and J. Allen, Phys. Rev. Lett. **55**, 418 (1985).

[26] M. Levy and J. P. Perdew, Phys. Rev. A **32**, 2010 (1985).

[27] R. Van Leeuwen and E. Baerends, Phys. Rev. A **49**, 2421 (1994).

[28] P. Mori-Sánchez, A. J. Cohen, and W. T. Yang, J. Chem. Phys. **125**, 201102 (2006).

[29] S. Kümmel and L. Kronik, Rev. Mod. Phys. **80**, 3 (2008).

[30] A. J. Cohen, P. Mori-Sánchez, and W. Yang, Science **321**, 792 (2008).

[31] P. A. Dirac, in *Mathematical Proceedings of the Cambridge Philosophical Society* (Cambridge Univ Press, 1930), vol. 26, pp. 376–385.

[32] J. C. Slater, Phys. Rev. **81**, 385 (1951).

[33] S. Vosko, L. Wilk, and M. Nusair, Can. J. Phys. **58**, 1200 (1980).

[34] J. P. Perdew and Y. Wang, Phys. Rev. B **45**, 13244 (1992).

[35] D. M. Ceperley and B. Alder, Phys. Rev. Lett. **45**, 566 (1980).

[36] J. P. Perdew, K. Burke, and Y. Wang, Phys. Rev. B **54**, 16533 (1996).

[37] A. D. Becke, Phys. Rev. A **38**, 3098 (1988).

[38] C. Lee, W. Yang, and R. G. Parr, Phys. Rev. B **37**, 785 (1988).

[39] J. P. Perdew, K. Burke, and M. Ernzerhof, Phys. Rev. Lett. **77**, 3865 (1996).

[40] J. P. Perdew, Phys. Rev. Lett. **55**, 1665 (1985).

[41] S. K. Ghosh and R. G. Parr, Phys. Rev. A **34**, 785 (1986).

[42] T. Van Voorhis and G. E. Scuseria, J. Chem. Phys. **109**, 400 (1998).

[43] J. P. Perdew, S. Kurth, A. Zupan, and P. Blaha, Phys. Rev. Lett. **82**, 2544 (1999).

[44] J. Tao, J. P. Perdew, V. N. Staroverov, and G. E. Scuseria, Phys. Rev. Lett. **91**, 146401 (2003).

[45] P. Hao, J. Sun, B. Xiao, A. Ruzsinszky, G. b. I. Csonka, J. Tao, S. Glindmeyer, and J. P. Perdew, J. Chem. Theory Comput. **9**, 355 (2012).

[46] R. M. Martin, *Electronic Structure: Basic Theory and Practical Methods* (Cambridge University Press, 2004).

[47] O. Gunnarsson and B. Lundqvist, Phys. Rev. B **13**, 4274 (1976).

[48] J. Perdew, Chem. Phys. Lett. **64**, 127 (1979).

[49] J. P. Perdew and A. Zunger, Phys. Rev. B **23**, 5048 (1981).

[50] J. F. Janak, Phys. Rev. B **18**, 7165 (1978).

[51] P. Mori-Sánchez, A. J. Cohen, and W. Yang, Phys. Rev. Lett. **100** (2008).

[52] W. Yang, A. J. Cohen, and P. Mori-Sánchez, J. Chem. Phys. **136**, 204111 (2012).

[53] T. Stein, J. Autschbach, N. Govind, L. Kronik, and R. Baer, J. Phys. Chem. Lett. **3**, 3740 (2012).

[54] D. J. Tozer, J. Chem. Phys. **119**, 12697 (2003).

[55] A. Dreuw and M. Head-Gordon, J. Am. Chem. Soc. **126**, 4007 (2004).

[56] M. J. Peach, A. M. Teale, T. Helgaker, and D. J. Tozer, J. Chem. Theory Comput. **11**, 5262 (2015).

[57] R. Armiento and S. Kümmel, Phys. Rev. Lett. **111**, 36402 (2013).

[58] E. Kraisler and L. Kronik, Phys. Rev. Lett. **110**, 126403 (2013).

[59] A. Seidl, A. Görling, P. Vogl, J. A. Majewski, and M. Levy, Phys. Rev. B **53**, 3764 (1996).

[60] E. K. U. Gross, E. Runge, and O. Heinonen, *Many-Particle Theory* (Hilger, Bristol, 1991).

[61] T. Helgaker, P. Jorgensen, and J. Olsen, *Molecular Electronic-Structure Theory* (John Wiley & Sons, 2014).

[62] R. T. Sharp and G. K. Horton, Phys. Rev. **90**, 317 (1953).

[63] J. D. Talman and W. F. Shadwick, Phys. Rev. A **14**, 36 (1976).

[64] J. Krieger, Y. Li, and G. Iafrate, Phys. Lett. A **146**, 256 (1990).

[65] A. D. Becke and E. R. Johnson, J. Chem. Phys. **124**, 221101 (2006).

[66] A. D. Becke, J. Chem. Phys. **98**, 5648 (1993).

[67] T. Leininger, H. Stoll, H.-J. Werner, and A. Savin, Chem. Phys. Lett. **275**, 151 (1997).

[68] R. Baer and D. Neuhauser, Phys. Rev. Lett. **94**, 043002 (2005).

[69] T. Yanai, D. P. Tew, and N. C. Handy, Chem. Phys. Lett. **393**, 51 (2004).

[70] U. Salzner and R. Baer, J. Chem. Phys. **131**, 231101 (2009).

[71] T. Stein, H. Eisenberg, L. Kronik, and R. Baer, Phys. Rev. Lett. **105**, 266802 (2010).

[72] R. Baer, E. Livshits, and U. Salzner, Annu. Rev. Phys. Chem. **61**, 85 (2010).

[73] L. Kronik, T. Stein, S. Refaely-Abramson, and R. Baer, J. Chem. Theory Comput. **8**, 1515 (2012).

[74] A. L. Fetter and J. D. Walecka, *Quantum Theory of Many-Particle Systems* (Dover Publications, 2003).

[75] F. Aryasetiawan and O. Gunnarsson, Reports Prog. Phys. **61**, 237 (1998).

[76] J. Schwinger, Proc. Natl. Acad. Sci. USA **37**, 452 (1951).

[77] A. Klein and R. Prange, Phys. Rev. **112**, 994 (1958).

[78] A. Klein, Phys. Rev. **121**, 950 (1961).

[79] L. Hedin, Phys. Rev. **139**, A796 (1965).

[80] F. J. Dyson, Phys. Rev. **75**, 1736 (1949).

[81] R. D. Mattuck, *A Guide to Feynmann Diagrams in the Many-Body Problem* (Dover Publications, 1992).

[82] C. Friedrich and A. Schindlmayr, NIC Series **31**, 335 (2006).

[83] A. Stan, N. E. Dahlen, and R. Van Leeuwen, J. Chem. Phys. **130**, 114105 (2009).

[84] C. Rostgaard, K. W. Jacobsen, and K. S. Thygesen, Phys. Rev. B **81**, 085103 (2010).

[85] F. Caruso, P. Rinke, X. Ren, M. Scheffler, and A. Rubio, Phys. Rev. B **86**, 081102 (2012).

[86] F. Caruso, P. Rinke, X. Ren, A. Rubio, and M. Scheffler, Phys. Rev. B **88**, 075105 (2013).

[87] M. S. Hybertsen and S. G. Louie, Phys. Rev. B **34**, 5390 (1986).

[88] F. Bruneval and M. A. Marques, J. Chem. Theory Comput. **9**, 324 (2012).

[89] V. Atalla, M. Yoon, F. Caruso, P. Rinke, and M. Scheffler, Phys. Rev. B **88**, 165122 (2013).

[90] D. A. Egger, S. Weissman, S. Refaely-Abramson, S. Sharifzadeh, M. Dauth, R. Baer, S. Kümmel, J. B. Neaton, E. Zojer, and L. Kronik, J. Chem. Theory Comput. **10**, 1934 (2014).

[91] R. M. Richard, M. S. Marshall, O. Dolgounitcheva, J. V. Ortiz, J.-L. Bredas, N. Marom, and C. D. Sherrill, J. Chem. Theory Comput. **12**, 595 (2016).

[92] L. Gallandi, N. Marom, P. Rinke, and T. Körzdörfer, J. Chem. Theory Comput. **12**, 605 (2016).

[93] J. W. Knight, X. Wang, L. Gallandi, O. Dolgounitcheva, X. Ren, J. V. Ortiz, P. Rinke, T. Körzdörfer, and N. Marom, J. Chem. Theory Comput. **12**, 615 (2016).

[94] E. Runge and E. K. U. Gross, Phys. Rev. Lett. **52**, 997 (1984).

[95] E. K. U. Gross and W. Kohn, Adv. Quantum Chem **21**, 287 (1990).

[96] E. Gross, J. Dobson, and M. Petersilka, in *Density Functional Theory II* (Springer, 1996), pp. 81–172.

[97] R. van Leeuwen, Phys. Rev. Lett. **80**, 1280 (1998).

[98] L. V. Keldysh, Sov. Phys. JETP **20**, 1018 (1965).

[99] G. Onida, L. Reining, and A. Rubio, Rev. Mod. Phys. **74**, 601 (2002).

[100] S. L. Adler, Phys. Rev. **126**, 413 (1962).

[101] N. Wiser, Phys. Rev. **129**, 62 (1963).

[102] E. Gross and W. Kohn, Phys. Rev. Lett. **55**, 2850 (1985).

[103] L. Reining, V. Olevano, A. Rubio, and G. Onida, Phys. Rev. Lett. **88**, 066404 (2002).

[104] F. Bruneval, F. Sottile, V. Olevano, R. Del Sole, and L. Reining, Phys. Rev. Lett. **94**, 186402 (2005).

[105] E. Salpeter and H. A. Bethe, Phys. Rev. **84**, 1232 (1951).

[106] M. Petersilka, U. J. Gossmann, and E. K. U. Gross, Phys. Rev. Lett. **76**, 1212 (1996).

[107] F. Sottile, V. Olevano, and L. Reining, Phys. Rev. Lett. **91**, 056402 (2003).

[108] P. Ghosez, X. Gonze, and R. Godby, Phys. Rev. B **56**, 12811 (1997).

[109] S. Botti, F. Sottile, N. Vast, V. Olevano, L. Reining, H.-C. Weissker, A. Rubio, G. Onida, R. Del Sole, and R. Godby, Phys. Rev. B **69**, 155112 (2004).

[110] S. Sharma, J. Dewhurst, A. Sanna, and E. Gross, Phys. Rev. Lett. **107**, 186401 (2011).

[111] S. Sharma, J. Dewhurst, A. Sanna, A. Rubio, and E. Gross, New J. Phys. **14**, 053052 (2012).

[112] S. Rigamonti, S. Botti, V. Veniard, C. Draxl, L. Reining, and F. Sottile, Phys. Rev. Lett. **114**, 146402 (2015).

[113] J. Berger, Phys. Rev. Lett. **115**, 137402 (2015).

[114] E. Rabani, R. Baer, and D. Neuhauser, Phys. Rev. B **91**, 235302 (2015).

[115] S. Refaely-Abramson, M. Jain, S. Sharifzadeh, J. B. Neaton, and L. Kronik, Phys. Rev. B **92**, 081204 (2015).

Chapter 3

Summary and Scope of the Thesis

In the preceding chapter of the thesis, an overview of density functional theory (DFT) and many-body perturbation theory has been provided and special attention has been paid to describing the problems that arise when practical calculations are made with the respective theories. More specifically, the theoretical description of the electron removal (and addition) energies are at the center of interest. In Chapters 4-7 I present work that I performed in the course of my Ph.D. research and that is aimed at addressing the questions introduced in Chapter 2.

The goal of my research is to improve the description and understanding of large (possibly infinite) systems, which exhibit a behavior at the boundary between molecules or nanocrystals and solids and for which distinct computational approaches are often used.

In Section 3.1 I present computational results on the electronic structure of solids using a newly developed exchange energy functional. This functional had previously been shown to significantly improve the description of electronic states in finite systems. In Section 3.2, I introduce work which analyzes in detail an error of standard functionals in describing the charge removal (and addition) energies and I show how it depends on the system size for 3D and 1D finite systems. I then focus on the description of the electronic structure of large 1D systems and describe a novel phenomenon (Section 3.3) in which the exchange interactions lead to spontaneous localization of quasiparticles, and charge removal (and possibly addition) energies become independent of the system length for very large systems. I further explore the description of the quasiparticles by many-body perturbation theory using the GW approximation. In this case, I have employed a newly developed stochastic formulation of the GW method. My work provides results of GW calculation for the largest polymers reported to date (Section 3.4).

3.1 Improved ground state electronic structure and optical dielectric constants with a semi-local exchange functional

A new generalized gradient approximation (GGA) functional (termed AK13) for exchange is employed to test its performance on representative set of solids. This GGA functional was constructed by Armiento and Kümmel (for references see Chapter 4) such that it provides a discontinuous jump in the corresponding exchange potential when an electron is added to the system investigated. This feature is consistent with the long sought derivative discontinuity (Section 2.2.1), which should be present in the (generally unknown) exact exchange-correlation functional.

In its original derivation of the AK13 functional, the discontinuous behavior of the potential is obtained as a constant potential shift depending on the energy of the highest occupied eigenstate and, while being fully within the Kohn-Sham approach of DFT, the AK13 exchange energy density functional exhibits features previously found only in orbital dependent functionals. For finite systems, its use was demonstrated to lead to physically correct exchange potentials and to yield eigenstate energies which approximate the quasiparticle energies well. For infinite periodic solids the same approach cannot be applied in a straightforward way due to the fact that the absolute energies of the eigenstates are not well defined (for further discussion of the meaning of Kohn-Sham eigenvalues in infinite periodic systems see Section 4.3). The work presented is mainly focused on the question how the functional describes the Kohn-Sham eigenstates in crystalline solids.

Three paradigm types of periodic solids which exhibit non-zero fundamental gap are studied: semiconductors, Mott insulators, and ionic crystals. First, the electronic band structure and band gaps are analyzed and compared with other computational and experimental results available. Further, the optical dielectric constants, which should be obtained exactly from DFT in principle, are calculated on different levels of theory (Section 4.5.2) and compared to experiment. Since the functional examined is of GGA type, it is compared to standard semi-local functionals. For illustration, the band structure and electronic density-of-states for α-Sn are shown in Figure 3.1.

For all systems investigated, the AK13 functional gives larger KS band gaps than a standard GGA, and for some AK13 even remedies a qualitative failure of standard semi-local functionals by opening the eigenvalue (Kohn-Sham) gap. The improved description of the individual KS eigenstates translates to an excellent agreement between the computed and experimental macroscopic dielectric constants. This suggests that the AK13 exchange functional can be used as an improved and inexpensive starting point for higher level DFT methods and especially beyond-DFT (GW) calculations.

This work has been published as:

Vojtěch Vlček, Gerd Steinle-Neumann, Linn Leppert, Rickard Armiento, Stephan Kümmel, *Improved Ground State Electronic Structure and Optical Dielectric Constants With a Semi-Local Exchange Functional*, Phys. Rev. B **91**, 035107 (2015).

I have performed all the calculations presented in the paper, designed the analysis of the results and performed it, and written the first draft of the paper.

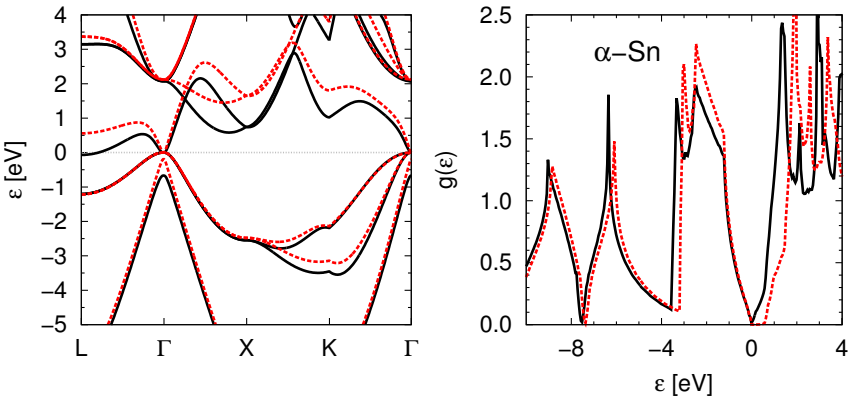

Figure 3.1: Bandstructure (left) and corresponding density-of-states (right) for crystalline α-Sn as obtained by calculations with the commonly used PBE generalized gradient approximation for exchange and correlation in black and the AK13 functional in the red dashed line. Band structures are shifted to have the Fermi energy at zero. While the PBE functional fails to predict the system as a small gap semiconductor (note the crossing of the Fermi level by a conduction band close to L critical point), the AK13 functional rectifies this deficiency.

3.2 Deviations from piecewise linearity in the solid-state limit with approximate density functionals

The piecewise linearity condition for the total energies (Section 2.2.2) is examined for periodic systems in the limit of their infinite size. For finite systems, the condition is defined unambiguously and can be calculated by adding or removing a fractional amount of charge from or to the system. Deviation from this condition indicates poor predictive capabilities for electronic structure, in particular of ionization potentials and fundamental band gaps. Moreover, the piecewise linearity of the total energies serves for a first-principles determination of the parameters of hybrid exchange-correlation functionals (introduced in the context of the generalized Kohn-Sham approach in Section 2.3.2). The significant deviation of standard (semi)local density functionals further leads to delocalization errors (cf. Section 2.2.2) which are connected to an inappropriate description of charge transfer. For infinite system, however, it is not straightforward to estimate this spurious behavior, as calculations with excess charge should be performed on the entire (infinite) system. Since the enhancement in the description of the electronic structure of finite systems translates to an improved prediction for periodic solids, as shown in Chapter 4, it stands to reason that deficiencies of the exchange-correlation functionals are present regardless of the system size.

As pointed out in Section 2.2.2, the curvature approaches vanishing values with increasing system. Such a behavior is observed even for functionals which yield poor predictions of electronic structure, and therefore cannot be used as a

diagnostic or constructive tool in solids. This indicates that the energy curvature is not a good measure of functional performance.

In our work, we consider two distinct examples of finite systems, namely nanocrystals and 1D molecular chains. In both cases, the systems studied are constructed from periodically repeated motives, either based on a unit-cell of a periodic crystal or the repeat unit in case of molecular chains. Within the system itself, the external (ionic) potential thus preserves translational periodicity, but the system considered is finite. We calculate the curvature upon charge removal and addition and find that if the excess charge delocalizes over the whole system, the energy curvature has distinctly different asymptotic behavior for 3D (nanocrystals) and quasi-1D (molecular chains) systems. Performing a detailed analysis of the expression for the curvature we connect it directly to the self-interaction term of the highest occupied state and demonstrate that the scaling behavior is consistent with electrostatic considerations. This behavior is illustrated in Figure 3.2.

For computations on periodic systems using large reference cell, we find that the energy curvature scales linearly with volume, i.e. with the number of unit cells constituting the reference cell. The rate of change of the energy curvature with volume of the reference cell is found to be a finite constant value for the approximate functional studied and to depend on the material itself. In addition, we demonstrate that if the excess charge associated with the curvature of charge removal or addition tends to delocalize over the entire system this rate of change of the curvature with system size should be zero for the exact exchange-correlation functional (as the curvature should vanish for any volume of the reference cell) and therefore may serve as a new useful measure of functional error in periodic solids.

For practical use, we show that the rate of change of the energy curvature can be obtained not only through computations with increasingly large periodic cells but preferably – and more efficiently – by considering changes in the band edge position with dense k-point sampling. Most importantly, we demonstrate that the difference between the scaling of the curvature in periodic and finite systems stems from the treatment of a compensating background charge inherently present in calculations with periodic boundary condition and that such the treatment removes part of the self-interaction.

This work has been published as:

Vojtěch Vlček, Helen R. Eisenberg, Gerd Steinle-Neumann, Leeor Kronik, Roi Baer, *Deviations from piecewise linearity in the solid-state limit with approximate density functionals*, J. Chem. Phys. **142**, 034107 (2015).

I have performed the calculations presented in the paper, worked on the theoretical developments shown and written the first draft of the paper jointly with Dr. Helen R. Eisenberg.

3.3 Spontaneous charge carrier localization in extended one-dimensional systems

In Section 3.2 (and in more detail in Chapter 5 we have shown that while the deviation from piecewise linearity can serve as a tool for determining the free parameters in the hybrid functionals, it will ultimately fail for very large and

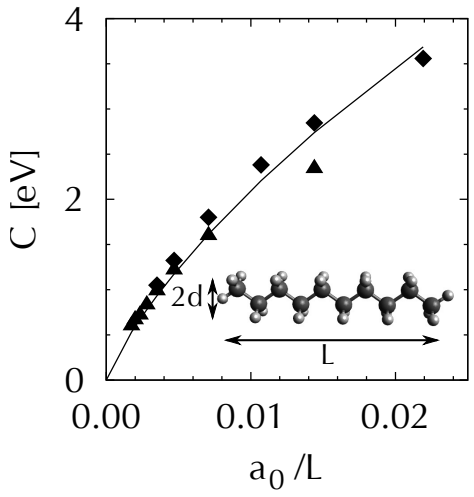

Figure 3.2: Deviation from piecewise linearity (i.e. energy curvature C) for charge removal from alkane chains of different length L and diameter d (indicated in the inset of the plot) is shown agains the inverse length of the molecule. The calculations were performed with localized bases cc-PVDZ and STO-3G shown by diamonds and triangles respectively. The black line represents an analytical expression based on self-interaction of homogeneous electron gas in a 1D system which is described in detail in Chapter 5.

infinite systems, since the hybrid functionals will collapse to their (semi)local form, which satisfies zero deviation. The solution proposed to this conundrum discussed in detail in Chapter 5 is based on the assumption that in a very large or infinite system, the excess charge (corresponding to quasiparticle, i.e. quasihole or quasielectron) would obey the symmetry of the underlying ionic lattice. In Chapter 6, however, we describe the possibility of a spontaneous charge carrier localization that would lead to energy curvature which remains finite even in the limit of infinite systems.

Here we exclude charge carrier localization in extended atomic systems due to disorder, point defects or distortions of the ionic lattice, since it is our goal to investigate the limiting behavior of an infinite periodic system. Hence we study only perfectly ordered structures constructed in a similar fashion as in Chapter 5: We consider 1D molecular chains of conjugated polymers (trans-polyacetylene and polythiophene illustrated in Figure 3.3) which we construct as completely planar and ideally periodic within the chain boundaries.

First we analyze the dependence of the ionization potentials estimated as the negative of the highest occupied eigenstate energy $-\varepsilon_H$, which is (in principle) exact in DFT (cf. Sections 2.2.1 and 2.2.2), and corresponds to the lowest energy of formation of a hole in the system. It has to be noted here that for the class of optimally tuned range-separated hybrid functionals, denoted as BNL*, such equivalence is enforced by tuning for the zero energy curvature condition (cf. Chapter 5). Our results clearly indicate that when the theory accounts for the presence of non-local exchange (either by using the BNL* functional or the Hartree-Fock method) the ionization potential converges to a constant value

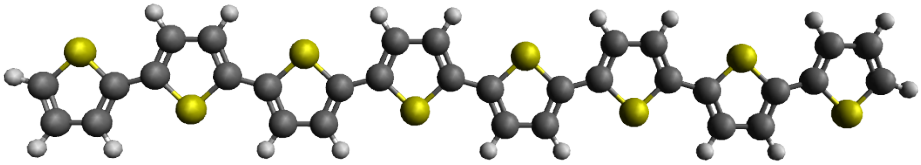

Figure 3.3: An example of a planar polythiophene molecule is shown with 4 repeat units (containing two thiophene rings each). Yellow, black and white spheres represent sulphur, carbon and hydrogen atoms, respectively.

which becomes independent of system size. Similar behavior is observed for other observables, namely optical absorption peaks and exciton binding energies estimated from TD DFT calculations. This energy stabilization occurs on length scales of several nanometers.

Further analysis of the DFT results reveal that the rapid stabilization of the ionization potential and its independence on the system length is associated with localization of the hole density. Based on the hole distribution along the backbone of the polymer, we calculate the hole characteristic size (for definition and procedure see Chapter 6), which shows two types of regimes illustrated in Figure 3.4: (i) for small systems, the strong quantum confinement dominates and the hole size increases linearly with system length; (ii) for large systems, the hole localizes and its size is independent of polymer length. We also present the connection between the hole localization and experimentally observed polaron formation in conjugated polymers.

In order to confirm that our results are not an artifact of the DFT calculations, i.e. that the phenomenon is observed even when the theoretical description does not rely on the mean field approximation, we perform additional computations using many body perturbation theory in the G_0W_0 approximation introduced in Section 2.4.3. Since the systems of interest are of significant size, we employ a stochastic GW approach recently developed by Neuhauser et al. (see Chapter 6 for reference and Chapter 7 for a detailed description of the method). This approach allows us to calculate the quasiparticle energies for all chains considered, representing thus the largest ever accomplished G_0W_0 computations for polymers, and confirm that the hole energies become independent of the length of the polymer in close agreement with the results obtained with BNL* functional.

This work has been accepted for publication:

Vojtěch Vlček, Helen R. Eisenberg, Gerd Steinle-Neumann, Daniel Neuhauser, Eran Rabani, Roi Baer, *Spontaneous charge carrier localization in extended one-dimensional systems*, Phys. Rev. Lett. (*in press*)

I have performed all the calculations presented in the manuscript, designed the analysis procedure and performed it, made the implementations necessary for the stochastic GW approach and written the first draft of the paper.

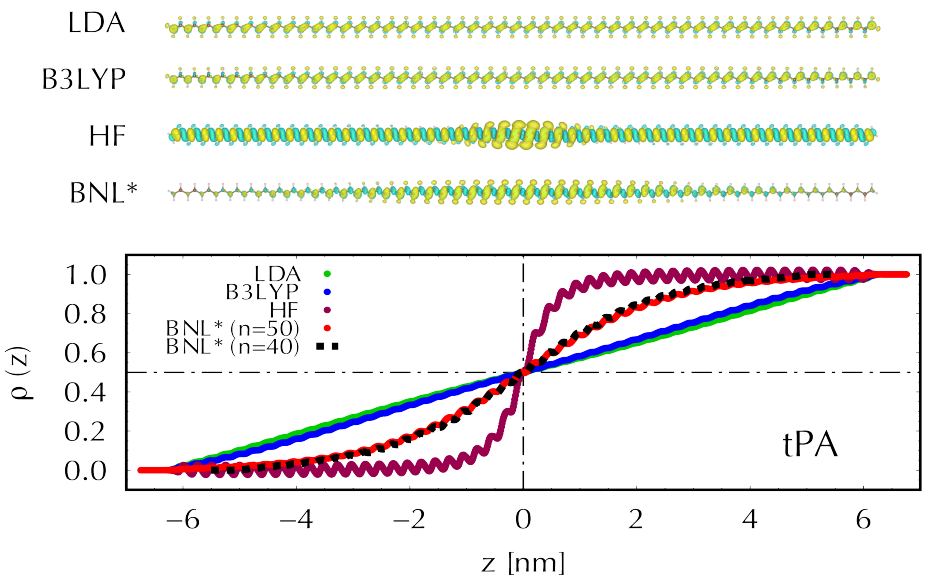

Figure 3.4: Difference in the densities of a neutral system and a cation of a trans-polyacetylene chain with 50 repeat units. Density differences are computed by Hartree-Fock and DFT calculations on various levels: LDA, B3LYP, and the optimally tuned range-separated hybrid functional BNL* (top panel). The isosurface plots present both positive (yellow) and negative (aqua) values due to the redistribution of the density upon ionization. While results obtained with LDA and B3LYP functionals lead to complete delocalization of the hole densities, BNL* and HF shown localization of the hole in the center of the polymer chain. HF results, however, suffer from spurious density fluctuations along the whole backbone of the polymer (for details see Chapter 6). The lower panel shows cumulative hole distribution ρ obtained by partial integration of the hole density along the polymer axis z. The distributions curves obtained for different methods are distinguished by colors in the graph. The narrow change of the integral value for in BNL* and HF results indicate the presence of a localized hole. For comparison a hole distribution obtained with BNL* for a shorter chain with 40 repeat units is shown by the black dashed line and indicates that the hole distribution no longer changes with increasing system size.

3.4 Stochastic GW calculations on large thiophene polymers

We investigate the phenomenon of spontaneous charge localization presented in Section 3.3 in more detail. For this, we directly aim at describing the ionization potentials, corresponding to the lowest quasihole energy, at the level of many-body perturbation theory within the GW approximation. As in Chapter 6, we rely on the use of the stochastic formulation of the GW approximation (see Chapter 6 and 7 for references and details), which allows us to calculate properties of systems with unprecedented sizes.

First, we present a more detailed derivation of the stochastic approach and describe the key ingredients of the formulation that improve the scaling of the algorithm with respect to system size. In this context, the algorithm described in Chapter 7 represents a modification of the original work of Neuhauser *et al.* as it provides quasiparticle correction (see Section 2.4.3 and Chapter 7) calculated directly for a given Kohn-Sham eigenstate obtained from the underlying DFT computations.

We then apply the stochastic GW approach to polythiophene polymer chains of increasing sizes and analyze the individual contributions to the quasiparticle shifts. We find that though we employ a "single shot" GW approach starting from Kohn-Sham DFT ground state calculation with the LDA functional, which does not exhibit localization of the quasihole (see Chapter 6), the predicted quasiparticle energies become independent of the length of the polymer chain (localization). We further analyze the individual contributions to the self-energy Σ, and find that the major part of the quasiparticle shift is supplied by the exchange part of Σ. While the magnitude of the polarization contribution remains almost constant, the exchange contribution decreases with increasing length of the polymer. For long chains of polythiophene, the ionization potential becomes independent of the systems size and this effect is driven by the exchange part of the self-energy. Our finding further supports the claims made in Section 3.3 and Chapter 6 and we moreover illustrate the strength of the GW approach.

We also investigate the possible localization in systems with higher dimensionality: We construct systems of three stacked planar polythiophene chains (see Chapter 7 for illustration) with interplanar distance typical for the condensed polythiophene phase. It has to be noted that in such systems there is a weak interaction among the individual chains which makes the system effectively two-dimensional. We again calculate the ionization potential for a set of stacked polymers using the stochastic GW method and reach extremely large systems containing up to 1446 valence electrons. By comparing the results for the single polymer chain and the polymer stacks of different length, we find that the higher dimensionality inhibits localization. By examining the individual contributions to Σ, we observe that while for the small systems, the behavior of the exchange and polarization parts for the stacked polymers is similar to that of the isolated chain, for large systems the exchange part of Σ for the stacks keeps decreasing with system length. The results are shown in Figure 3.5. Based on this observation, we conjecture that either: (i) The localization phenomenon is limited to 1D systems. (ii) Alternatively, the length scale of localization is much smaller in 1D systems and it increases with the dimensionality of the system.

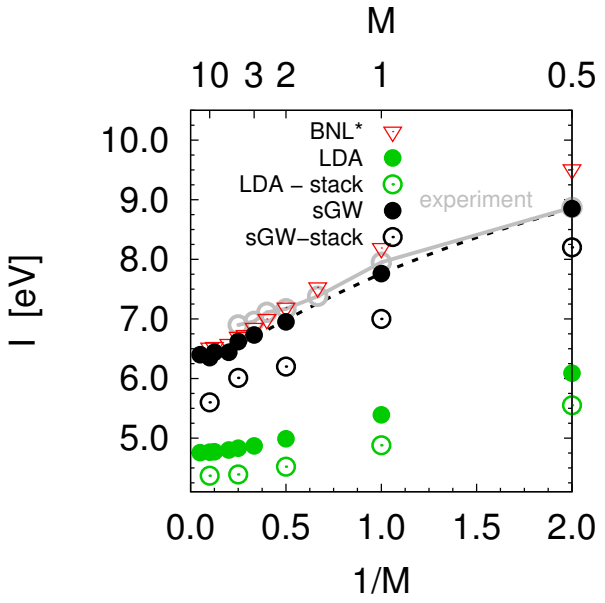

Figure 3.5: Ionization potentials I for polythiophene polymers of different sizes (given in the number of repeat units M - for details see Chapter 6 and Chapter 7). The filled green circles represent DFT calculations with the local density approximation, used as a starting point for "one-shot" GW computations shown in filled black circles. The calculations for three polythiophene molecules stacked on top of each other are shown in open green and black circles for LDA and GW results, respectively. The calculations with optimally tuned range-separated hybrid functional (BNL*) for an isolated polymer strand are shown in red triangles and experimental results for isolated molecules are presented for comparison. For single polymer chains, we observe that I becomes independent of system size when $M > 5.5$, while localization is not observed for the stacked system considered.

This work will be submitted for publication as:

Vojtěch Vlček, Eran Rabani, Daniel Neuhauser, Roi Baer, *Stochastic GW calculations on large thiophene polymers*, to be submitted to J. Chem. Theory Comput.

I have performed all the calculations presented in the manuscript, made all necessary implementations for the stochastic GW approach, and written the first draft of the paper.

Chapter 4

Improved Ground State Electronic Structure and Optical Dielectric Constants With a Semi-Local Exchange Functional

Vojtěch Vlček[1], Gerd Steinle-Neumann[1], Linn Leppert[2], Rickard Armiento[3], Stephan Kümmel[2]

4.1 Abstract

A recently published generalized gradient approximation functional within density functional theory (DFT) has shown, in a few paradigm tests, an improved KS orbital description over standard (semi-)local approximations. The characteristic feature of this functional is an enhancement factor that diverges like $s\ln(s)$ for large reduced density gradients s which leads to unusual properties. We explore the improved orbital description of this functional more thoroughly by computing the electronic band structure, band gaps, and the optical dielectric constants in semiconductors, Mott insulators, and ionic crystals. Compared to standard semi-local functionals, we observe improvement in both the band gaps and the optical dielectric constants. In particular, the results are similar to those obtained with orbital functionals or by perturbation theory methods in that it opens band gaps in systems described as metallic by standard (semi-)local density functionals, e.g., Ge, α-Sn, and CdO.

[1]Bayerisches Geoinstitut, Universität Bayreuth, 95440 Bayreuth, Germany
[2]Theoretische Physik IV, Universität Bayreuth, 95440 Bayreuth, Germany
[3]Department of Physics, Chemistry and Biology (IFM), Linköping University, 58183 Linköping, Sweden

4.2 Introduction

The Kohn-Sham (KS) [1] approach to density functional theory (DFT) [2] has become the standard tool for electronic structure computations in solid state physics and materials science. It owes its success to the generally favorable compromise between accuracy and computational efficiency offered by (semi-)local approximations to the exchange-correlation (xc) functional. However, (semi-)local approximations are far from flawless. In particular, for KS single particle states that are supposed to be very localized, (semi-)local functionals frequently give orbitals that are too delocalized and too high in energy. This shortcoming is a widely recognized problem, which is often discussed as a consequence of various aspects of the self-interaction error, arguably the major source of error in DFT calculations (see, e.g., Ref. [3] for an expanded discussion).

There is a large library of methods that aim for an improved description of localized states, and the development of new approaches is an active field of research. Higher-order or beyond DFT methods, such as hybrid functionals [4] (e.g., Ref. [5]), exact exchange with the optimized effective potential (xOEP) [6, 7] and the GW method [8] represent a viable solution, which however come at vastly increased computational expense. While the quality of the orbital description in KS-DFT is an inherently difficult topic, as the KS states do not directly represent electron quasiparticle states in the usual sense, a comparison with the above mentioned higher-order methods shows that the (semi-)local functionals tend to overdelocalize the KS orbitals in general. Other methods aiming at remedying this problem require non-fundamental species- and environment-dependent parameters (DFT+U),[9] or abandon the variational KS-DFT framework, e.g., model potentials such as the Becke-Johnson potential [10] and its modifications, e.g., by Tran and Blaha (TB-mBJ) [11] or others. [12] However, some of us recently developed a standard semi-local generalized gradient approximation (GGA) functional that improves the KS orbital description, while it still remains fully within the KS-DFT framework, the Armiento-Kümmel functional (AK13) [13]. Unfortunately, this functional comes with its own tradeoff: a lower accuracy of the total energy, clearly demonstrated in the supplementary material of Ref. [13] and further commented on by Ref. [14]. It is nevertheless encouraging that it is *at all possible* for a semi-local functional to make a significant qualitative improvement of the orbital description compared to results of other (semi-)local functionals. The purpose of the present paper is to more closely investigate the nature of this improvement in the context of crystalline solids.

From both the pragmatic and the fundamental perspective it is highly desirable to have xc functionals which qualitatively capture the important physics of a system. As discussed above, one such aspect is the improved localization of the KS orbitals seen with higher-order methods. Physical properties calculated from properly localized KS orbitals often compare favorably with experimental results (independently of how one justifies this practice, cf. Sections 4.3 and 4.8). In this work we study the Kohn-Sham band structure and optical dielectric constants for a variety of solids, including Mott insulators, semiconductors and insulators. Our focus is not to examine the accuracy with which the various methods reproduce experimental results, but rather, the extent to which the AK13 functional shares the qualitative overall improvement of higher-order methods over standard (semi-)local functionals. As explained, such improve-

ments can be expected to bring the results of properties derived from the KS orbitals closer to the experimental values.

The rest of the paper is organized as follows: Section 4.3 gives a more in-depth discussion of the interpretation of the KS orbitals and the KS band gap; in Section 4.4 we summarize the essentials of the construction of the AK13 functional; Section 4.5 covers the computational details of our study; in Sections 4.6 and 4.7 we present and discuss the results for band gaps and optical dielectric constants, respectively; Section 4.8 provides an outlook and a summary of the results obtained here.

4.3 KS orbitals and the KS band gap: relation to Physical Properties

A self-consistent KS calculation gives as its results a total ground state energy E and a set of eigenvalues $\{\varepsilon_i\}$. The energy E is the central observable of ground-state DFT, and there is no doubt about its physical meaning. Contrary to E, it is not guaranteed that the $\{\varepsilon_i\}$ have a well defined physical meaning; even for the exact xc functional only the highest occupied one[15] can be interpreted as the first ionization potential I. In early DFT the eigenvalues were thus denied any meaning at all [16]. However, experience has shown that the KS band-structure, i.e., the $\{\varepsilon_i\}$ obtained in periodic-boundary condition calculations for crystals, is extremely useful for practical purposes [17, 18], despite the absolute energy of the eigenvalues and the KS potential already have an unknown absolute energy offset relative to the vacuum level and we are thus restricted only to the eigenvalue differences (see also footnote [1]). By now it has been firmly established that relative energies of *occupied* KS eigenstates can accurately approximate ionization potentials I [19], and, e.g., photoemission experiments have even confirmed the physical interpretability of orbitals themselves [20–22].

The situation is very different for the *unoccupied* eigenvalues, which cannot be associated with electron affinities A or inverse photoemission spectra energies. This is even true for the exact xc functional, due to the derivative discontinuity Δ_{xc} [23]. Because of Δ_{xc}, the relative energies between the occupied and unoccupied KS orbitals are incorrect. As a result of this the KS gap, defined as the energy difference between the lowest unoccupied (ε_L) and highest occupied (ε_H) KS eigenvalue $E_g^{\mathrm{KS}} = \varepsilon_L - \varepsilon_H$, is in general not equal to the fundamental gap [24–27], defined as $E_g = I - A$. The two gaps differ by Δ_{xc}, i.e.,

$$E_g = E_g^{\mathrm{KS}} + \Delta_{\mathrm{xc}}. \tag{4.1}$$

Despite the fact that E_g^{KS} does not represent the fundamental gap E_g, KS eigenvalues are a very important result of electronic structure calculations for at least three reasons:

(i) Regardless of the fact that the E_g^{KS} from (semi-)local functionals typically underestimates the experimental gap noticeably, experience for periodic systems

[1] In the context of periodic solids, it is only meaningful to look at the relative energies of the KS orbitals as their absolute values cannot be related to the vacuum level. This should be clear from the observation that the work function of a real solid depends on the surface, and thus, the absolute levels are affected by regions not included in the infinite periodic model.

shows that the shape and general features of KS bands are often physically meaningful and have pragmatically been used with great success [18, 28, 29].

(ii) For finite systems, E_g^{KS} represents the energy of an excitation which can be described (approximately) as an electron and hole being close to each other [30], and, as such, it cannot be interpreted as a good approximation for E_g. A better interpretation of KS eigenvalue differences is as a zero order approximation of excitation energies [31, 32].

(iii) The KS band structure often serves as an input for calculating the quasiparticle bandstructure in the GW approximation [8, 33, 34]. It has also been argued that the xc potential can be interpreted as the best local approximation to the self-energy in Dyson's equation [35].

As outlined in the Introduction (Section 4.2), independent of the question of interpretation of the eigenvalues, xOEP tends to improve the similarity of the KS band structure with that from higher-order and quasiparticle theory.[34, 36–39] Also, hybrid functionals which include (some) generalized KS exact exchange improve band-structure prediction [40]. The magnitude of self-interaction errors [41, 42] and the question of whether the KS or the generalized KS scheme is used [43] are both important for the interpretability of eigenvalues. The considerable improvement from full or partial exact exchange or self-interaction corrections, however, comes at the high computational price of having to evaluate many exchange- or Coulomb-integrals. The recently developed AK13 functional spurs hopes that these deficiencies can be mitigated at the computational cost of a standard (semi-)local functional.

4.4 Semi-local DFT with an improved orbital description

The AK13 is an exchange-only density functional, which was inspired by the exchange potential derived by Becke and Johnson [10], $v_x^{\mathrm{BJ}}(\mathbf{r})$. It can be expressed in terms of the charge density $n(\mathbf{r})$ and its KS *potential* for atoms approximates that of xOEP. By requiring the exchange potential to have the same asymptotic properties as $v_x^{\mathrm{BJ}}(\mathbf{r})$, one can derive [13] the following restriction on a corresponding GGA exchange energy functional:

$$E_x = A_x \int n(\mathbf{r}) F(s) \mathrm{d}\mathbf{r} \tag{4.2}$$

with

$$F(s) \to cs \ln(s) \quad \text{for} \quad s \to \infty, \tag{4.3}$$

where $A_x = -(3/4)(3/\pi)^{1/3}$ in Hartree atomic units. $F(s)$ is the enhancement factor, c a numerical constant, and s the reduced density gradient

$$s = \frac{|\nabla n(\mathbf{r})|}{2\left(3\pi^2\right)^{1/3} n(\mathbf{r})}. \tag{4.4}$$

The AK13 functional implements this requirement and a few other restrictions by the following expression for the enhancement factor

$$F(s) = 1 + B_1 s \ln\left(1+s\right) + \left(\mu_{\mathrm{GE}} - B_1\right) s \ln\left[1 + \ln\left(1+s\right)\right], \tag{4.5}$$

where $\mu_{\mathrm{GE}} = 10/81$, and $B_1 = 3/5\mu_{\mathrm{GE}} + 8\pi/15$ is a constant which determines the strength of the discontinuity of the potential. All the constants in the above expression were obtained from theoretical considerations for the exchange potential outside of a finite system and semi-infinite surfaces, i.e., Eq. (4.5) contains no empirical parameter.

The AK13 exchange functional is a KS-DFT functional of GGA form, i.e., it is semi-local in $n(\mathbf{r})$, and thus allows computations at a cost similar to other (semi-)local functionals. However, it was argued in Ref. [13] that any functional whose KS potential takes a non-zero asymptote outside a finite system requires some care in the definition of the zero of energy in the KS system. Specifically, to interpret the potential and KS eigenvalues in the ways discussed in Section 4.3, they must first be shifted with precisely the constant value that aligns the potential asymptote to zero, c_{shift}. However, this shift can be disregarded for infinite crystalline solids for two reasons:

(i) As discussed in the preceding section, there is no absolute zero of the potential associated with the vacuum level in infinite periodic solids.

(ii) As the extent of the system is infinite, the exchange potential does not asymptotically approach any constant value that could be associated with c_{shift}.

One of the quantities considered in the present work is the fundamental band gap. According to Eq. (4.1) this is the KS gap plus the contribution from the derivative discontinuity Δ_{xc}. Standard (semi-)local xc functionals have no derivative discontinuity, $\Delta_{\mathrm{xc}} = 0$, while one can show that the AK13 potential for finite systems jumps discontinuously when the ensemble-averaged particle number in DFT [23] is changed across an integer [13]. This feature is traditionally closely associated with the derivative discontinuity since the shift of the potential should be equal to Δ_{xc}. The shift of the AK13 potential comes entirely from c_{shift}, which changes discontinuously when a new orbital is occupied. This property of AK13 suggests a strong advantage over other (semi-)local functionals in this respect. In Ref. [13] there is an explicit formula for the potential shift,

$$c^i_{\mathrm{shift}} \to -\frac{A_x^2 Q_x^2}{2}\left(1 \pm \sqrt{1 - \frac{4\epsilon_i}{A_x^2 Q_x^2}}\right) \tag{4.6}$$

and the derivative discontinuity takes the form of

$$\Delta_{\mathrm{xc}} = c^{H+1}_{\mathrm{shift}} - c^{H}_{\mathrm{shift}}, \tag{4.7}$$

where the eigenvalues are counted in i, H is the index of the highest occupied eigenvalue, and $Q_x = (\sqrt{2}/(3(3\pi^2)^{1/3}))B_1$. Unfortunately, this formula requires knowledge of the correct absolute (unshifted) KS eigenvalues of the calculation. As explained above, these are not available in a computation of a crystalline solid.

Ongoing work is aimed at resolving the problem of calculating the potential shift for AK13 in periodic systems, and of realizing the AK13 idea of a non-vanishing asymptotic constant in a different way. However, in this paper we focus on the orbital improvement and band gap obtained for the AK13 KS orbitals themselves. Hence, we follow a frequent practice used for band structure calculations using xOEP and hybrid functionals: we make no attempt to further widen the gap with Δ_{xc}, even though it is clear that this contribution exists. One should also note that it has been suggested that in Δ_{xc} the exchange

and correlation parts may have a tendency to cancel in a way that makes this contribution small for certain classes of systems [3, 37].

4.5 Computational Details

4.5.1 Electronic Structure Calculations

We perform band structure calculations for crystalline solids using KS-DFT in the projector augmented wave (PAW) formalism [44] as implemented in the Vienna Ab-initio Simulation Package (VASP) [45–48]. We have implemented the AK13 functional in this code and compute the electronic structure both with this functional and with the widely used generalized-gradient approximation by Perdew, Burke and Ernzerhof (PBE) [49]. The cutoff energy for the plane wave expansion and the k-point meshes are chosen to converge the total energy and the eigenvalues of the occupied bands to 1 meV (obtained self-consistently for both PBE and AK13). The experimental lattice constants and other computational parameters are given in the appendix (Table 4.3). Spin polarization is only taken into account for NiO, where both PBE and AK13 predict antiferromagnetic order.

Where possible, we compare the KS band gap from our calculations to results from xOEP and the TB-mBJ potential [11] from the literature. The latter is a modification of $v_x^{\mathrm{BJ}}(\mathbf{r})$ with the aim to better reproduce experimental gaps.

4.5.2 Optical Dielectric Constants

We also investigate how the AK13 functional affects the optical dielectric constant. We first evaluate the independent-particle polarizability χ^0, following the approach by Baroni and Resta [50] and Gajdoš *et al.* [51]. χ^0 can be written as [52, 53]

$$\chi^0_{\mathbf{G},\mathbf{G}'}(\mathbf{q},\omega) = \lim_{\eta\to 0}\frac{2}{\Omega}\sum_{i,j,\mathbf{k}} w_{\mathbf{k}}\frac{f(\varepsilon_{i,\mathbf{k}+\mathbf{q}}) - f(\varepsilon_{j,\mathbf{k}})}{\varepsilon_{i,\mathbf{k}+\mathbf{q}} - \varepsilon_{j,\mathbf{k}} - \omega + i\eta} \times \langle\psi_{i,\mathbf{k}+\mathbf{q}}| e^{i(\mathbf{G}+\mathbf{q})\cdot\mathbf{r}} |\psi_{j,\mathbf{k}}\rangle \langle\psi_{j,\mathbf{k}}| e^{-i(\mathbf{G}'+\mathbf{q})\cdot\mathbf{r}'} |\psi_{i,\mathbf{k}+\mathbf{q}}\rangle . \quad (4.8)$$

$\chi^0_{\mathbf{G},\mathbf{G}'}$ for given reciprocal lattice vectors $\mathbf{G}$ and $\mathbf{G}'$, depends on the wave-vector $\mathbf{q}$ and the frequency ω. For simplicity we drop the spin dependence of the KS single particle eigenstates and eigenenergies, $\psi_{j,\mathbf{k}}$ and $\varepsilon_{j,\mathbf{k}}$. With the Fermi occupation function $f(\varepsilon_{j,\mathbf{k}})$ varying between 0 and 1, the spin degeneracy is accounted for by the prefactor $2/\Omega$, where Ω denotes the unit-cell volume. A small parameter η is present in order to shift the poles of the function in the complex plane away from the real axis. In Eq. (4.8) the summation goes over all single particle states i, j and over all k-points with weighting factor $w_{\mathbf{k}}$.

The dielectric matrix can be expressed in terms of the independent-particle polarizability [50, 54] as

$$\epsilon_{\mathbf{G},\mathbf{G}'}(\mathbf{q},\omega) = 1 - \frac{\nu_{\mathbf{G},\mathbf{G}'}(\mathbf{q})\,\chi^0_{\mathbf{G},\mathbf{G}'}(\mathbf{q},\omega)}{1 - \sum_{G''}\chi^0_{\mathbf{G},\mathbf{G}''}(\mathbf{q},\omega)\,f^{\mathrm{xc}}_{\mathbf{G}'',\mathbf{G}'}}, \quad (4.9)$$

where f^{xc} is the xc kernel

$$f^{\mathrm{xc}}_{\mathbf{G}'',\mathbf{G}'} = \frac{\delta^2 E_{\mathrm{xc}}}{\delta n_{\mathbf{G}''} \delta n_{\mathbf{G}'}} \tag{4.10}$$

and ν is the Coulomb kernel:

$$\nu_{\mathbf{G},\mathbf{G}'}(\mathbf{q}) = \frac{4\pi}{|\mathbf{G}+\mathbf{q}| \cdot |\mathbf{G}'+\mathbf{q}|}. \tag{4.11}$$

The macroscopic dielectric matrix $\epsilon_{\mathrm{mac}}(\omega)$ is calculated as the long wavelength limit ($q \to 0$) of the inverse dielectric matrix [50, 51], i.e.,

$$\epsilon_{\mathrm{mac}}(\omega) = \left(\lim_{q \to 0} \epsilon^{-1}_{0,0}(\mathbf{q}, \omega) \right)^{-1}. \tag{4.12}$$

Here we consider three levels of approximation to ϵ_{mac}. On the most rigorous level we combine Eqs. (4.9) and (4.12), denoted hereafter as $\epsilon^{\mathrm{DFT}}_{\mathrm{mac}}$. This constant is exact in principle within KS-DFT, i.e., it depends only on the approximations made in solving the KS equations.

If the influence of the xc kernel in Eq. (4.9) is neglected (by setting $f^{\mathrm{xc}} = 0$) we obtain the dielectric constant in the random phase approximation (RPA) [55, 56], $\epsilon^{\mathrm{RPA}}_{\mathrm{mac}}$. Furthermore, if we neglect the local field (NLF), corresponding to the off-diagonal elements of $\epsilon^{-1}_{\mathbf{G},\mathbf{G}'}(\mathbf{q}, \omega)$, we obtain a dielectric constant

$$\epsilon^{\mathrm{NLF}}_{\mathrm{mac}} = \lim_{\omega \to 0} \epsilon_{0,0}(\omega). \tag{4.13}$$

In practice, one can avoid the sum over unoccupied KS single particle states on all three levels of theory (DFT, RPA and NLF). This is achieved by employing density functional perturbation theory to evaluate the first order correction to the wave function with respect to the wave vector $\mathbf{q}$ in Eq. (4.8). For more details we refer to Refs. [50] and [51].

4.6 Band Structures and Gaps

4.6.1 Results

Table 4.1 shows the KS band gaps E^{KS}_g calculated with PBE and AK13 functionals, and previously published values for the xOEP functional and the TB-mBJ potential at experimental lattice constants (Table 4.3). We here regard PBE as representative of all standard (semi-)local functionals, since the differences in orbital description on unrelaxed structures are usually small. For all systems the AK13 functional gives a considerably larger E^{KS}_g than the PBE functional, bringing it towards better agreement with xOEP, TB-mBJ, and the experimental value.

Note that Ge, α-Sn and CdO are predicted as metallic by PBE, whereas xOEP, TB-mBJ and AK13 all open band gaps. For these systems the band structure and the electronic density of states are shown in Figure 4.1. For Ge, the PBE functional predicts a vanishingly small gap, whereas AK13 opens a significant band gap (0.6 eV). Similarly, PBE predicts α-Sn to be a metal, with bands crossing at the zone center and close to the Brillouin zone boundary near

	PBE	AK13	TB-mBJ	xOEP	Exp
C (diamond)	4.1	4.8	4.9 [11]	5.4 [37]	5.5 [57]
Si	0.6	1.6	1.0 [58] – 1.2 [11]	1.4 [59]	1.1 [60]
SiC	1.4	2.2	2.3 [11]	2.5 [37]	2.4 [61]
α-Sn	-0.1	0.0			0.1 [62]
Ge	0.0	0.6	0.7 [58]	1.0 [37]	0.7 [63]
GaAs	0.5	1.4	1.6 [64]	1.5 [59]	1.4 [65]
MgO	4.7	6.6	7.2 [11] – 8.3 [58]	7.8 [66]	7.8 [67]
NaCl	5.1	9.8			9.0 [68]
CaF_2	7.3	9.8			11.8 [69]
ZnO	0.8	2.0	2.7 [70] – 3.4 [58]		3.4 [71]
CdO	-0.4	0.7	1.8 [72]		2.3 [73]
NiO	0.7	1.4	4.2 [11]	4.1 [38]	4.0 [74] – 4.2 [75]

Table 4.1: KS band gaps from the current calculations (PBE and AK13) in comparison to band gaps computed with the Tran-Blaha modified-Becke Johnson potential (TB-mBJ), exact KS exchange (xOEP), and experiments (Exp). References are given in the brackets.

the high symmetry point L. The AK13 functional changes the dispersion of the unoccupied bands significantly, including a shift of the valence pocket near L to a conduction band, and describes the system as a semiconductor with zero band gap. For CdO the AK13 functional opens an indirect gap $\mathrm{L} \to \Gamma$. Opening of the gap can be seen in the density of states $\mathrm{g}(\varepsilon)$ as well (Figure 4.1).

To investigate the possible influence of a correlation functional we also calculated band gaps using the AK13 exchange functional and the correlation functional of the local density approximation (LDA) for a few solids. The difference to band gaps using no correlation were minor, at the order of $0.1 - 0.2$ eV and similar relative shifts between the computations with and without LDA correlation were observed for eigenvalues of occupied and unoccupied bands close to the Fermi level.

4.6.2 Discussion

For the band gaps (Table 4.1), there is a qualitative difference between xOEP, TB-mBJ, and experimental values, on the one hand, and PBE, on the other hand. This observation corroborates a picture of something missing from standard (semi-)local functionals. From the computed band gaps and the band structure in Figure 4.1 it should be clear that the AK13 functional gives a distinctly different orbital description from PBE in the systems studied, with a band structure closer to what is provided by xOEP, for example. If the difference stems from the orbital description of PBE being inaccurate due to overdelocalization, it appears that AK13 has, at least partly, addressed this deficiency. A natural consequence of mitigating the overdelocalization is the contraction in the bandwidth which can be seen in the band structures (Figure 4.1, Table 4.4) and is even more pronounced in the density of states. The issue of describing localized states in semi-local DFT was outlined in the introduction and discussed in more detail in Ref. [13]. It is worth noting that band-width contraction was previously also noted in the KS band structures obtained with the TB-mBJ potential

[58].

One may at this point ask if not the better agreement with experimental results of the also arguably semi-local KS *potential* of TB-mBJ makes AK13 superfluous. With respect to this question we make four observations:

(i) One of the primary strengths of DFT is its rigorous theoretical framework that underpins every calculation. The BJ model potential is a construct that directly models the KS potential. It is an ingenious potential construction, but as such, its corresponding energy functional is not merely unknown, it does not exist [76, 77], and this deficiency cannot easily be corrected [78]. Since the KS equations are derived from variational calculus of an energy equation that involves the energy xc functional, the use of BJ-type potentials has a very weak formal theoretical basis.

(ii) As mentioned above, the TB-mBJ exchange potential *has been fitted to experimental band gap values*, whereas AK13 was constructed without any empirical parameters.

(iii) There should be a positive contribution from Δ_{xc} to the gap (Eq. 4.1), therefore Kohn-Sham gaps that underestimate experimental gaps are consistent with the general theoretical expectation.

(iv) As seen from our results for AK13 exchange with LDA correlation, the correlation functional generally has a smaller impact on the band structure than exchange, but it is not completely irrelevant. The fitting done in the construction of TB-mBJ includes LDA correlation, whereas AK13 was developed to only model exchange, and so far there is no correlation functional constructed to match the features of AK13.

The more general question about the value of a KS functional that yields qualitatively improved KS gaps will be taken up again in Section 4.8 – in light of the fundamental difference between E_g and E_g^{KS}.

4.7 Optical dielectric constants

4.7.1 Results

Our computed optical dielectric constants are shown in Table 4.2. For most of the systems, there are significant but not overly clear differences in the results. If we neglect the results for Ge and NiO (discussed below), the average difference between PBE and experimental values is ca. +16% which is similar to what has previously been reported for LDA [51]. For AK13 the average difference is instead negative and of significantly reduced magnitude, ca. −4%. In the first-order approximation, one may consider the optical dielectric constant to be inversely proportional to the KS band gap, this results for AK13 can thus be regarded as a consequence of opening the E_g^{KS}. Nevertheless, as indicated in Section 4.5.2, the density functional perturbation theory is used and the actual result depends on the band structure of the system.

If we focus on the small band gap systems, the differences are clearer. For Ge, the PBE functional gives optical dielectric constants that are several orders of magnitude higher than the experimental value (ca 10^3). For NiO the values differ roughly by a factor of two. There are also less striking, but still major differences for α-Sn and CdO.

We find that at all levels of theory ($\epsilon_{\mathrm{mac}}^{\mathrm{NLF}}$, $\epsilon_{\mathrm{mac}}^{\mathrm{RPA}}$ and $\epsilon_{\mathrm{mac}}^{\mathrm{DFT}}$) AK13 generally

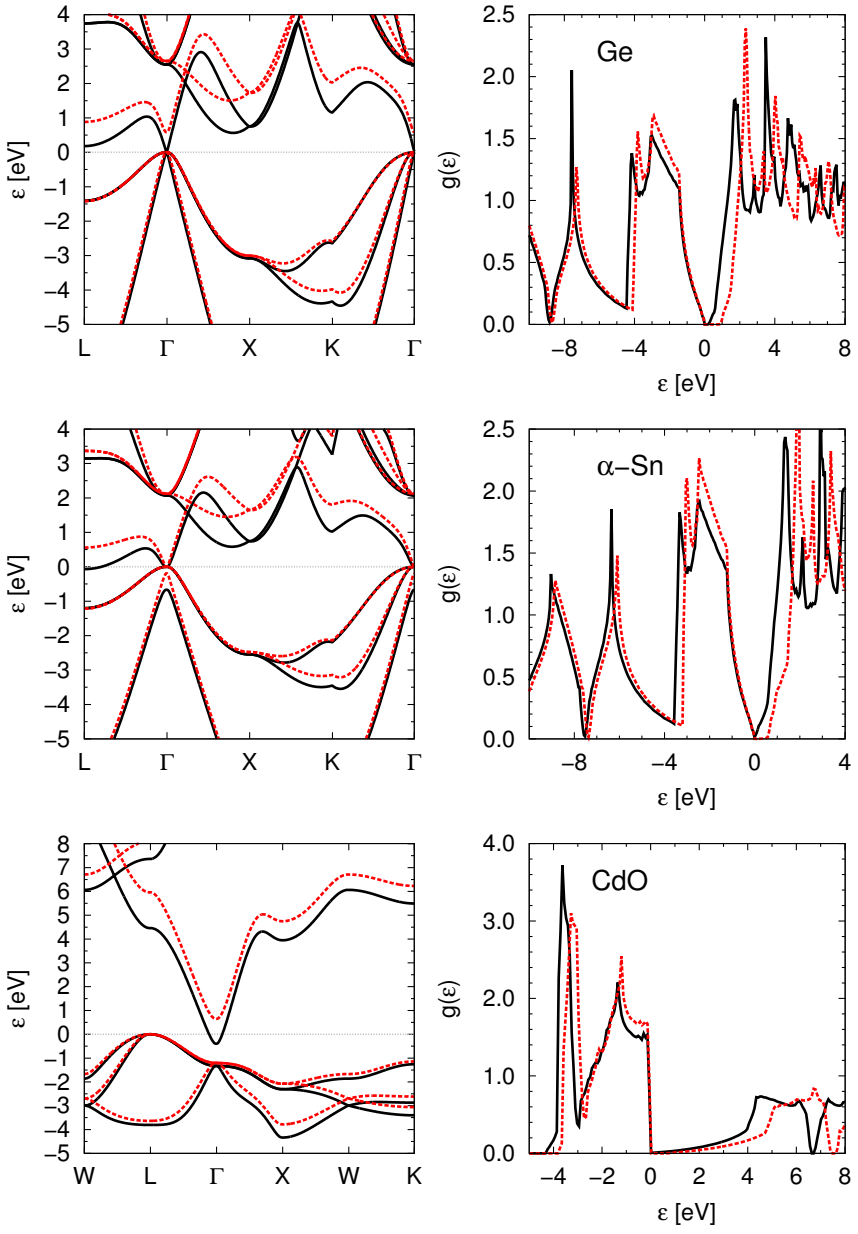

Figure 4.1: Bandstructure (left) and the density of states (right) for Ge (top), α-Sn (middle) and CdO (bottom). PBE results are shown with a solid black line, dashed red lines represent the AK13 results. The Fermi energy is chosen as the zero of energy, and is also indicated by the horizontal gray dotted line for the band structure.

	$\epsilon_{\text{mac}}^{\text{NLF}}$		$\epsilon_{\text{mac}}^{\text{RPA}}$		$\epsilon_{\text{mac}}^{\text{DFT}}$		
	PBE	AK13	PBE	AK13	PBE	AK13	Exp
C (diamond)	6.0	5.6	5.5	5.2	5.8	5.8	5.7 [57]
Si	13.5	9.8	12.1	8.7	12.9	10.1	11.9 [57]
SiC	7.2	6.2	6.6	5.6	7.0	6.4	6.5 [57]
α-Sn	28.9	21.3	26.8	19.8	28.2	22.5	24 [79, 80]
Ge	$\sim 10^3$	14.7	$\sim 10^3$	13.4	$\sim 10^3$	15.6	15.8 [81]
GaAs	14.4	9.7	13.1	8.7	13.9	10.2	10.9 [82]
MgO	3.2	2.6	3.0	2.4	3.2	2.8	3.0 [83]
NaCl	2.8	2.1	2.3	1.7	2.5	2.1	2.3 [84]
CaF_2	2.4	2.0	2.3	1.9	2.3	2.1	2.0 [85]
ZnO	5.1	3.6	4.8	3.4	5.0	3.7	3.7 [86]
CdO	7.2	4.9	6.9	4.7	7.1	5.1	5.3 [87]
NiO	22.0	10.3	21.7	10.1	23.1	11.4	5.7 [88]

Table 4.2: The macroscopic dielectric constant computed for PBE and AK13 functionals at the three different levels of approximation discussed in Section 4.4.2. The different approximations are denoted by their respective abbreviations given in the superscripts: NLF (neglect of local fields), RPA (random phase approximation) and DFT (calculated on the DFT level). References for the experimental results are provided in the brackets.

gives a lower value of the optical dielectric constant than PBE. At the RPA level, both functionals give the lowest values, and when accounting for the xc kernel, i.e., at the DFT level, the dielectric constant increases. While a detailed numerical comparison between the various methods and experiments is not the focus of our work, we note that going from the RPA to DFT level (i.e., taking into account the xc kernel) shifts the dielectric constant of PBE further away from the experimental value, while the AK13 results are brought closer towards the experimental data. The same behavior as seen here for PBE has been reported previously for LDA [50].

To investigate the influence of correlation on the dielectric constants, we performed calculations for a few solids using AK13 exchange and LDA correlation. Correlation changes the values, but not to an extent important for the conclusions of this work. In our tests, correlation has the strongest influence on the dielectric constants of α-Sn, leading to a decrease in the value by 10% for all levels of approximation.

4.7.2 Discussion

As explained in Sections 4.2 and 4.3, in systems where standard (semi-)local functionals give an overdelocalized orbital description, we expect properly localized KS orbitals to give dielectric constants in better qualitative agreement with experimental results due to their increased similarity to the true quasiparticle electron states. Hence, our central argument is that the fact that AK13 functional moves the dielectric constant distinctly towards the experimental result compared to PBE is a clear indicator of an improved orbital description.

The differences between PBE and AK13 in dielectric constants (Table 4.2) for large gap systems are not major, so we focus in the following on the systems

for which PBE predicts a metallic state or a very small band gap: Ge, α-Sn and CdO.

The large value of the dielectric constant of Ge with PBE is directly related to the zero or vanishingly small direct gap: In the limit of $\mathbf{q} \to 0$ and $\omega \to 0$, the fraction in the sum in Eq. (4.8) can simply be viewed as a derivative of the occupation function with respect to the KS eigenstate energy at given wavevector $\mathbf{k}$, $\partial f\left(\varepsilon_{i,\mathbf{k}}\right)/\partial\varepsilon_{i,\mathbf{k}}$. In the case of Ge (see Figure 4.1), the PBE valence and conduction band are very close to each other at Γ, providing a vanishing band gap, which gives a very large contribution to ϵ_{mac}. Opening the gap by using the AK13 functional thus reduces the values of the optical dielectric constants at all levels of theory and leads to results comparable to experiments.

For the other two solids of interest, α-Sn and CdO, the values of ϵ_{mac} do not indicate a similar behavior. In the case of CdO this can be explained by the fact that the conduction band has its minimum at a $\mathbf{k}$ vector different from the wave vector of the highest occupied KS eigenstate (Figure 4.1); there is thus no zero or vanishingly small direct gap.

For α-Sn both the PBE and AK13 functional provide a vanishing direct gap at Γ. The divergence in the derivative of the occupation function is balanced by other terms in Eqs. (4.8) and (4.9), however. Applying the AK13 functional reduces the value of ϵ_{mac} relative to the PBE results and brings its value closer to the experimental data.

From Eq. (4.9) we see that the contribution of the xc functional both enters via the KS orbital shapes used in Eq. (4.8), and more directly via the xc kernel f^{xc}. Nevertheless, the difference between AK13 and PBE remains roughly equal across all level of theory $\epsilon_{\mathrm{mac}}^{\mathrm{NLF}}$, $\epsilon_{\mathrm{mac}}^{\mathrm{RPA}}$, and $\epsilon_{\mathrm{mac}}^{\mathrm{DFT}}$. Since the xc kernel is only present on the DFT level of theory, the primary difference between PBE and AK13 dielectric constants cannot only come from this term; rather, the differences originate from qualitative differences in the KS orbitals (cf. Figure 4.1 for α-Sn).

4.8 Outlook and Summary

It is a worthwhile task to consider the results that we have obtained with the AK13 functional here in the context of the derivation of the AK13 functional as reviewed in Section 4.4, and the fundamental theorems of DFT that we reviewed in Sections 7.2 and 4.3. While AK13 yields clear improvements, there are steps in its derivation that are non-unique. Therefore, one could hope to further improve the results by extending and modifying the AK13 approach. Three lines of further development and possible modification appear naturally.

First, the AK13 functional is for exchange only. A compatible correlation functional can change the gaps. While previous experience [37] and our results using LDA correlation indicate that typical (semi-)local correlation functionals change gaps by about 0.1 eV, i.e., quite moderately, correlation corrections can be larger in general. Specifically, one would expect that they affect so-called strongly correlated systems such as NiO, where indeed the AK13 exchange functional shows the largest deviation of all solids considered here.

Second, even without introducing correlation the AK13 functional itself could be changed. The derivation of the AK13 approach [13] was guided by

conditions inferred from the asymptotic behavior of the exchange potential of finite systems. Instead, one could try to optimize the AK13 functional for solids, e.g. by fitting to experimental band gaps in the spirit of the TB-mBJ potential. Third, and in a somewhat similar vein, one could also try to obtain improved energetics together with physical eigenvalues by changing the enhancement factor in Eq. (4.5), e.g., via changing B_1.

In this work we deliberately pursue neither of these options. One of our reasons is that using the parameters that are present in the AK13 approach as *fit parameters* would lead away from the first principles character of the AK13 concept. More important yet is another reason: Fitting the parameters in AK13 such that its KS gaps match experimental band gaps would ignore that the fundamental gap in KS DFT is built from the KS gap *and* Δ_{xc} (Eq. 4.1). Therefore, there is no fundamental reason to expect that such fitting would lead to a functional with transferable accuracy for unoccupied eigenvalues and band gaps. Indeed, it is a reoccurring experience that reliable eigenvalues and binding energies are not easily obtained from one and the same functional [89–91].

While we therefore argue that trying to obtain *quantitatively* accurate predictions for experimental gaps from KS gaps is futile, we also argue that it is nevertheless very important to have functionals that predict the electronic density of states in a *qualitatively* correct way. A hallmark problem of standard (semi-)local functionals is that they do not properly capture localization effects. As a consequence, the ordering of the KS orbitals can be wrong, leading to a qualitatively wrong KS gap and other qualitative failures, e.g., grossly misleading predictions for charge transfer [92, 93]. On the other hand, when the Slater determinant comprised of KS orbitals captures the physics of the true many-body wavefunction in a qualitatively correct way, then reliable understanding and insight can already be gained from the KS states. This has been demonstrated impressively, e.g., by photoemission experiments [20–22]. We have shown here that the AK13 functional can remedy some of the worst qualitative failures of typical (semi-)local functionals. This is an important step forward for two reasons. The first is a conceptual one and *within DFT*: The KS band gap is an important contribution to the true gap, and even the exact Δ_{xc} contribution will not yield correct results when added to a qualitatively wrong KS gap. The second goes *beyond DFT*: Today, results from DFT methods are not only valuable in and of themselves, but are also important as input to higher order methods such as the GW approach. The accuracy of such methods, specifically GW, for systems with a complex electronic structure can depend sensitively on the DFT input [34, 94–96]. A functional such as AK13 that remedies the worst failures already on the DFT level may serve as a better starting point than standard (semi-)local functionals.

In summary, we have compared KS band gaps and optical dielectric constants obtained with AK13 to results from established DFT approaches (PBE, xOEP, TB-mBJ) and experiments. The AK13 functional gives larger KS band gaps than a standard GGA and brings a *qualitative* improvement in computed macroscopic dielectric constants for some systems. In particular, for Ge, CdO and α-Sn the AK13 functional opens a band gap and thus remedies a qualitative failure of the standard (semi-)local functionals. As such, the AK13 bandstructure may serve as an improved and inexpensive starting point for higher level DFT methods [97] or beyond-DFT (GW) calculations.

4.9 Acknowledgments

Computations were performed at the Leibniz Supercomputing Centre of the Bavarian Academy of Sciences and the Humanities. This work was supported by the Deutsche Forschungsgemeinschaft (DFG) under contract STE1105/8-1 (GSN) and SFB840 project B1 (SK). RA acknowledges financial support from the Swedish Research Council (VR) Grant No. 621-2011-4249 and the Linnaeus Environment at Linköping on Nanoscale Functional Materials (LiLi-NFM) funded by VR.

4.10 Appendix

In Table 4.3 the computational parameters for the electronic structure calculations are summarized.

In Table 4.4 we present widths of the conduction and first valence band calculated with the PBE and AK13 functionals, together with results from experiments and computations using TB-mBJ [58], where available. This follows the discussion in Ref. [58] where the localization of electronic bands (band dispersion) is considered. With the exception of Ge all the calculations show smaller band widths than the experiments. PBE yields the largest band dispersion, while the AK13 and TB-mBJ results have similar widths.

	a_0	k-points	E^C
C (diamond)	3.567 [98]	22×22×22	1800
Si	5.431 [99]	22×22×22	1200
SiC	4.358 [100]	22×22×22	1600
α-Sn	6.490 [101]	22×22×22	1400
Ge	5.657 [98]	22×22×22	1400
GaAs	5.654 [98]	22×22×22	1000
MgO	4.213 [102]	22×22×22	1600
NaCl	5.653 [103]	24×24×24	1200
CaF_2	5.463 [104]	24×24×24	1400
ZnO	3.234, 5.177 [105]	22×22×16	1100
CdO	4.696 [106]	24×24×24	1100
NiO	4.183 [107]	12×12×12	1200

Table 4.3: Computational parameters used in the current calculations. The experimental lattice constants in Å (with the appropriate references given as square brackets) are provided together with the k-point meshes and energy cut-off energies for the planewave expansion E^C in eV used here. The lattice constants are given for the conventional unit cells. Note that for ZnO the first value represents the length of the a- and b-axes and the latter value is for the c-axis. It is important to mention that the k-point mesh for NiO is given for the supercell used to generate the antiferromagnetic order. For the calculation of the dielectric constants for ZnO a smaller E^C (1000 eV) and a coarser k-point mesh (16×16×16) is used.

	PBE		AK13		TB-mBJ		Exp.
	V	C_1	V	C_1	V	C_1	V
C (diamond)	21.5	6.1	21.6	6.4			23.0 [108]
Si	12.0	3.4	11.6	3.2	11.7	3.5	12.5 [109]
SiC	8.5	5.8	8.1	5.4			
α-Sn	10.7	3.2	10.4	3.5			
Ge	12.8	3.9	12.5	3.9	12.3	4.1	12.6 [109]
GaAs	6.8	3.9	6.5	3.4			
MgO	4.6	6.8	4.0	6.8	3.7	6.1	4.8 [110]
NaCl	1.9	3.9	1.2	2.5			
CaF_2	2.7	2.1	2.1	0.3			
ZnO	6.2	7.0	5.9	6.8	5.4	6.6	9.0 [111]
CdO	4.3	7.0	3.8	6.8			
NiO	7.6	1.2	7.0	0.6			

Table 4.4: Valence band widths (V) and first conduction band width (C_1) from the current calculations using the PBE and AK13 functionals in eV. TB-mBJ and experimental values are taken from the literature where available. References are provided in the brackets for each experimental value and the TB-mBJ results are from Ref. [58].

Bibliography

[1] W. Kohn and L. J. Sham, Phys. Rev. **140**, A1133 (1965).

[2] P. Hohenberg and W. Kohn, Phys. Rev. **136**, 864 (1964).

[3] S. Kümmel and L. Kronik, Rev. Mod. Phys. **80**, 3 (2008).

[4] A. D. Becke, The Journal of Chemical Physics **98**, 5648 (1993).

[5] J. Heyd, G. Scuseria, and M. Ernzerhof, The Journal of Chemical Physics **118**, 8207 (2003).

[6] R. T. Sharp and G. K. Horton, Phys. Rev. **90**, 317 (1953).

[7] J. D. Talman and W. F. Shadwick, Phys. Rev. A **14**, 36 (1976).

[8] L. Hedin, Phys. Rev. **139**, A796 (1965).

[9] V. I. Anisimov, F. Aryasetiawan, and A. I. Lichtenstein, J. Phys.: Condens. Matt. **9**, 767 (1997).

[10] A. D. Becke and E. R. Johnson, J. Chem. Phys. **124**, 221101 (2006).

[11] F. Tran and P. Blaha, Phys. Rev. Lett. **102**, 226401 (2009).

[12] E. Räsänen, S. Pittalis, and C. R. Proetto, J. Chem. Phys. **132**, 044112 (2010).

[13] R. Armiento and S. Kümmel, Phys. Rev. Lett. **111**, 036402 (2013).

[14] T. F. T. Cerqueira, M. J. T. Oliveira, and M. A. L. Marques, J. Chem. Theory Comput. **10**, 5625 (2014).

[15] C.-O. Almbladh and U. von Barth, Phys. Rev. B **31**, 3231 (1985).

[16] R. G. Parr and W. Yang, *Density Functional Theory of Atoms and Molecules* (Oxford Science Publications, Oxford, 1989).

[17] O. Gunnarsson and K. Schönhammer, Phys. Rev. Lett. **56**, 1968 (1986).

[18] Z. H. Levine and D. C. Allan, Phys. Rev. Lett. **63**, 1719 (1989).

[19] D. P. Chong, O. V. Gritsenko, and E. J. Baerends, J. Chem. Phys. **116**, 1760 (2002).

[20] P. Puschnig, S. Berkebile, A. J. Fleming, G. Koller, K. Emtsev, T. Seyller, J. D. Riley, C. Ambrosch-Draxl, F. P. Netzer, and M. G. Ramsey, Science **326**, 702 (2009).

[21] M. Dauth, T. Körzdörfer, S. Kümmel, J. Ziroff, M. Wiessner, A. Schöll, F. Reinert, M. Arita, and K. Shimada, Phys. Rev. Lett. **107**, 193002 (2011).

[22] D. Lüftner, T. Ules, E.-M. Reinisch, G. Koller, S. Soubatch, F. S. Tautz, M. G. Ramsey, and P. Puschnig, Proc. Natl. Acad. Sci. **111**, 605 (2014).

[23] J. P. Perdew, R. G. Parr, M. Levy, and J. L. Balduz, Phys. Rev. Lett. **49**, 1691 (1982).

[24] J. P. Perdew and M. Levy, Phys. Rev. Lett. **51**, 1884 (1983).

[25] L. J. Sham and M. Schlüter, Phys. Rev. Lett. **51**, 1888 (1983).

[26] R. W. Godby, M. Schlüter, and L. J. Sham, Phys. Rev. Lett. **56**, 2415 (1986).

[27] L. Kronik, T. Stein, S. Rafaely-Abramson, and R. Baer, J. Chem. Theory Comput. **8**, 1515 (2012).

[28] M. S. Hybertsen and S. G. Louie, Phys. Rev. B **34**, 5390 (1986).

[29] X. Zhu and S. G. Louie, Phys. Rev. B **43**, 14142 (1991).

[30] E. J. Baerends, O. V. Gritsenko, and R. van Meer, Phys. Chem. Chem. Phys. **15**, 16408 (2013).

[31] A. Görling, Phys. Rev. A **54**, 3912 (1996).

[32] C. Filippi, C. J. Umrigar, and X. Gonze, J. Chem. Phys. **107**, 9994 (1997).

[33] G. Onida, L. Reining, and A. Rubio, Rev. Mod. Phys. **74**, 601 (2002).

[34] P. Rinke, A. Qteish, J. Neugebauer, C. Freysoldt, and M. Scheffler, New J. Phys. **7**, 126 (2005).

[35] P. Duffy, D. P. Chong, M. E. Casida, and D. R. Salahub, Phys. Rev. A **50**, 4707 (1994).

[36] M. Städele, J. A. Majewski, P. Vogl, and A. Görling, Phys. Rev. Lett. **79**, 2089 (1997).

[37] M. Städele, M. Moukara, J. A. Majewski, P. Vogl, and A. Görling, Phys. Rev. B **59**, 10031 (1999).

[38] E. Engel and R. N. Schmid, Phys. Rev. Lett **103**, 036404 (2009).

[39] M. Betzinger, C. Friedrich, A. Görling, and S. Blügel, Phys. Rev. B **85**, 245124 (2012).

[40] T. M. Henderson, J. Paier, and G. E. Scuseria, Phys. Status Solidi B **248**, 767 (2011).

[41] J. P. Perdew and A. Zunger, Phys. Rev. B **23**, 5048 (1981).

[42] T. Körzdörfer, S. Kümmel, N. Marom, and L. Kronik, Phys. Rev. B **79**, 201205(R) (2009).

[43] T. Körzdörfer and S. Kümmel, Phys. Rev. B **82**, 155206 (2010).

[44] D. Vanderbilt, Phys. Rev. B **41**, 7892 (1990).

[45] G. Kresse and J. Furthmüller, Phys. Rev. B **54**, 11169 (1996).

[46] G. Kresse and J. Furthmüller, Comput. Mat. Sci. **6**, 15 (1996).

[47] G. Kresse and J. Hafner, Phys. Rev. B **49**, 14251 (1994).

[48] G. Kresse and J. Hafner, Phys. Rev. B **47**, 558 (1993).

[49] J. P. Perdew, K. Burke, and M. Ernzerhof, Phys. Rev. Lett. **77**, 3865 (1996).

[50] S. Baroni and R. Resta, Phys. Rev. B **33**, 7017 (1986).

[51] M. Gajdoš, K. Hummer, G. Kresse, J. Furthmüller, and F. Bechstedt, Phys. Rev. B **73**, 045112 (2006).

[52] S. L. Adler, Phys. Rev. **126**, 413 (1962).

[53] N. Wiser, Phys. Rev. **129**, 62 (1963).

[54] P. E. Van Camp, V. E. Van Doren, and J. T. Devreese, Phys. Rev. B **24**, 1096 (1981).

[55] H. Ehrenreich and M. H. Cohen, Phys. Rev. **115**, 786 (1959).

[56] P. Nozières and D. Pines, Phys. Rev. **109**, 762 (1958).

[57] P. Y. Yu and M. Cardona, *Fundamentals of Semiconductions* (Springer-Verlag, Berlin, 2001).

[58] D. Waroquiers, A. Lherbier, A. Miglio, M. Stankovski, S. Poncé, M. J. T. Oliveira, M. Giantomassi, G. M. Rignanese, and X. Gonze, Phys. Rev. B **87**, 075121 (2013).

[59] A. Fleszar, Phys. Rev. B **64**, 245204 (2001).

[60] R. S. Muller and R. I. Kamins, *Device Electronics for Integrated Circuits* (Wiley, New York, 1986), 2nd ed.

[61] R. G. Humphreys, D. Bimberg, and W. J. Choyke, Solid State Commun. **39**, 163 (1981).

[62] A. W. Ewald and E. E. Kohnke, Phys. Rev. **97**, 607 (1955).

[63] O. Madelung, ed., *Semiconductors: Intrinsic Properties of Group IV Elements and III-V, II-VI, and I-VII compounds*, vol. 22a (Springer, Berlin, 1985).

[64] H. Jiang, J. Chem. Phys. **138**, 134115 (2013).

[65] J. L. Shay, Phys. Rev. B **2**, 803 (1970).

[66] T. Kotani, Phys. Rev. B **50**, 14816 (1994).

[67] R. C. Whited, C. J. Flatten, and W. C. Walker, Solid State Commun. **13**, 1903 (1973).

[68] D. M. Roessler and W. C. Walker, Phys. Rev. **166**, 599 (1968).

[69] T. Tsujibayashi, K. Toyoda, S. Sakuragi, M. Kamada, and M. Itoh, App. Phys. Lett. **80**, 2883 (2002).

[70] D. Koller, F. Tran, and P. Blaha, Phys. Rev. B **83**, 195134 (2011).

[71] D. C. Reynolds, D. C. Look, B. Jogai, C. W. Litton, G. Cantwell, and W. C. Harsch, Phys. Rev. B **60**, 2340 (1999).

[72] H. Dixit, R. Saniz, S. Cottenier, D. Lamoen, and B. Partoens, J. Phys.: Condens. Matter **24**, 205503 (2012).

[73] F. P. Koffyberg, Phys. Rev. B **13**, 4470 (1976).

[74] S. Hüfner, Adv. Phys. **43**, 183 (1994).

[75] S. L. Dudarev, G. A. Botton, S. Y. Savrasov, C. J. Humphreys, and A. P. Sutton, Phys. Rev. B **57**, 1505 (1998).

[76] A. Karolewski, R. Armiento, and S. Kümmel, J. Chem. Theory Comput. **5**, 712 (2009).

[77] A. P. Gaiduk and V. N. Staroverov, The Journal of Chemical Physics **131**, 044107 (2009).

[78] A. Karolewski, R. Armiento, and S. Kümmel, Phys. Rev. A **88**, 052519 (2013).

[79] C. F. Lavine and A. W. Ewald, J. Phys. Chem. Solids **32**, 1121 (1971).

[80] R. E. Lindquist and A. W. Ewald, Phys. Rev. **135**, A191 (1964).

[81] R. F. Potter, *Handbook of Optical Constants of Solids* (Academic, New York, 1985).

[82] K. G. Hambleton, C. Hilsum, and B. R. Holeman, Proc. Phys. Soc. (UK) **77**, 1147 (1961).

[83] A. E. Huges and B. Henderson, *Point defects in solids* (Plenum Press, New York, 1972).

[84] J. R. Hardy and A. M. Karo, Phys. Rev. B **26**, 3327 (1982).

[85] T. Passerat de Silans, I. Maurin, P. Chaves de Souza Sugundo, S. Saltiel, M. P. Gorza, M. Ducloy, D. Bloch, D. de Sousa Meneses, and P. Echegut, J. Phys.: Condens. Matter **21**, 255902 (2009).

[86] H. Yoshikawa and A. Sadao, Jpn. J. Appl. Phys. **36**, 6237 (1997).

[87] H. Finkenrath, H. Köhler, and M. Lochmann, Z. Angew. Phys **21**, 512 (1966).

[88] W. Reichardt, V. Wagner, and W. Kress, Journal of Physics C: Solid State Phys. **8**, 3955 (1975).

[89] E. Johnson, private communication (2014).

[90] P. Verma and R. J. Bartlett, J. Chem. Phys. **140**, 18A534 (2014).

[91] T. Schmidt, E. Kraisler, A. Makmal, L. Kronik, and S. Kümmel, J. Chem. Phys. **140**, 18A510 (2014).

[92] S.-H. Ke, H. U. Baranger, and W. Yang, J. Chem. Phys. **126**, 201102 (2007).

[93] D. Hofmann and S. Kümmel, Phys. Rev. B **86**, 201109(R) (2012).

[94] N. Marom, X. Ren, J. E. Moussa, J. R. Chelikowsky, and L. Kronik, Phys. Rev. B **84**, 195143 (2011).

[95] T. Körzdörfer and N. Marom, Phys. Rev. B **86**, 041110 (2012).

[96] V. Atalla, M. Yoon, F. Caruso, P. Rinke, and M. Scheffler, Phys. Rev. B **88**, 165122 (2013).

[97] J. Klimeš and G. Kresse, J. Chem. Phys. **140**, 054516 (2014).

[98] R. W. G. Wyckoff, *Crystal Structures* (New York, Interscience Publishers, 1963), 2nd ed.

[99] D. Toebbens, N. Stuesser, K. Knorr, H. Mayer, and G. Lampert, J. Appl. Phys. **45**, 1456 (1974).

[100] Z. Li and C. Bradt, J. Mat. Sci. **21**, 4366 (1986).

[101] J. Thewlis and A. Davey, Nature **174**, 1011 (1954).

[102] J. Zhang, Phys. Chem. Min. **27**, 145 (2000).

[103] D. Walker, P. K. Verma, L. M. D. Cranswick, R. L. Jones, S. M. Clark, and S. Buhre, Am. Min. **89**, 204 (2004).

[104] S. Speziale and T. S. Duffy, Phys. Chem. Min. **29**, 465 (2002).

[105] H. Sowa and H. Ahsbahs, J. Appl. Cryst. **39**, 169 (2006).

[106] J. Zhang, Phys. Chem. Min. **26**, 644 (1999).

[107] A. Leineweber, H. Jacobs, and S. Hull, Inorg. Chem. **40**, 5818 (2001).

[108] I. Jiménez, L. J. Terminello, D. G. J. Sutherland, J. A. Carlisle, E. L. Shirley, and F. J. Himpsel, Phys. Rev. B **56**, 7215 (1997).

[109] K. H. Hellwege and A. M. Hellwege, eds., *Landolt-Börnstein, Zahlenwerte und Funktionen aus Naturwissenschaften und Technik* (Springer Verlag, New York, 1983).

[110] L. H. Tjeng, A. R. Vos, and G. A. Sawatzky, Surf. Sci. **235**, 269 (1990).

[111] U. Özgür, Y. I. Alivov, C. Liu, A. Teke, M. A. Reshchikov, S. Doan, V. Avrutin, S.-J. Cho, and H. Morkoc, J. Appl. Phys. **98**, 041301 (2005).

Chapter 5

Deviations from piecewise linearity in the solid-state limit with approximate density functionals

Vojtěch Vlček[1,2,3], Helen R. Eisenberg[2,3], Gerd Steinle-Neumann[1], Leeor Kronik[4], Roi Baer[2]

5.1 Abstract

In exact density functional theory (DFT) the total ground-state energy is a series of linear segments between integer electron points, a condition known as "piecewise linearity". Deviation from this condition is indicative of poor predictive capabilities for electronic structure, in particular of ionization energies, fundamental gaps, and charge transfer. In this article, we take a new look at the deviation from linearity (i.e., curvature) in the solid-state limit by considering two different ways of approaching it: a large finite system of increasing size and a crystal represented by an increasingly large reference cell with periodic boundary conditions. We show that the curvature approaches vanishing values in both limits, even for functionals which yield poor predictions of electronic structure, and therefore can not be used as a diagnostic or constructive tool in solids. We find that the approach towards zero curvature is different in each of the two limits, owing to the presence of a compensating background charge in the periodic case. Based on these findings, we present a new criterion for functional construction and evaluation, derived from the size-dependence of the curvature, along with a practical method for evaluating this criterion. For

[1]Bayerisches Geoinstitut, Universität Bayreuth, D-95440 Bayreuth, Germany
[2]Fritz Haber Center for Molecular Dynamics, Institute of Chemistry, The Hebrew University of Jerusalem, Jerusalem 91904, Israel
[3]These two authors contributed equally to this work.
[4]Department of Materials and Interfaces, Weizmann Institute of Science, Rehovoth 76100, Israel

large finite systems we further show that the curvature is dominated by the self-interaction of the highest occupied eigenstate. These findings are illustrated by computational studies of various solids, semiconductor nanocrystals, and long alkane chains.

5.2 Introduction

Kohn-Sham (KS) density functional theory (DFT) [1, 2] is a widely used first-principles approach to the many-electron problem. It is based on mapping the system of N interacting electrons into a unique non-interacting system with the same ground state electron density [3, 4]. In the non-interacting system the density is determined by $n(\mathbf{r}) = \sum_i f_i |\psi_i(\mathbf{r})|^2$ where $\psi_i(\mathbf{r})$ $(i = 1, 2, ...)$ are normalized single particle eigenstates and f_i are the corresponding occupation numbers. The eigenstates are determined from the KS equations

$$\hat{H}\psi_i = \varepsilon_i \psi_i, \tag{5.1}$$

where ε_i are the (monotonically increasing) KS eigenvalues (see footnote [1]) and

$$\hat{H} = -\frac{1}{2}\nabla^2 + v_H(\mathbf{r}) + v_{XC}(\mathbf{r}) + v_{ext}(\mathbf{r}) \tag{5.2}$$

is the KS Hamiltonian (atomic units are used throughout). In Eq. (5.2), $v_H(\mathbf{r})$ is the Hartree potential, $v_{XC}(\mathbf{r})$ the exchange-correlation (XC) potential and $v_{ext}(\mathbf{r})$ is the external potential operating on the electrons in the interacting system. While DFT in general, and the KS equation in particular, are exact in principle, the XC potential functional is always approximated in practice and thus defines the level of theory applied.

The exact XC energy functional, $E_{XC}[n]$, from which the XC potential is derived via the relation $v_{XC}(\mathbf{r}) = \delta E_{XC}[n]/\delta n(\mathbf{r})$, is known to satisfy a number of constraints (e.g., Ref. [5]). One constraint, on which we focus here, is the *piecewise-linearity* property [6]. Perdew *et al.* [6] have argued that the ensemble ground-state energy $E(N)$ as a function of electron number, N where $N_0 - 1 \leq N \leq N_0$, must be a series of linear segments between the integer electron points N_0. Within the KS formalism this requirement translates directly into a condition on the XC energy functional, $E_{XC}[n]$.

An important manifestation of piecewise-linearity is the relation between the highest occupied eigenvalue, ε_H, and the ionization potential, $I(N_0) \equiv E(N_0 - 1) - E(N_0)$. These considerations have been originally developed for finite systems; infinite systems are discussed in detail below. For the exact functional, piecewise-linearity dictates that $I = -dE/dN$. In addition, Janak's theorem [7] states that for any (exact or approximate) XC functional, the highest occupied eigenvalue obeys

$$\varepsilon_H = \frac{dE_{KS}}{df_H}, \tag{5.3}$$

where E_{KS} is the KS estimate for the energy of the interacting system. For any change in electron number N, the same change occurs in f_H, the occupation

[1] For spin unpolarized (polarized) KS systems the value of the occupation number f_i is equal to 2 (1) if $\varepsilon_i < \varepsilon_H$, equal to 0 if $\varepsilon_i > \varepsilon_H$ and $0 \leq f_i \leq 2\,(1)$ if $\varepsilon_i = \varepsilon_H$, where ε_H, the highest occupied eigenvalue, is determined such that $\sum_i f_i$ is equal to the total number of electrons $N = \int n(\mathbf{r})\, d^3r$. The lowest eigenvalue for which $f_i = 0$ is referred to as ε_L.

number of the highest occupied eigenstate of the non-interacting system. Thus we find the result $I = -\varepsilon_H$ for a KS theory which uses the exact XC functional (i.e. for which $E_{KS} = E$). This exact condition, known as the *ionization potential theorem*, [6, 8–10] can be conveniently restated in terms of the energy curvature, C, defined as the second derivative of the total energy functional with respect to the fractional electron number,

$$C = \frac{d^2E}{dN^2} = \frac{d^2E_{KS}}{df_H^2} = \frac{d\varepsilon_H}{df_H}, \tag{5.4}$$

where Janak's theorem has been used in the third equality. Fulfillment of piecewise-linearity implies that $C = 0$, i.e. that the curvature is zero.

Despite the importance of piecewise-linearity, it has long been known that standard application of commonly used functional classes, such as the local density approximation (LDA), the generalized gradient approximation (GGA), or conventional hybrid functionals with a fixed fraction of Fock exchange (e.g. Ref. [11]), grossly disobeys this condition. In practice, a substantial, non-zero curvature is observed. The $E_{KS}(f_H)$ curve is typically strongly convex (see, e.g. Refs. [12–21]) and, correspondingly, $-\varepsilon_H$ can underestimate I by as much as a factor of two [22, 23].

The lack of piecewise-linearity in approximate functionals further affects the prediction of the fundamental gap, E_g, defined as the difference between the minimum energy needed for electron removal and the maximum energy gained by electron addition. Even with the exact functional, the KS eigenvalue gap, $\varepsilon_L - \varepsilon_H$ (where ε_L is the energy of the lowest unoccupied eigenstate), need not equal E_g [24, 25]. Instead,

$$E_g = \varepsilon_L - \varepsilon_H + \Delta_{XC}, \tag{5.5}$$

where Δ_{XC} is the derivative discontinuity [6, 21, 26–28] - a spatially-constant "jump" in the XC potential as the integer number of particles is crossed. This discontinuity is itself a consequence of piecewise linearity: The discontinuous change of slope in the energy as a function of electron number must also be reflected in the energy computed from the KS system. Some of it is contained in the kinetic energy of the non-interacting electrons, but the rest must come from a discontinuity in the XC potential [6]. Note that within the generalized KS (GKS) scheme (see footnote [2]) part of the discontinuity in the energy may also arise from a non-multiplicative (e.g., Fock) operator [29–31]. Therefore the derivative discontinuity in the XC potential may be mitigated and in some cases even eliminated [31–34].

For any approximate (G)KS scheme, E_g can be expressed as [35]

$$E_g = \varepsilon_L - \varepsilon_H + \frac{1}{2}\left(C^{hole} + C^{elec}\right) + \Delta_{XC}, \tag{5.6}$$

where C^{hole} and C^{elec} are the curvatures associated with electron removal and addition, respectively. The curvatures act as "doppelgänger" for the missing derivative discontinuity. Whereas in the exact functional all curvatures are zero and the difference between E_g and the eigenvalue gap is given solely by Δ_{XC}, for

[2] where the interacting-electron system is mapped into a partially interacting electron gas that is still represented by a single Slater determinant [29].

standard approximate (semi-)local (LDA and GGA) or hybrid functionals, employed in the absence of ensemble corrections, Δ_{XC} is zero and the addition of the average curvature compensates quantitatively for the missing derivative discontinuity term [35]. In the most general case, both a remaining curvature and a remaining derivative discontinuity will contribute to the difference between E_g and $\varepsilon_L - \varepsilon_H$.

For small finite systems, the criterion of piecewise linearity (i.e., zero curvature) has been employed to markedly improve the connection between eigenvalues and ionization potentials or fundamental gaps, and often also additional properties, in at least four distinct ways: (i) In the imposition of various corrections on existing underlying exchange-correlation functionals [35–40]; (ii) In first-principles ensemble generalization of existing functional forms [41, 42]; (iii) In the construction and evaluation of novel exchange-correlation functionals [43, 44]; And (iv) in non-empirical tuning of parameters within hybrid functionals [45, 46], especially range-separated ones [33, 34, 47, 48].

Unfortunately, this remarkable success of the piecewise-linearity criterion does not easily transfer to large systems possessing delocalized orbitals. For example, for a LDA treatment of hydrogen-passivated silicon nanocrystals (NCs), the fundamental gap computed from total energy differences approaches the KS eigenvalue gap with increasing NC size [49, 50]. The same conclusion was drawn from GGA studies of electron and hole addition to an increasingly large periodic cell of ZnO [51]. As mentioned above, for LDA $\Delta_{XC} = 0$. Taken together with Eq. (5.6), this implies that as system size grows the average curvature becomes vanishingly small and piecewise linearity is approached [15]. Despite this, the ionization potential obtained this way does not agree with experiment [52].

This limitation is intimately related to the vanishing ensemble correction to the band gap of periodic solids [42] and even to the failure of time-dependent DFT for extended systems [53, 54]. This is a disappointing state of affairs, because the zero curvature condition that has been used so successfully for small finite systems, both diagnostically and constructively, appears to be of little value for extended systems, even though the problem it is supposed to diagnose is still there.

In this article, we take a fresh look at this problem, by considering the evolution of curvature with system size. We approach the bulk limit in two different ways: (i) Calculations for an increasingly large but finite system (namely nanocrystals and molecular chains). (ii) Calculations for a crystal represented by an increasingly large reference cell with periodic boundary conditions. We show that in both cases the curvature approaches zero. However, it doesn't do so in the same fashion, due to the presence of a compensating background charge in the periodic system. Based on these findings, we present a new criterion for functional construction and an assessment derived from the size-dependence of the curvature, along with a practical method for evaluating this criterion. We further show that the curvature for large finite systems is dominated by the self-interaction of the highest occupied eigenstate. These findings are illustrated by computational studies of semiconductor NCs and long alkane chains.

5.3 Energy curvature in large finite systems

5.3.1 General considerations

We first examine finite systems, in which, as noted above, curvature effects have been already studied extensively. As a first step in our general theoretical considerations, we express the curvature of a finite system as the rate of change in the energy of the highest-occupied KS-eigenstate as an electronic charge q is removed or added (see footnote [3]) to the system:

$$C = \frac{d\varepsilon_H}{dq} = \left\langle \psi_H \left| \frac{d\hat{H}}{df_H} \right| \psi_H \right\rangle . \tag{5.7}$$

The first equality is a restatement of Eq. (5.4), combined with the fact that the removed (added) charge is taken from (inserted into) the highest occupied eigenstate ψ_H, (see footnote [4]) while the second is due to the Hellmann-Feynman theorem [55, 56]. As the derivative in Eq. (5.7) is applied only to the terms of the Hamiltonian $\hat{H}$ that are functionals of the density, $n(\mathbf{r})$, we can write the curvature as [57]:

$$C = \int n_H(\mathbf{r}) \int \left[\frac{1}{|\mathbf{r}-\mathbf{r}'|} + f_{XC}(\mathbf{r},\mathbf{r}') \right] \frac{dn(\mathbf{r}')}{df_H} d^3r' \mathrm{d}^3r, \tag{5.8}$$

where $f_{XC}(\mathbf{r},\mathbf{r}') = \delta^2 E_{XC}[n]/\delta n(\mathbf{r})\delta n(\mathbf{r}')$ is the exchange-correlation kernel and $n_i(\mathbf{r}) \equiv |\psi_i(\mathbf{r})|^2$ is the density of the i^{th} KS eigenstate. Using the fact that the electron density is given by $n(\mathbf{r}) = \sum_i f_i n_i(\mathbf{r})$, it follows that

$$\frac{dn(\mathbf{r})}{df_H} = n_H(\mathbf{r}) + n_{relax}(\mathbf{r}), \tag{5.9}$$

where the first term on the right hand side is the density of the highest occupied KS eigenstate and the second term, $n_{relax}(\mathbf{r}) \equiv \sum_i f_i \left(dn_i(\mathbf{r}) / df_H \right)$, describes the eigenstate density relaxation upon charge removal/addition. The curvature can therefore be expressed as:

$$\begin{aligned} C = &\iint \frac{n_H(\mathbf{r})\, n_H(\mathbf{r}')}{|\mathbf{r}-\mathbf{r}'|} d^3r' d^3r \\ &+ \iint \frac{n_H(\mathbf{r})\, n_{relax}(\mathbf{r}')}{|\mathbf{r}-\mathbf{r}'|} d^3r' d^3r + C_{XC}. \end{aligned} \tag{5.10}$$

The first term in Eq. (5.10) is twice the electrostatic interaction energy of $n_H(\mathbf{r})$ with itself; the second term is twice the electrostatic interaction energy between $n_H(\mathbf{r})$ and the relaxation density, $n_{relax}(\mathbf{r})$; the last term,

$$C_{XC} = \iint n_H(\mathbf{r}) \left[n_H(\mathbf{r}') + n_{relax}(\mathbf{r}') \right] f_{XC}(\mathbf{r},\mathbf{r}')\, d^3r' d^3r, \tag{5.11}$$

[3] In this paper all systems are treated strictly in the closed shell spin-unpolarized ensemble, so any removal or addition of small amounts of electronic charge preserves the unpolarized spin nature of the system.

[4] Obviously the lowest-unoccupied eigenstate becomes the highest-occupied one upon charge addition.

is the contribution of the exchange-correlation kernel to the curvature. As discussed in the introduction, for the exact exchange-correlation functional the curvature is identically zero and therefore the two electrostatic (Hartree) terms must be canceled out by the exchange-correlation kernel term.

In the LDA, the approximate exchange-correlation kernel is of the form: [58] $f_{XC}^{LDA}(\mathbf{r},\mathbf{r}') = \delta(\mathbf{r}-\mathbf{r}')\,\tilde{f}_{XC}^{LDA}(n(\mathbf{r}))$. The expression for the exchange-correlation contribution to the curvature then simplifies to

$$C_{XC}^{LDA} = \int n_H(\mathbf{r})\left[n_H(\mathbf{r}) + n_{relax}(\mathbf{r})\right]\tilde{f}_{XC}^{LDA}(n(\mathbf{r}))\,d^3r, \tag{5.12}$$

which does not generally cancel the Hartree terms in Eq. (5.10). This is consistent with the above-mentioned deviations from piecewise-linearity found in LDA calculations of small molecules.

5.3.2 Energy curvature in large finite three-dimensional systems

To gain insight into the behavior of curvature as a function of system size, we first consider an electron gas consisting of N_e electrons distributed uniformly in a finite volume Ω with periodic boundary conditions. For such a system, $n_i(\mathbf{r}) = \frac{1}{\Omega}$ and there is no eigenstate relaxation i.e. $n_{relax}(\mathbf{r}) = 0$. Therefore the general curvature expression of Eq. (5.10) includes only the electrostatic self-interaction and XC terms and, using LDA, can be simplified to

$$\begin{aligned}\bar{C} &= \frac{1}{\Omega^2}\iint_\Omega \frac{1}{|\mathbf{r}-\mathbf{r}'|}d^3r'd^3r + \frac{\tilde{f}_{XC}^{LDA}(n)}{\Omega} \\ &= \frac{\bar{D}}{\Omega^{1/3}} + \frac{\tilde{f}_{xc}^{LDA}(n)}{\Omega},\end{aligned} \tag{5.13}$$

where we have used the fact that for a given uniform density, $n = N_e/\Omega$, the LDA XC kernel is constant. Note that the bar over C and D is used to denote quantities relating to a uniform electron density. The first term in Eq. (5.13) is twice the electrostatic self-interaction energy of a unit charge, which is characterized by a volume-independent shape factor $\bar{D} = \frac{1}{\Omega^{5/3}}\iint_\Omega \frac{1}{|\mathbf{r}-\mathbf{r}'|}\mathrm{d}^3r'd^3r$. Analytical integration yields $\bar{D} = \frac{6}{5}(\frac{4\pi}{3})^{1/3}E_H a_0 \approx 52.5\ eVa_0$ for a sphere, where E_H and a_0 are the atomic Hartree and Bohr units for energy and length, respectively. For a cube and a parallelepiped of the shape of a diamond primitive cell, numerical integration yields $\bar{D} \approx 51.2\ eVa_0$ and $49.0\ eVa_0$, respectively, with the former value in agreement with electrostatic energy calculations reported in Ref. [59].

Note that expressions containing powers of Ω and $\Omega^{-1/3}$, as in Eq. (5.13), are often encountered also in the theory for computation of charged defects within periodic unit cells [51, 60–63], and in both cases they are of electrostatic origin. However, here we analyze the removal or addition of fractional charge that is delocalized across a finite system, whereas the other analysis studied the removal or addition of an integer charge that is localized on a defect within a periodic system [51, 63].

Clearly, the curvature of this uniform-electron-gas based example decays to zero as the system size increases. Specifically, in the limit of an infinitely large uniform electron gas limit, where LDA is an exact result, the exact DFT

condition of zero curvature is indeed obeyed. However, for a uniform electron gas confined to a finite volume, LDA predicts non-zero curvature as it is not an exact functional for these systems [64].

In Eq. (5.13), the curvature for large systems is dominated by the $\bar{D}\Omega^{-1/3}$ term, which arises from the electrostatic self-interaction of the highest occupied eigenstate. It stands to reason that such a term, with a general prefactor D, can be expected not just for this idealized system, but also for realistic large but finite systems for which LDA is a reasonable approximation.

To test this hypothesis, we focused on the elemental group IV solids - diamond, silicon, and germanium - for which LDA is well-proven to be a good approximation for ground-state properties [65, 66] and for which the electronic states are sufficiently delocalized to compare to analytical arguments relying on the uniform electron gas. For each solid, we constructed a set of increasingly large nanocrystals in two stages. First, we replicated the primitive unit cell of the bulk crystal an equal number of times in each of the lattice vector directions, using the experimental lattice constant, thereby creating a finite but periodic supercell. Second, we removed unbound atoms and passivated any remaining dangling bonds with hydrogen atoms. In this way, hydrogen-passivated NCs containing up to 325 Si, C, or Ge atoms, as well as a passivation layer containing up to 300 H atoms, were formed. For each of the NCs constructed this way, we calculated the LDA energy curvature for both charge removal and charge addition. All calculations were performed using NWCHEM [67] with the cc-PVDZ basis set for the smaller NCs and the STO-3G basis set for the larger NCs. The curvature was estimated by a finite difference approximation to Eq. (5.4), $C = \Delta\varepsilon_H/\Delta f_H$, where we calculated ε_H for the neutral system and for systems where an incremental small fractional charge was removed from, or added to, the entire system.

The resulting curvature for each of the systems studied is shown in Figure 5.1, as a function of $\Omega^{-\frac{1}{3}}$. Clearly, in the limit of large system volume, Ω, all three compounds exhibit the limiting form expected, i.e., a curvature given by $C = D\Omega^{-1/3}$, for both electron removal and addition. Furthermore, by fitting our results for NCs with edges larger than 14 a_0 to the expected dependence, we obtained $D \approx 43.5\text{eV}a_0$ for all three materials. This "universal value" is reasonable in light of the fact that the highest occupied eigenstate for all three materials has a similar spatial distribution, making the Hartree self-interaction contribution similar. Moreover, it deviates from the ideal uniform-electron-gas parallelepiped by only ∼20%, a difference that can be attributed to the non-uniform structure of the highest occupied eigenstate obtained within LDA (Eq. 5.10). For smaller nanocrystals, the term scaling as Ω^{-1} is non-negligible and therefore the curvature departs from the ideal $\Omega^{-1/3}$ behavior, as observed in Figure 5.1. Therefore, we conclude that the curvature expression given by the right-hand side of Eq. (5.13), derived for the uniform electron gas, is indeed applicable also for realistic systems possessing delocalized electronic states and that the self-repulsion term dominates the curvature as the system grows.

Interestingly, further support for the limiting $D\Omega^{-1/3}$ dependence of the curvature is obtained from the results of past LDA-based studies of the quantum size effect in spherical silicon [49] and germanium [68] nanocrystals. In these studies, the fundamental gap, computed from total energy differences of the anionic, neutral, and cationic system, was compared to the KS eigenvalue gap. The difference was observed [49, 50, 68] to scale as $\sim \Omega^{-1/3}$. This observation

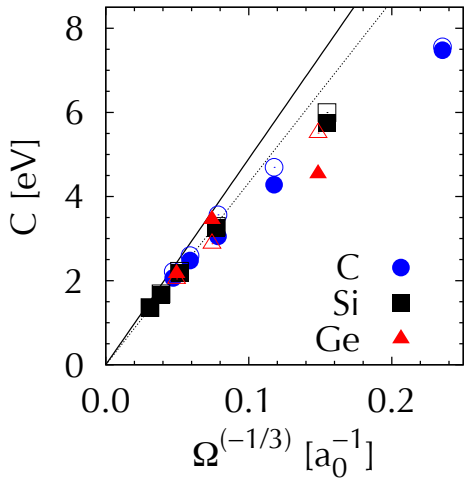

Figure 5.1: Curvature, C, obtained within the local density approximation for electron removal (solid symbols) or addition (hollow symbols) for diamond (blue circles), silicon (black squares), and germanium (red triangles) nanocrystals, as a function of $\Omega^{-\frac{1}{3}}$, where Ω is the nanocrystal volume. The dotted line represents a least-squares fit to the asymptotic dependence. The solid line represents the asymptotic dependence expected from Eq. (5.13) for a uniform electron gas of the same size and shape as the nanocrystals.

is easily explained within our theory as a direct consequence of the non-zero curvature [35]: Eq. (5.6) shows that for (semi-)local functionals (without an explicit derivative discontinuity), the difference between the fundamental and the KS eigenvalue gap is in fact equal to the average curvature for electron addition and removal and must exhibit the same trends as a consequence. This conclusion is further supported by the value of $D = 39.5\,eVa_0$ and $D = 41.1\,eVa_0$, deduced for the spherical silicon and germanium NCs, respectively, from the data of Ref. [49] and Ref. [68]. These values are indeed very close to the value of $D = 43.5\,eVa_0$ which we obtained above from explicit curvature calculations for the diamond-structured NCs. Note that the change in shape does not cause a significant difference in the value of D, consistent with our uniform electron gas calculations.

5.3.3 Energy curvature in large finite one-dimensional systems

The above-demonstrated dominance of the electrostatic term in the size-dependence of the curvature suggests that it must be strongly influenced by dimensionality. To test this, we again consider twice the Hartree energy as given in Eq. (5.10), evaluated for a unit-charge uniform electron gas, confined to a cylinder of length L and radius d such that $L \gg d$, as an approximation for the curvature of a long but finite one-dimensional system. This energy can be

computed analytically [69] to obtain:

$$C \approx \frac{2}{L} \ln\left(2e^{-3/4}\frac{L}{d}\right), \quad L \gg d. \tag{5.14}$$

This indicates that, as in the three-dimensional case, the curvature vanishes as the system grows arbitrarily long - an observation also consistent with the results of Mori-Sanchez *et al.* for hydrogen chains [15]. However, the curvature does not decay as L^{-1}, as perhaps could be naively expected, but rather as $L^{-1}\ln\left(\frac{2e^{-3/4}L}{d}\right)$. The relaxation and exchange-correlation terms are expected to scale as L^{-1}. However they do not significantly affect the curvature when $L > 50a_0$, as for very large L the logarithmic term dominates the L^{-1} term.

To test whether this prediction carries over to realistic one-dimensional systems, we considered alkane chains of increasing length, L, whose width d is fixed by definition (see inset of Figure 5.2). These alkane chains provide a useful model of a quasi-one-dimensional system that is well-described by LDA [70]. We investigated chains containing up to 240 C atoms and again used NWCHEM [67] with the cc-PVDZ and the STO-3G basis sets. The computed curvature for electron removal is shown in Figure 5.2, as a function of a_0/L, and compared with the prediction of Eq. (5.14). Clearly, for large L the curvature is once again very well approximated by the electrostatic self-interaction of a uniformly smeared unit charge.

5.4 Energy curvature in periodic systems

5.4.1 General Considerations

In solid-state physics, it is common practice to employ periodic boundary conditions for the description of crystalline solids [71]. To understand the bulk limit of curvature calculations in such a scenario, we consider a reference cell of total volume Ω_{RC}, containing N repeating unit cells (with unit cell volume Ω_{UC}), using Born - von Karman periodic boundary conditions [71]. In other words, the reference cell is treated as a *finite but topologically periodic* system [42, 64]. In such a system, the infinite bulk limit is approached with increasing size of the reference cell (see footnote [5]).

To compute the curvature, we remove (or add) an electronic charge Q_{RC} from (or to) the reference cell, denoted below by a "hole" (or "elec") superscript where appropriate. We focus mostly on electron removal for simplicity. Owing to the periodic boundary conditions, electron removal from the reference cell implies removal of the same charge from each of its periodic images. As there are an infinite number of repeated reference cells, the removed electronic charge is effectively infinite, leading to divergences in the Coulomb potential. Therefore, a uniform compensating negative charge, of density Q_{RC}/Ω_{RC}, is introduced to the reference cell. This keeps the infinite periodic crystal neutral and avoids the divergent behavior [73, 74].

As before, the curvature C_{RC}, defined with respect to the reference cell, is computed as the rate of change of the highest occupied KS-eigenvalue with

[5] Alternatively, the bulk limit can be approached using the concept of k-point sampling of the unit cell. [72] For now, we do not pursue this alternative, but we discuss it extensively below

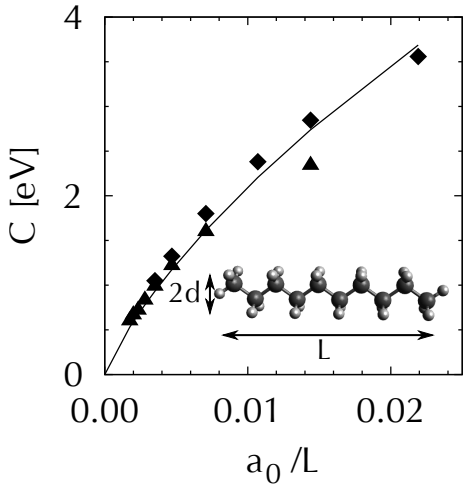

Figure 5.2: Curvature, C, obtained within the local density approximation for electron removal from alkane chains, as a function of a_0/L, where L is the chain length. The line represents the asymptotic dependence expected from Eq. (5.14) for a unit-charge uniform electron gas of the same length as the chain and a radius of $d = 2a_0$. Triangles and diamonds represent data obtained using the cc-PVDZ and STO-3G basis sets, respectively. Inset: the decane molecule as an example of an alkane chain, with d and L shown explicitly.

respect to removed charge, $C_{RC} = d\varepsilon_H/dQ_{RC}$. By construction (and assuming no symmetry breaking), the hole formed by charge removal exhibits a periodic structure commensurate with the repeating unit-cell and therefore $Q_{RC} = NQ_{UC}$, where Q_{UC} is the charge removed from each of the N unit cells that comprise the reference cell. In the limit of large N, ε_H is expected to become independent of the size of the reference cell, i.e., of N. Therefore

$$C_{RC} = \frac{d\varepsilon_H}{dQ_{RC}} = \frac{1}{N}\frac{d\varepsilon_H}{dQ_{UC}} \equiv \frac{C_{UC}}{N}, \tag{5.15}$$

where $C_{UC} \equiv d\varepsilon_H/dQ_{UC}$ is the "unit-cell curvature", which in the limit of large N is independent of the reference cell size (see footnote [6]).

Clearly, the curvature C_{RC} for the infinite crystal does depend on the reference cell size. As the reference cell grows ($N \to \infty$, $\Omega_{RC} \to \infty$), we find $C_{RC} \to 0$ for any underlying functional. This result should be contrasted with the exact DFT condition of piecewise linearity, where the curvature given by Eq. (5.15) should be strictly zero for *any* reference cell size and not just in the infinite cell limit. In other words, as for the NCs, in the infinite system limit piecewise-linearity is obtained irrespective of the underlying XC functional and therefore does not provide useful information for functional construction or evaluation. However, in the exact theory we also expect $C_{UC} = 0$. Therefore, a non-vanishing unit-cell curvature, C_{UC}, represents a measure of the spurious XC functional behavior even in periodic infinite solids and may prove useful in future analysis.

5.4.2 LDA calculations of topologically periodic reference cells

To examine the considerations and conclusions of the previous section, we performed LDA calculations for increasingly large periodic reference cells of selected semiconductors and insulators, using the LDA-optimized lattice vectors of a neutral unit cell (see footnote [7]).

As mentioned above, the reference cell is considered to be finite but topologically periodic. Therefore, all calculations are carried out using only the single k-point (at Γ). This makes curvature calculations straightforward both conceptually and practically, as charge is removed from the highest occupied KS eigenstate as in the finite-system calculations above. The energy derivatives needed for the evaluation of the curvature (Eq. 5.15) were calculated using finite differences of the highest occupied energy eigenvalue, ε_H, for the neutral and incrementally charged reference cell.

The results of such calculations for increasingly large reference cells of diamond and silicon are summarized in Figure 5.3 (see footnote [8]). As shown in the top panel of Figure 5.3, the reference cell curvature indeed decreases

[6] The same dependence on N can be obtained by considering the curvature directly as the second derivative of the energy, i.e., $C_{RC} = d^2E_{RC}/dQ_{RC}^2$, because E_{RC} and Q_{RC} are both extensive quantities and therefore proportional to N.

[7] We performed non-spin-polarized calculations using norm-conserving pseudopotentials within the Quantum-ESPRESSO [75] and ABINIT [76, 77] packages, which use a planewave basis with periodic boundary conditions. All results were converged for plane-wave kinetic energy cut-off.

[8] LDA erroneously predicts bulk germanium to be semi-metallic (see, e.g., Ref. [78]). Therefore, germanium is omitted from Figure 5.3

monotonically and vanishes in the large N limit, in agreement with the above theoretical considerations. At the same time, the bottom panel of Figure 5.3 shows that the unit cell curvature is not zero and for large N approaches a constant, material-dependent value, such that Eq. (5.15) is obeyed.

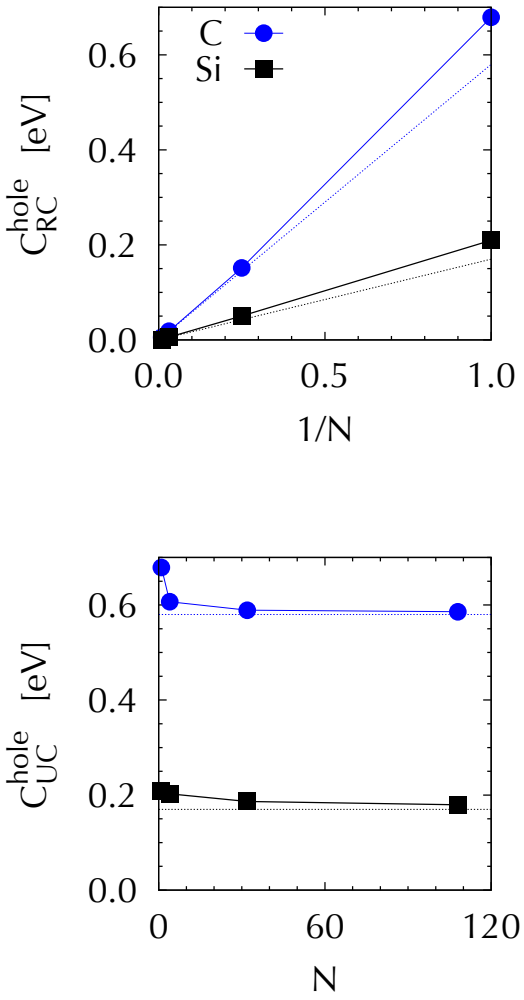

Figure 5.3: Computed charge removal curvature for silicon (black squares) and diamond (blue circles) crystals: (Top) Reference cell curvature, C^{hole}_{RC}, as a function of N^{-1}. (Bottom) unit cell curvature, C^{hole}_{UC}, as a function of N, the number of primitive unit-cells in the reference cell. Solid lines are a guide for the eye. Dotted lines represent the asymptotic dependence on N (Top), or the converged values of C_{UC} (Bottom), obtained through Brillouin-zone sampling described in Section 5.4.4.

5.4.3 Finite versus periodic cell: A seeming paradox and its resolution

In the limit of an arbitrarily large system, one would expect surface effects to be negligible and so, naively, that the limiting behavior of large periodic and non-periodic systems to be the same. However, we already showed both analytically and numerically that in fact the limiting behavior is not the same. For the finite system, the curvature asymptotically scales as $\Omega^{-1/3}$, where Ω is the volume of the finite, non-periodic system, whereas for the topologically periodic system the curvature asymptotically scales as Ω_{RC}^{-1}, where Ω_{RC} is the reference cell volume.

This apparent paradox can be reconciled by recalling that in a periodic system, electron addition/removal must be accompanied by the addition of a compensating, uniformly distributed background charge of opposite sign, so as to avoid divergence of the Coulomb potential and energy [73]. For a non-periodic system, however, no compensating charge is necessary. This background charge strongly affects curvature considerations [74]. To understand why, consider that if surface effects are neglected then Eq. (5.10), developed above for non-periodic systems, can be applied to the reference cell of a periodic system. However, while n_{relax} integrates to zero in the reference cell, n_H integrates to 1. Therefore, n_H must be replaced by a background-neutralized density, $\rho_H(\mathbf{r}) \equiv n_H(\mathbf{r}) - \frac{1}{\Omega_{RC}}$, before it can be inserted in Eq. (5.10). Therefore, Eq. (5.10) yields the following expression for the curvature in the periodic case, $C^{periodic}$:

$$\begin{aligned} C^{periodic} = & \iint_{\Omega_{RC}} \frac{\rho_H(\mathbf{r})\,\rho_H(\mathbf{r}')}{|\mathbf{r}-\mathbf{r}'|} d^3r' d^3r \\ & + \iint_{\Omega_{RC}} \frac{\rho_H(\mathbf{r})\,n_{relax}(\mathbf{r}')}{|\mathbf{r}-\mathbf{r}'|} d^3r' d^3r + C_{XC}. \end{aligned} \tag{5.16}$$

With all densities being unit-cell periodic, we can define

$$\tilde{n}_j(\mathbf{G}) = \frac{1}{\Omega_{UC}} \int_{\Omega_{UC}} n_j(\mathbf{r})\, e^{i\mathbf{G}\cdot\mathbf{r}} d^3r$$

as the Fourier-component of $n_j(\mathbf{r})$ corresponding to the reciprocal unit-cell lattice vector, $\mathbf{G}$. For charge-neutral systems, the $\mathbf{G} = \mathbf{0}$ component must be zero. By noting that $\tilde{n}_H(\mathbf{G} \neq \mathbf{0}) = \tilde{\rho}_H(\mathbf{G} \neq \mathbf{0})$, because the two densities differ only by a constant, we obtain:

$$\begin{aligned} C^{periodic} = & 4\pi\Omega_{RC} \sum_{\mathbf{G}\neq 0} \frac{\tilde{n}_H(\mathbf{G})\,\tilde{n}_H(\mathbf{G})^*}{G^2} \\ & + 4\pi\Omega_{RC} \sum_{\mathbf{G}\neq 0} \frac{\tilde{n}_H(\mathbf{G})\,\tilde{n}_{relax}(\mathbf{G})^*}{G^2} + C_{XC}. \end{aligned} \tag{5.17}$$

The KS-eigenstate densities, $n_j(\mathbf{r})$, are normalized over the reference cell and therefore $n_H(\mathbf{r})$ and $n_{relax}(\mathbf{r})$, as well as their Fourier components, must scale as Ω_{RC}^{-1}. Because $\mathbf{G}$ depends only on the unit cell and is independent of Ω_{RC}, Eq. (5.17) shows that $C^{periodic}$ scales as Ω_{RC}^{-1}. Thus, we obtain a curvature that scales with inverse system volume, consistent with Eq. (5.15) above. We note that similar reasoning as to the effect of the compensating charge has also been used in the study of charged defects in periodic systems [51, 63].

One can also compare the terms in Eq. (5.10) and Eq. (5.16), obtaining the following expression for the difference in their curvature:

$$C^{finite} - C^{periodic} = \iint_{\Omega_{RC}} \frac{\left(2n_H(\mathbf{r}) - \frac{1}{\Omega_{RC}} + n_{relax}(\mathbf{r})\right)\frac{1}{\Omega_{RC}}}{|\mathbf{r}-\mathbf{r}'|} d^3r' d^3r. \tag{5.18}$$

Dimensional analysis reveals that the above curvature difference scales as $\Omega_{RC}^{-1/3}$.

As discussed in Section 5.3, $\Omega^{-1/3}$ scaling was also obtained for the non-periodic case from the self-interaction energy of the highest-occupied eigenstate. Furthermore, because the background charge must systematically cancel the divergence in the electronic electrostatic energy, the prefactor of the $\Omega_{RC}^{-1/3}$ dependence in the above equation must be equal and opposite to that deduced from Eq. (5.10). Therefore, overall the $\Omega_{RC}^{-1/3}$ scaling must vanish in $C^{periodic}$ and only the Ω_{RC}^{-1} scaling remains.

To summarize, the scaling behavior of a non-periodic and a periodic system really is different, but this is not owing to topology *per se*, but rather stems from the effects of the uniform background charge, used in periodic calculations only. Before concluding this issue, however, two more comments are in order. First, for finite systems described with (semi-)local functionals, the scaling is self-interaction dominated and therefore positive (see, e.g., Refs. [12, 16, 17, 35]). Upon elimination of this effect by the compensating background, curvature can be either positive or negative (which we show below to be the case). This is somewhat reminiscent of the behavior of the exact-exchange functional (see, e.g., Ref. [12]), where self-interaction is eliminated and the curvature is typically mildly negative. Second, for periodic systems we assumed throughout that the removed/added charge is delocalized throughout the reference cell. If this is not the case, e.g., if a molecule or a localized defect is computed within a large supercell, scaling arguments no longer apply and the results will resemble those of finite systems. This explains, among other things, why a Hubbard-like U term for localized states in an otherwise periodic system is indeed useful, as long as the correction is limited to the vicinity of the localized site (see, e.g., Refs. [36, 79]).

5.4.4 Brillouin zone sampling

In Section 5.4.2 we have considered the infinite solid limit by constructing increasingly large topologically-periodic reference cells. While pedagogically useful, this procedure is too cumbersome and computationally expensive to be used for routine unit-cell curvature calculations. In practice, the infinite-solid limit is much easier to reach by using k-point sampling of the Brillouin zone corresponding to a single periodic unit cell [71]. One can then show that a single unit cell with uniform sampling of N k-points is completely equivalent, mathematically and physically, to a reference cell comprised of N unit cells within the single k-point (the Γ point) treatment [72]. The infinite solid limit thus simply corresponds to an arbitrarily dense k-point sampling.

Obviously, practical calculations must involve a finite number of k-points. This is of little consequence to ground-state calculations of semiconductors and insulators, as results tend to converge quickly with the number of k-points [72]. However, it raises a serious issue for electron removal/addition calculations.

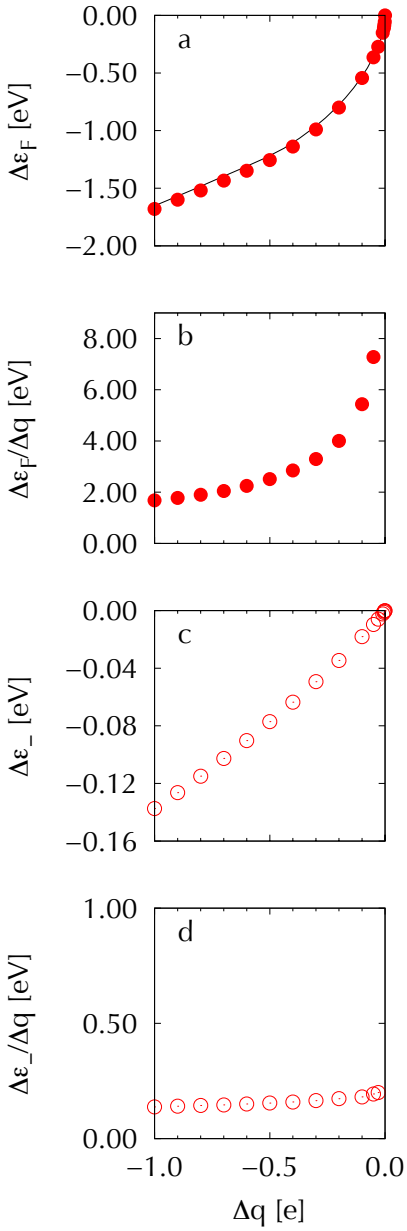

Figure 5.4: Charge removal in a unit cell of silicon, with $16 \times 16 \times 16$ k-point sampling. Panel a: change in Fermi level position, $\Delta\varepsilon_F$, as a function of the removed charge, Δq. Solid line: change in ε_F expected from the uncharged density of states curve given by Eq. (5.19). Panel b: Numerical derivative of the results in panel a, $\Delta\varepsilon_F/\Delta q$, as a function of Δq. Panel c: change in position of valence band maximum, $\Delta\varepsilon_-$, as a function of Δq. Panel d: Numerical derivative of the results in panel c, $\Delta\varepsilon_-/\Delta q$, as a function of Δq.

Naively, one would think that the above-discussed determination of curvature from $d\varepsilon_H/dq$ should be generalized to the case of k-point sampling by considering $d\varepsilon_F/dq$, where ε_F is the Fermi level. This is because for a ground-state, zero-temperature solid, ε_F denotes the energy of the highest occupied state by definition. However, in practice one always removes/adds a finite amount of charge, q, rather than a truly infinitesimal charge. Therefore, charge is generally removed from all eigenstates with energy greater than ε_F, where the latter is determined by the charge conservation condition

$$nN - q = \int_{-\infty}^{\varepsilon_F} g(\varepsilon)\, d\varepsilon, \tag{5.19}$$

with $g(\varepsilon)$ the density of states (DOS). Once charge is removed not only from the highest-energy state, but rather from many states, the piecewise linearity condition no longer applies. Therefore the entire theoretical edifice on which all previous considerations were based breaks down. This difficulty persists even if the second derivative of the total energy, rather than the first derivative of the Fermi energy, is considered. One could, perhaps, hope that extrapolation of $d\varepsilon_F/dq$ to $q \to 0$, where charge really is removed only from the highest occupied eigenstate, would still lead to the correct result. Unfortunately, this is not the case, and in fact $d\varepsilon_F/dq$ erroneously diverges for $q \to 0$ [80].

The above considerations are illustrated numerically in Figure 5.4, where the dependence of ε_F on q (Figure 5.4a) and its derivative (Figure 5.4b) were computed for a primitive unit cell of silicon with a $16 \times 16 \times 16$ k-point sampling scheme. Clearly, and as expected from Eq. (5.19), the Fermi energy follows closely the integrated density of states of the uncharged system (shown as a solid line), whose derivative diverges.

Fortunately, an equally simple, yet accurate, procedure is to consider instead the valence band maximum (or the conduction band minimum for charge addition), which we denote here as ε_-. For $q \to 0$ it too must tend to the correct limit as charge is removed only from the highest occupied state. For finite q it is, of course, incorrect, but as it does not incorporate DOS effects its derivative is not expected to diverge. This is illustrated numerically in Figure 5.4 as well, for the same silicon example, where both the weaker dependence of ε_- on q (note the energy scale in Figure 5.4c) and the convergence of its derivative for small q (see Figure 5.4d) is apparent.

In the calculations of Figure 5.4, the removal of charge q from a unit cell, sampled by N k-points, is in fact equivalent to the removal of the same charge from a reference cell whose volume is N times larger. However, as the same charge is removed from the unit-cell, irrespective of the number of k-points, $\Delta\varepsilon_-/\Delta q$ is directly comparable to the non-vanishing unit-cell curvature, C_{UC}. This is directly verified in Figure 5.5, which compares, for silicon, unit-cell curvature values, C_{UC}, obtained from increasingly large single k-point reference cells (as in Figure 5.3) with those obtained from increasingly dense k-point sampling of a unit cell. Clearly, the results are indeed equivalent.

The fact that it is $d\epsilon_-/dq$, rather than $d\epsilon_F/dq$, which predicts the correct curvature, has profound consequences for the piecewise linearity criterion. As by definition $dE/df_H = \epsilon_F$, it is incorrect in the solid state to apply the expression d^2E/dN^2 given in Eq. (5.4) for finite systems. d^2E/dN^2 is no longer equivalent to a calculation based on the first derivative of ϵ_H, and use of the energy criterion

would necessarily yield the undesired $d\epsilon_F/dq$, instead of the useful $d\epsilon_-/dq$ and therefore should be avoided. The only exception is when a single k-point is used, as then $\epsilon_- = \epsilon_F$.

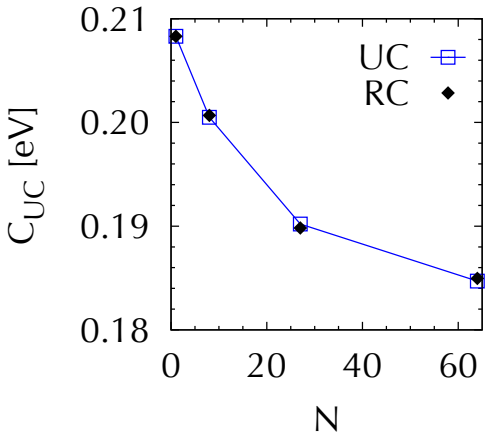

Figure 5.5: Unit cell curvature, C_{UC}, obtained from single k-point calculations of a reference cell containing N unit cells (filled diamonds) and from N k-point calculations of a single unit cell (hollow squares), as a function of N. Lines joining the results of the N k-point calculations are a guide to the eye.

Finally, with the above scheme, we efficiently calculate unit-cell curvatures for charge removal and addition in a variety of semiconductors and insulators, obtained in the limit of sufficiently dense k-point sampling of the primitive unit-cell. The results are summarized in Table 5.1. Note that, just like the total energy per unit cell, C_{UC} will generally depend on the choice of unit cell (e.g., primitive vs. conventional).

From the results it is clear that for all systems considered the unit cell curvature in LDA is a non zero, material-dependent property. Furthermore, once convergence has been reached it is independent of the density of the k-point sampling. This is to be contrasted with the reference cell curvature discussed earlier, which was not only dependent on the reference cell size, but went to zero in the infinite limit for all functionals. As noted in the preceding section, C_{UC} can have both positive and negative values (illustrated by the results in Table 5.1), owing to the presence of the neutralizing background. Note that Eq. (5.6) should not be used for periodic solids, since, as noted above, the energies of the ionized systems are generally incorrect for a periodic LDA calculation. Consequently, C_{UC} values do not directly correspond to LDA correction terms. However, the deviation of C_{UC} from zero is still a useful indicator on which to build future correction schemes.

	Crystal Structure	C_{UC} (eV)	
		Charge removal	Charge addition
AlAs	Zinc-blende	0.26	-0.65
AlN	Zinc-blende	0.94	-0.92
AlP	Zinc-blende	0.33	-0.66
AlSb	Zinc-blende	0.16	-0.57
C	Diamond	0.58	-0.62
GaP	Zinc-blende	0.36	-0.65
MgO	Rock-salt	1.6	-0.73
Si	Diamond	0.17	-0.54
SiC	Zinc-blende	0.59	-0.64

Table 5.1: Energy curvature for the unit cell, C_{UC}, for charge removal and addition, calculated for various solids.

5.5 Conclusions

In this article, we have examined the solid-state limit of energy curvature, i.e., of deviations from piecewise-linearity, focusing on (semi-)local functionals. We considered two different limits: finite systems, with volume $\Omega \to \infty$, as well as topologically periodic systems with a reference cell (to which the periodic boundary conditions are applied) of volume $\Omega_{RC} \to \infty$. We found that in all cases piecewise-linearity - albeit possibly with the wrong slope - is obtained in the solid-state limit, even from functionals that grossly disobey it for a finite system. However, using both analytical considerations and practical calculations of representative systems, we found that the zero curvature limit is reached in very different ways. Therefore, while using the demand of zero curvature for functional construction and evaluation is not, as such, useful in the solid-state limit, its size-dependence does contain useful information.

For large finite systems, we found that curvature scales as $\Omega^{-1/3}$ for three-dimensional systems (e.g., nanocrystals) and as $\frac{2}{L}\ln\left(2e^{-3/4}\frac{L}{d}\right)$, where L is the length and d is the width, for quasi-one-dimensional systems (e.g., molecular chains). This scaling behavior was found to be dominated by electrostatics and traced to the self-interaction term of the highest occupied state.

For large reference cell periodic systems, we found that the curvature C_{RC} scales as $C_{RC} = C_{UC}\Omega_{UC}/\Omega_{RC}$, where C_{UC} and Ω_{UC} are the unit-cell curvature and volume respectively. C_{UC} (for an approximate functional) is a non-vanishing material-dependent quantity that is independent of the reference cell, and therefore may serve as a new useful measure of functional error in periodic solids. As mentioned in the Introduction (Section 5.2), for molecular systems deviation from piecewise linearity has already been used extensively for functional evaluation, tuning, and correction [35–48]. We hope that, with time, similar approaches that use our new criterion could emerge for the solid state.

Furthermore, we have been able to calculate this curvature in two ways: either directly from the definition by using increasingly large periodic reference cells or, more usefully, by considering changes in the band edge position upon charge removal/addition in unit cells with dense k-point sampling. Last but not least, we rationalized the difference between the periodic and non-periodic case as resulting from the automatic elimination of the electrostatic self-interaction of

the highest-occupied eigenstate via the addition of a compensating background charge in periodic systems.

We believe that these results should prove useful for further development, evaluation, and application of novel exchange-correlation functionals suitable for the solid-state.

5.6 Acknowledgments

We thank Eli Kraisler, Sivan Refaely-Abramson (Weizmann Institute), and Stephan Kümmel (Universität Bayreuth) for useful discussions. Work at the Weizmann Institute was supported by the European Research Council. Work at the Hebrew University of Jerusalem was supported by the Israel Science Foundation Grant No. 1219-12. VV acknowledges travel support by the Minerva Foundation. Some of the computations (VV) were performed at the Leibniz Supercomputing Centre of the Bavarian Academy of Sciences and the Humanities.

Bibliography

[1] P. Hohenberg and W. Kohn, Phys. Rev. **136**, B864 (1964).

[2] W. Kohn and L. J. Sham, Phys. Rev. **140**, A1133 (1965).

[3] M. Levy, Phys. Rev. A **26**, 1200 (1982).

[4] E. H. Lieb, Int. J. Quantum Chem. **24**, 243 (1983).

[5] J. P. Perdew and S. Kurth, *A Primer in Density Functional Theory* (Springer, 2003).

[6] J. P. Perdew, R. G. Parr, M. Levy, and J. L. Balduz, Phys. Rev. Lett. **49**, 1691 (1982).

[7] J. Janak, Phys. Rev. B **18**, 7165 (1978).

[8] M. Levy, J. P. Perdew, and V. Sahni, Phys. Rev. A **30**, 2745 (1984).

[9] C.-O. Almbladh and U. von Barth, Phys. Rev. B **31**, 3231 (1985).

[10] J. P. Perdew and M. Levy, Phys. Rev. B **56**, 16021 (1997).

[11] A. D. Becke, J. Chem. Phys. **98**, 1372 (1993).

[12] P. Mori-Sánchez, A. J. Cohen, and W. T. Yang, J. Chem. Phys. **125**, 201102 (2006).

[13] A. Ruzsinszky, J. P. Perdew, G. I. Csonka, O. A. Vydrov, and G. E. Scuseria, J. Chem. Phys. **126**, 104102 (2007).

[14] O. A. Vydrov, G. E. Scuseria, and J. P. Perdew, J. Chem. Phys. **126**, 154109 (2007).

[15] P. Mori-Sánchez, A. J. Cohen, and W. Yang, Phys. Rev. Lett. **100**, 146401 (2008).

[16] A. J. Cohen, P. Mori-Sánchez, and W. T. Yang, Science **321**, 792 (2008).

[17] A. J. Cohen, P. Mori-Sánchez, and W. T. Yang, Phys. Rev. B **77**, 115123 (2008).

[18] R. Haunschild, T. M. Henderson, C. A. Jiménez-Hoyos, and G. E. Scuseria, J. Chem. Phys. **133**, 134116 (2010).

[19] M. Srebro and J. Autschbach, J. Phys. Chem. Lett. **3**, 576 (2012).

[20] J. D. Gledhill, M. J. Peach, and D. J. Tozer, J. Chem. Theory Comput. **9**, 4414 (2013).

[21] A. J. Cohen and P. Mori-Sánchez, J. Chem. Phys. **140**, 044110 (2014).

[22] D. J. Tozer, Phys. Rev. A **58**, 3524 (1998).

[23] M. J. Allen and D. J. Tozer, Mol. Phys. **100**, 433 (2002).

[24] J. P. Perdew and M. Levy, Phys. Rev. Lett. **51**, 1884 (1983).

[25] L. J. Sham and M. Schluter, Phys. Rev. Lett. **51**, 1888 (1983).

[26] J. P. Perdew and M. Levy, Phys. Rev. B **31**, 6264 (1985).

[27] E. Sagvolden and J. P. Perdew, Phys. Rev. A **77**, 012517 (2008).

[28] A. J. Cohen and P. Mori-Sánchez, J. Chem. Phys. **140**, 044110 (2014).

[29] A. Seidl, A. Görling, P. Vogl, J. A. Majewski, and M. Levy, Phys. Rev. B **53**, 3764 (1996).

[30] S. Kümmel and L. Kronik, Rev. Mod. Phys. **80**, 3 (2008).

[31] W. Yang, A. J. Cohen, and P. Mori-Sánchez, J. Chem. Phys. **136**, 204111 (2012).

[32] H. R. Eisenberg and R. Baer, Phys. Chem. Chem. Phys. **11**, 4674 (2009).

[33] T. Stein, H. Eisenberg, L. Kronik, and R. Baer, Phys. Rev. Lett. **105**, 266802 (2010).

[34] L. Kronik, T. Stein, S. Refaely-Abramson, and R. Baer, J. Chem. Theory Comput. **8**, 1515 (2012).

[35] T. Stein, J. Autschbach, N. Govind, L. Kronik, and R. Baer, J. Phys. Chem. Lett. **3**, 3740 (2012).

[36] M. Cococcioni and S. de Gironcoli, Phys. Rev. B **71**, 035105 (2005).

[37] S. Lany and A. Zunger, Phys. Rev. B **80**, 085202 (2009).

[38] I. Dabo, A. Ferretti, N. Poilvert, Y. L. Li, N. Marzari, and M. Cococcioni, Phys. Rev. B **82**, 115121 (2010).

[39] J. D. Chai and P. T. Chen, Phys. Rev. Lett. **110**, 033002 (2013).

[40] A. Ferretti, I. Dabo, M. Cococcioni, and N. Marzari, Phys. Rev. B **89**, 195134 (2014).

[41] E. Kraisler and L. Kronik, Phys. Rev. Lett. **110**, 126403 (2013).

[42] E. Kraisler and L. Kronik, J. Chem. Phys. **140**, 18A540 (2014).

[43] M. Kuisma, J. Ojanen, J. Enkovaara, and T. T. Rantala, Phys. Rev. B **82**, 115106 (2010).

[44] R. Armiento and S. Kümmel, Phys. Rev. Lett. **111**, 36402 (2013).

[45] N. Sai, P. F. Barbara, and K. Leung, Phys. Rev. Lett. **106**, 226403 (2011).

[46] V. Atalla, M. Yoon, F. Caruso, P. Rinke, and M. Scheffler, Phys. Rev. B **88**, 165122 (2013).

[47] R. Baer, E. Livshits, and U. Salzner, Annu. Rev. Phys. Chem. **61**, 85 (2010).

[48] J. Autschbach and M. Srebro, Acc. Chem. Res. **47**, 2592 (2014).

[49] S. Öğüt, J. R. Chelikowsky, and S. G. Louie, Phys. Rev. Lett. **79**, 1770 (1997).

[50] R. W. Godby and I. D. White, Phys. Rev. Lett. **80**, 3161 (1998).

[51] S. Lany and A. Zunger, Phys. Rev. B **80**, 85202 (2009).

[52] U. Salzner, J. Phys. Chem. A **114**, 10997 (2010).

[53] G. Onida, L. Reining, and A. Rubio, Rev. Mod. Phys. **74**, 601 (2002).

[54] A. F. Izmaylov and G. E. Scuseria, J. Chem. Phys. **129**, 034101 (2008).

[55] J. Hellman, *Einführung in die Quantenchemie* (Deuticke, Leipzig, 1937).

[56] R. P. Feynman, Phys. Rev. **56**, 340 (1939).

[57] U. Salzner and R. Baer, J. Chem. Phys. **131**, 231101 (2009).

[58] M. Petersilka, U. J. Gossmann, and E. K. U. Gross, Phys. Rev. Lett. **76**, 1212 (1996).

[59] D. Finocchiaro, M. Pellegrini, and P. Bientinesi, J. Comput. Phys. **146**, 707 (1998).

[60] M. Leslie and N. Gillan, J. Phys. C: Solid State Phys. **18**, 973 (1985).

[61] E. V. Kholopov, Phys. Usp. **47**, 965 (2004).

[62] G. Makov and M. Payne, Phys. Rev. B **51**, 4014 (1995).

[63] C. Freysoldt, J. Neugebauer, and C. G. Van de Walle, Phys. Rev. Lett. **102**, 016402 (2009).

[64] P. M. W. Gill and P. F. Loos, Theor. Chem. Acc. **131**, 1069 (2012).

[65] R. Godby, M. Schlüter, and L. Sham, Phys. Rev. B **36**, 6497 (1987).

[66] J. R. Chelikowsky and M. L. Cohen, in *Handbook on Semiconductors*, edited by T. S. Moss and P. T. Landsberg (Elsevier, Amsterdam, the Netherlands, 1992), p. 59.

[67] M. Valiev, E. J. Bylaska, N. Govind, K. Kowalski, T. P. Straatsma, H. J. J. Van Dam, D. Wang, J. Nieplocha, E. Apra, T. L. Windus, et al., Comput. Phys. Commun. **181**, 1477 (2010).

[68] D. V. Melnikov and J. R. Chelikowsky, Phys. Rev. B **69**, 113305 (2004).

[69] O. Ciftja, Physica B **407**, 2803 (2012).

[70] L. Segev, A. Salomon, A. Natan, D. Cahen, L. Kronik, F. Amy, C. K. Chan, and A. Kahn, Phys. Rev. B **74**, 165323 (2006).

[71] N. W. Ashcroft and N. D. Mermin, *Solid State Physics* (Holt, Rinehart and Winston, 1976).

[72] W. E. Pickett, Computer Physics Reports **9**, 115 (1989).

[73] J. Ihm, A. Zunger, and M. L. Cohen, J. Phys.: Condens. Matter **12**, 4409 (1979).

[74] S. Sharma, J. Dewhurst, N. Lathiotakis, and E. Gross, Phys. Rev. B **78**, 201103 (2008).

[75] P. Giannozzi, S. Baroni, N. Bonini, M. Calandra, R. Car, C. Cavazzoni, D. Ceresoli, G. L. Chiarotti, M. Cococcioni, I. Dabo, et al., J. Phys.: Condens. Matter **21**, 395502 (19pp) (2009).

[76] X. Gonze, J.-M. Beuken, R. Caracas, F. Detraux, M. Fuchs, G.-M. Rignanese, L. Sindic, M. Verstraete, G. Zerah, F. Jollet, et al., Computational Materials Science **25**, 478 (2002).

[77] X. Gonze, G.-M. Rignanese, M. Verstraete, J.-M. Beuken, Y. Pouillon, R. Caracas, F. Jollet, M. Torrent, G. Zerah, M. Mikami, et al., Z. Kristallogr. **220**, 558 (2005).

[78] J. Heyd, J. E. Peralta, G. E. Scuseria, and R. L. Martin, J. Chem. Phys. **123**, 174101 (2005).

[79] I. Solovyev, P. Dederichs, and V. Anisimov, Phys. Rev. B **50**, 16861 (1994).

[80] C. Kittel, *Introduction to Solid State Physics* (Wiley, 1966).

Chapter 6

Spontaneous charge carrier localization in extended one-dimensional systems

Vojtěch Vlček[1,2], Helen R. Eisenberg[1], Gerd Steinle-Neumann[2], Daniel Neuhauser[3], Eran Rabani[4,5], Roi Baer[1,6]

6.1 Abstract

Charge carrier localization in extended atomic systems has been described previously as being driven by disorder, point defects or distortions of the ionic lattice. Here we show for the first time by means of first-principles computations that charge carriers can spontaneously localize due to a purely electronic effect in otherwise perfectly ordered structures. Optimally-tuned range-separated density functional theory and many-body perturbation calculations within the GW approximation reveal that in trans-polyacetylene and polythiophene the hole density localizes on a length scale of several nanometers. This is due to exchange-induced translational symmetry breaking of the charge density. Ionization potentials, optical absorption peaks, excitonic binding energies and the optimally-tuned range parameter itself all become independent of polymer length as it exceeds the critical localization scale. Moreover, we find that lattice disorder and the formation of a polaron result from the charge localization in contrast to the traditional view that lattice distortions precede charge localiza-

[1]Fritz Haber Center for Molecular Dynamics, Institute of Chemistry, The Hebrew University of Jerusalem, Jerusalem 91904, Israel

[2]Bayerisches Geoinstitut, Universität Bayreuth, 95440 Bayreuth, Germany

[3]Department of Chemistry and Biochemistry, University of California, Los Angeles California 90095, U.S.A.

[4]Department of Chemistry, University of California and Materials Science Division, Lawrence Berkeley National Laboratory, Berkeley, California 94720, U.S.A.

[5]The Sackler Center for Computational Molecular and Materials Science, Tel Aviv University, Tel Aviv 69978, Israel

[6]On sabbatical in the Department of Chemistry, University of California, Berkeley California 94720, U.S.A.

tion. Our results can explain experimental findings that polarons in conjugated polymers form instantaneously after exposure to ultrafast light pulses.

6.2 Results, Discussion and Conclusions

Spatial localization in extended systems has been a central topic in physics, since the pioneering work of Anderson [1] and Mott [2], and more recently in the context of many-body localization [3]. It also forms an important theme in the materials science of extended conjugated systems where the dynamics of charges carrier are described in terms of localized polarons [4–10]. One way to identify charge localization is through the dependence of its energy (e.g., ionization potential or electron affinity) on the system size L. In 1D systems, if the charge remains delocalized, then according to a simple *non-interacting* picture, its energy converges to the bulk limit as $1/L^{\alpha}$ with $\alpha = 1$ for a metal or $\alpha = 2$ otherwise. However if charge localizes within a critical length scale l_c, the energy will become independent of L for $L > l_c$.

Charge localization in conjugated systems can occur in several ways: Attachment by point defects [9], lattice disorder effects [5, 10], and formation of self-bound charged polarons and neutral solitons by local distortion of the nuclear lattice [11–14]. However, it still remains an open question whether localization can occur in disorder-free transitionally invariant systems. This question has received much attention recently in the context of many-body localization [15–18].

In this letter we provide evidence from first-principles computations for a new mechanism of localization in 1D conjugated systems, in which the electrons form their own nucleation center without the need to introduce disorder into the Hamiltonian. This challenges the widely accepted picture in which the electronic eigenstates localize only after coupling with the lattice distortion [19]. To illustrate this mechanism, we study the electronic structure and the charge distribution in large one-dimensional systems with ideal geometries (ordered structures). We focus on two representative conjugated polymers, trans-polyacetylene (tPA) and polythiophene (PT), with increasing lengths $L = M\ell_1$ up to $M = 70$ and $M = 20$, respectively (ℓ_1 is the length of the repeat unit). Besides their practical significance [6], tPA and PT also exhibit interesting physical phenomena, in which polarons, bipolarons and solitons affect charge mobility and localization [4, 12, 20–22].

In Figure 6.1 we plot the ionization potentials (IPs) for both tPA (panel a) and PT (panel b) polymers taken as a negative of the highest occupied eigenstate energy of the neutral system -ε_H as a function of the number of repeat units, M. To illustrate the effect of localization we focus on the ionization potential, representing the energy of positive charge carrier (hole), rather than on the electron affinity, representing the energy of the negative charge carrier (electron), since we find the former to localize on shorter length scales (see below). Several levels of theory are used: Hartree-Fock (HF) theory, density functional theory (DFT) within the local density approximation (LDA) [31], the optimally-tuned BNL* [32–34] range-separated hybrid functional [35], and the B3LYP [36] approximation, and, finally, the G_0W_0 many-body perturbation technique [37] within the stochastic formulation (sGW) [38]. The LDA and to some extent the B3LYP approximation lack sufficient exact exchange, while HF

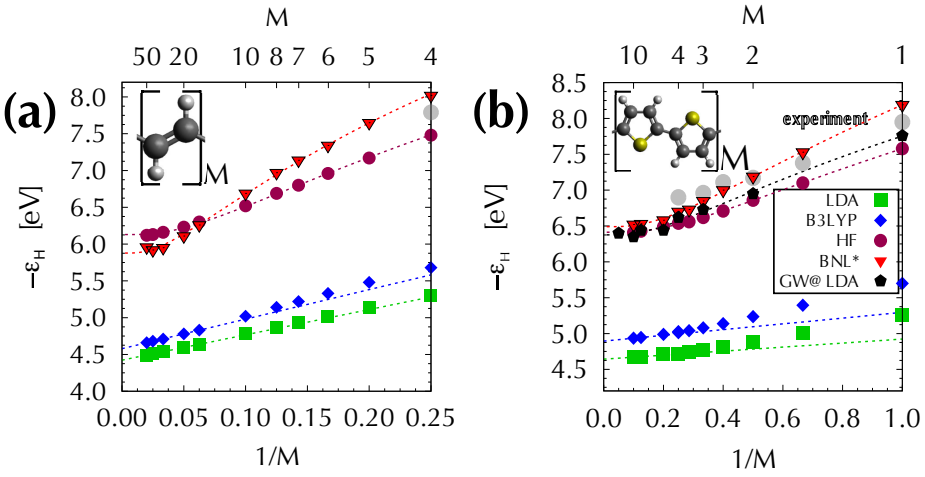

Figure 6.1: Ionization potentials (estimated using the highest occupied eigenenergies ε_H) for **(a)** trans-polyacetylene and **(b)** polythiophene shown against the inverse number of repeat units M in the respective polymer. The repeat unit for each polymer is illustrated in the corresponding insets (C, H and S are shown by black, white and yellow spheres, respectively). Results obtained from different computational approaches are indicated by colors and labelled in the figure. Experimental data for the ionization potentials (gray circles) were taken from Refs. [23–25] and references therein. The dashed lines represent a numerical fit to $-\varepsilon_H(M) = -\varepsilon_H(\infty) + \frac{\Delta\varepsilon}{M}$ for LDA and B3LYP ($\varepsilon_H(\infty)$ and $\Delta\varepsilon$ are fitting parameters) and to $-\varepsilon_H(M) = -\varepsilon_H(\infty) + \Delta\varepsilon \exp\left(-\sqrt{M/M_0}\right)$ for HF, BNL*, and GW. The parameters of the fit are provided in the Supplementary material.

lacks correlations and screening effects. BNL* provides a systematic description of correlations and exact exchange through the process of optimal tuning [39]. G_0W_0 is based on many-body perturbation theory and includes exchange, correlation and screening effects and is widely acknowledged as a technique going beyond the mean-field approaches [40].

Functional	Polymer	ℓ_c/nm	$-\varepsilon_H(\infty)$/eV	σ_∞/nm
HF	tPA	4.9	6.12	0.8
	PT	3.1	6.41	0.9
BNL*	tPA	7.9	5.87	2.3
	PT	4.3	6.69	1.4
GW	PT	4.2	6.4	-

Table 6.1: The critical length l_c and the asymptotic values of the ionization potential $-\varepsilon(\infty)$ and the second moment σ_∞ of the hole density distribution as predicted by HF, BNL* and GW for tPA and PT chains.

The LDA and B3LYP computations yield IPs that are considerably smaller than the experimental values (Figure 6.1), consistent with previous computational studies on shorter polymer chains [41, 42] and with general theoretical

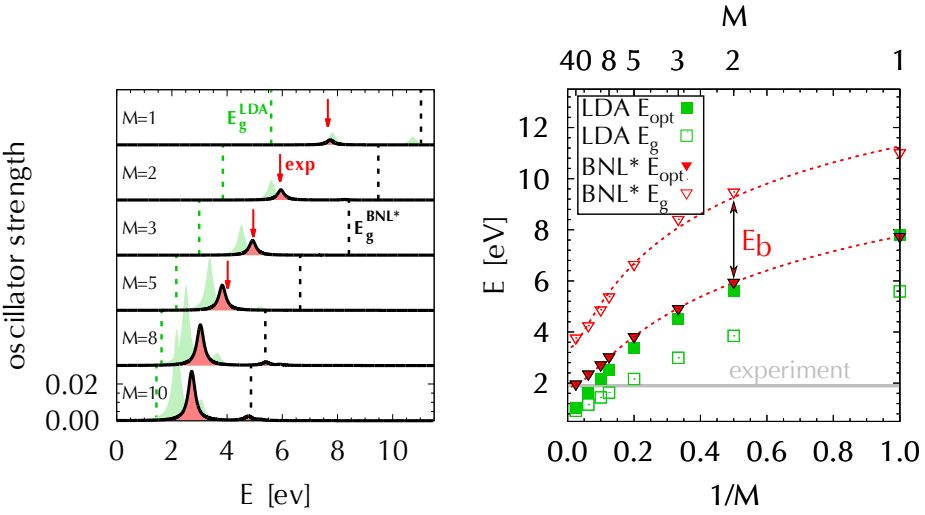

Figure 6.2: **(a)** Calculated optical spectra for selected tPA polymers of various lengths (numbers of repeat units M). All calculations were performed with the cc-pvTZ basis set using TDDFT within the BNL* functional (solid black line with red fill) and LDA functional (green filled curve). The fundamental band gaps are shown by dashed vertical lines in corresponding colors. Red arrows indicate experimental absorption peak positions (Refs. [26–29] and references therein). **(b)** Position of the first maxima of the absorption E_{opt} and the fundamental band gap E_g obtained with BNL* and LDA functionals as function of inverse number of repeat units. Results for the two longest polymers were calculated using the 3-21G basis set, other results are obtained using cc-pvTZ. The exciton binding energy is the difference between E_g and the peak maximum is illustrated by an arrow. The horizontal full line represents the experimental energy of the maximum absorption for the infinite system (1.9 eV) [30].

arguments [43, 44]. These IP values approach their bulk limit asymptotically linearly as M^{-1} (see Supplementary Material, Section 6.4, Table 6.4) for the range of sizes studied and they do not fit the purely non-interacting asymptotic dependence of M^{-2}. By contrast, HF IPs are significantly closer to the experimental values, deviating by less than 0.4 eV. The HF IPs also initially drop as polymer size increases, but for a polymer of length exceeding a critical length l_c they quickly converge to an asymptotic value $-\varepsilon_H(\infty)$, indicating localization of the hole. This is documented in Table 6.1 and the related discussion in the Supplementary material (cf. Figure 6.5), in which the derivative of $-\varepsilon_H$ with respect to the system size is analyzed. The computed IPs using BNL* and sGW are in even better agreement with the available experimental data than those of HF (Figure 6.1). They also show a localization transition for tPA chains longer than 7.9 nm and PT polymers longer than 4.3 nm (details of this estimate are provided in the Supplementary material). Using the results for polymers of intermediate size (which do not exhibit localization yet) we can linearly extrapolate to the limit $M \to \infty$ and estimate the value of ionization potential if no localization occurs; this yields IP values smaller by ≈ 0.5 eV which can be

viewed as the energy of spontaneous localization. While the asymptotic values of the ionization potentials predicted by HF, BNL* and sGW are similar, the BNL* and sGW critical length scales ℓ_c are larger than those predicted by HF. This result is consistent with the tendency of HF to over-localize holes in finite systems [45, 46].

To further strengthen the validity of the BNL* treatment (and indirectly the G_0W_0 which agrees with the BNL*), in Figure 6.2 we compare its predicted optical excitations E_{opt} and *fundamental gaps* $E_g = \varepsilon_L - \varepsilon_H$ (where ε_L is the energy of the lowest unoccupied eigenstate of the neutral system) in tPA to experimental results, where available [26–29] (see Supplementary Material, Table 6.6). The absorption spectra shown in the left panel of Figure 6.2 were calculated using (adiabatic) time-dependent DFT [33, 47, 48]. It is seen that the BNL* approach provides excellent agreement for optical gaps E_{opt}^{BNL*} in comparison with experimental data. This is also illustrated in the right panel of Figure 6.2, where the optical gaps E_{opt} are plotted as a function of $1/M$ and for the largest system studied our results yield the value of the experimental optical gap of the infinite system [30, 49]. In the right panel of Figure 6.2 we also plot the fundamental gap E_g^{BNL*}. The values of E_g^{BNL*} for small systems are in excellent agreement with previous G_0W_0 results [25]. Furthermore, E_g^{BNL*} does not localize for the tPA lengths studied. Since, ε_H^{BNL*} localizes within a length scale of 7.9 nm the persistent change in E_g^{BNL*} for larger polymers must result from a continued change in the eigenenergy ε_L^{BNL*}. This suggests that added negative charge does not yet localize for the tPA sizes studied and this may explain why the finite size gaps are larger than the G_0W_0 gap of 2.1 eV for $L \to \infty$ [20, 50, 51]. Note, however, that the G_0W_0 gaps are rather sensitive to the size of the unit cell and small changes of 0.005 nm in the position of the atoms can lead to significant fluctuation of 2.0 to 4.2 eV in the gaps [52]. Since there are no experimental measurements of the fundamental gap when $L \to \infty$, it still remains an open question as to the length scale at which *electrons* localize (as opposed to hole localization, which already occurs at the system sizes studied). To reach system sizes at which the electron localizes will probably require use of stochastic approach for BNL* [53]. Finally, panel b of Figure 6.2 shows that the exciton binding energy $E_b = E_g - E_{opt}$ is on the order of $E_g/2$ for the larger systems, a value typical of other 1D conjugated systems [54], indicating that neutral excitations are dominated by electron-hole interactions.

Up to now we have studied localization only from the point of view of energy changes. It is instructive to also study localization in terms of the *hole density,* which is the difference $\Delta n(\mathbf{r}) = n^N(\mathbf{r}) - n^{N-1}(\mathbf{r})$ between the ground state density of the neutral (N) and the positively charged $(N-1)$ systems. For non-interacting electrons this quantity equals the density of the highest occupied eigenstate, which is not localized. For interacting electrons, however, $\Delta n(\mathbf{r})$ must be calculated as the difference of densities obtained from two *separate* self-consistent field DFT calculations and can thus exhibit a different behavior. We have also ascertained that the same localization pattern emerges even when an infinitesimal charge $q \to 0$ is removed, showing that localization of the hole density occurs in the linear response regime.

Isosurface plots of the hole densities Δn are given in the upper left and middle panels of Figure 6.3 for the various methods (excluding sGW). In the lower left and middle panels we show the *cumulative* hole densities $\rho(z) =$

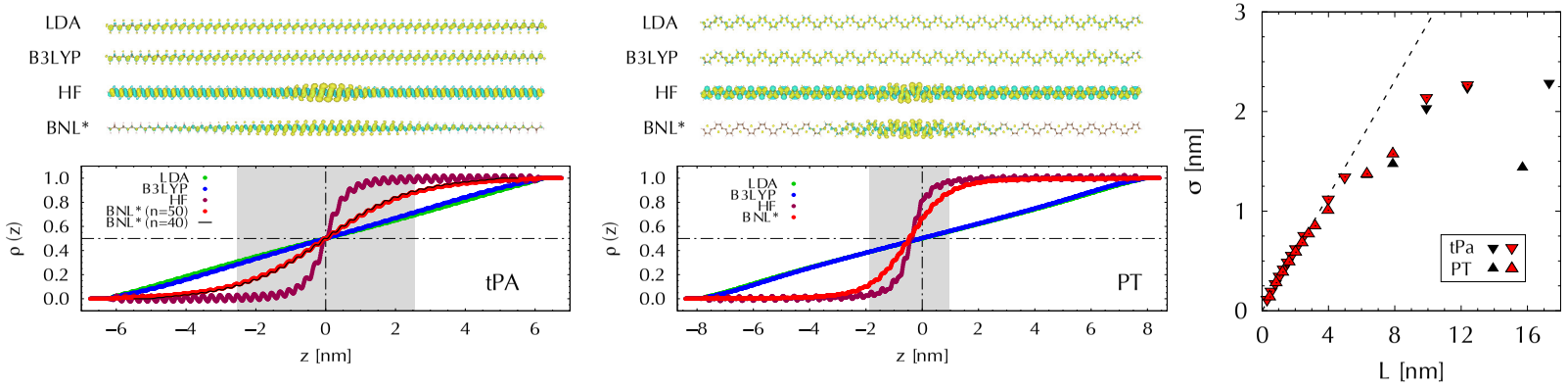

Figure 6.3: Left and middle panels: The hole densities (top), $\Delta n(\mathbf{r})$, for the corresponding labelled methods in long strands of $M = 50$ repeat tPA units (left) and $M = 20$ repeat PT units (middle). The hole is shown as a yellow (aqua) $0.00025a_0^{-3}$ (-$0.00025a_0^{-3}$) density isosurface. In the bottom panels we plot the cumulative density, $\rho(z)$, for different functionals. The cumulative curve for a tPA polymer with $M = 40$ (black line) is practically indistinguishable from $M = 50$ though their length differs by 2.5 nm. Gray areas in the plots show the value of the second cumulant (σ) for the corresponding BNL* hole density, which are plotted in the right panel for different polymer lengths. The dashed straight line in the right panel is the fully delocalized result ($\sigma = L/\sqrt{12}$). Note that for the larger system we used a smaller basis (3-21G, black symbols) which closely follows the results using a larger basis (cc-pvTZ, red symbols).

$\int_{-\infty}^{z} \mathrm{d}z' \int_{-\infty}^{\infty} \mathrm{d}y' \int_{-\infty}^{\infty} \mathrm{d}x' \Delta n(\mathbf{r}')$. In both types of representations it is evident that LDA and B3LYP do not show localization of the hole density in any of the systems studied and in $\rho(z)$ they show linear monotonic increase. By contrast, the HF and BNL* charge distributions localize as observed by change of $\rho(z)$ near the center of the chain. In PT this transition in $\rho(z)$ occurs around one of the S atoms closest to the center of the polymer, due to the lack of mirror plane symmetry. For polymers with $L > \ell_c$, the BNL* hole density hardly changes; this is illustrated by the overlapping $\rho(z)$ of polymers with two distinct length that differ by 25% from each other (M=40 and M=50). This implies that the size of the hole is no longer influenced by the polymer terminal points and is thus independent of system size.

The extent of hole localization can be described by the second cumulant $\sigma = \sqrt{\int \Delta n(\mathbf{r}') (z' - \bar{z})^2 \, d\mathbf{r}'}$ (where $\bar{z} = \int \Delta n(\mathbf{r}') \, z' d\mathbf{r}'$). This is shown in the right panel of Figure 6.3 for BNL*. For small sizes, σ increases as $L/\sqrt{12}$, consistent with a uniform hole density spread over the entire polymer. As L increases beyond ℓ_c, BNL* σ converge to an asymptotic value, σ_∞ (Table 6.1), while those of LDA continue to follow the linear $L/\sqrt{12}$ law (not shown).

It is important to note that the hole density $\Delta n(\mathbf{r})$ is dominated by the minority-spin density changes: the orbitals having the same spin as the removed electron redistribute such as to localize the hole density near the chain center. On the other hand, the majority-spin orbitals remain nearly unperturbed and thus do not contribute to $\Delta n(\mathbf{r})$. This fact reveals that localization is driven by attractive non-local exchange interactions, existing solely between like-spin electrons and the attractive interactions stabilizes the localized hole by ≈ 0.5 eV. This notion is further supported by the fact that localization only appears in methods that account for non-local exchange (HF, BNL*, and G_0W_0).

One of the interesting ramifications of the IP stabilization for polymer length $L > l_c$ is the simultaneous stabilization of the BNL* range-separation parameter γ. This is because in the absence of hole localization the tuning criterion [39], $I + \varepsilon_H = 0$ is expected to become automatically satisfied when (semi)local functionals are used in the limit of infinite system size [45, 55–57] forcing γ (and with it the non-local exchange part of the functional) to drop eventually to zero. It is only through localization that we are able to continue tuning, and the range parameter attains finite asymptotic values of $\gamma^{tPA} = 2.7$ nm^{-1} and $\gamma^{PT} = 3.1$ nm^{-1}. The leveling of γ with L was reported for PT [58], however, it was not previously clear whether γ would level-off for tPA.

While HF supports partial localization (Figure 6.3), its hole density also exhibits oscillations along the entire polymer length that do not diminish with system size. These indicate a rigid shift of charge between neighboring atoms: From double to single C-C bonds in tPA and from S to nearby C atoms for PT. This is consistent with the tendency of HF to eliminate bond-length alternation in the entire tPA polymer chain [59]. In order to examine this effect we have relaxed the structure of charged tPA with M=50 both for HF and BNL. The HF results confirm the elimination of the bond length alternation and a contraction of the central bond due to the charge extraction, as shown in the left panel of Figure 6.4. BNL* on the other hand eliminates the bond-length alternation only in the proximity of the localized hole density (right panel of Figure 6.4), consistent with a localized polaron model.

In summary, using first principles density functional theory and many-body

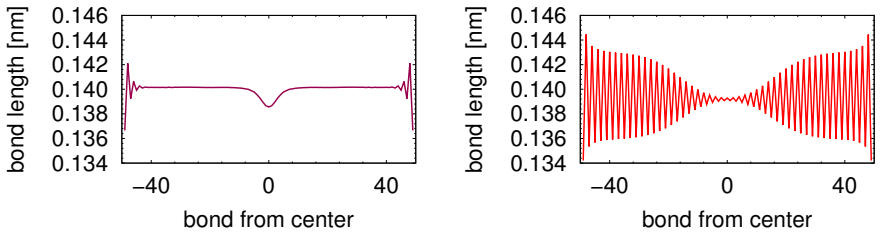

Figure 6.4: The C-C bond length in the charged $M = 50$ tPA polymer as predicted by HF (left panel) and BNL* (right panel) obtained with the 3-21G basis set. In BNL*, a polaron appears in the center of the polymer chain as a reduction of the bond-length alternation, while in the region about 40 C-C bonds away from the polaron, the alternation is increased to 0.007 nm, similar to the experimental value of 0.008 nm for neutral chains [60].

perturbation theory, we have shown that positive charge carriers can localize in 1D conjugated polymers due to a spontaneous, purely electronic symmetry breaking transition. In this case, localization is driven by non-local exchange interactions and thus cannot occur when (semi)local density functional approximations are used. HF theory, which has non-local exchange, shows a localization transition in a relatively small length-scale but predicts complete annihilation of bond-length alternation upon ionization, irrespective of polymer length. BNL*, which through tuning includes a balanced account of local and non-local exchange effects, provides an accurate description of the optical gap in comparison to experiments and shows a localization transition with a length scale (estimated from the leveling off of the IPs) that agrees well with the sGW approach. Moreover, BNL* predicts a localized disruption of the bond-length alternation.

The localization phenomenon is driven by the same-spin attractive non-local exchange interactions and therefore, cannot be explained in terms of classical electrostatics. There is no reason to assume that the observed emergence of the localization length ℓ_c in finite systems will not readily occur also in infinite systems, where hole states near the top of the valence band are necessarily infinitely degenerate.

6.3 Acknowledgements

We thank professors Ulrike Salzner and Leeor Kronik for illuminating discussions on polymers and localization in large systems. R.B. and D.N. are supported by The Israel-USA Binational Science Foundation (Grant No. 201250). V.V. is supported by Minerva Stiftung of the Max Planck Society, R.B. gratefully acknowledges support for his sabbatical visit by the Pitzer Center and the Kavli Institute of the University of California, Berkeley. D.N. and E.R. acknowledge support by the NSF, grants CHE-1112500 and CHE-1465064, respectively. This research used resources of the National Energy Research Scientific Computing Center, a DOE Office of Science User Facility supported by the Office of Science of the U.S. Department of Energy under Contract No. DE-AC02-05CH11231, and at the Leibniz Supercomputing Center of the Bavarian Academy of Sciences

and the Humanities.

6.4 Supplementary material

6.4.1 Methods

DFT

Calculations were performed using NWCHEM [61] with the cc-pVTZ and 3-21G basis sets (the latter for the long systems). We model the polymers as planar chains with M identical repeat units, of length ℓ_1^{tPA}=0.247 nm for a tPA repeat unit which contains 2 carbon atoms and $\ell_1^{PT} = 0.782$ nm for a thiophene repeat unit which contains two thiophene rings (see insets in Figure 6.1). The identical repeat units for each polymer were obtained as the central units of B3LYP/cc-pVTZ optimized chains with 8 repeat units for tPA and 4 repeat units for PT. Cartesian coordinates of of the repeat units in Å, used to model tPA and PT, are given in Tables 6.2 and 6.3. Note that in the case of PT we also model polymers with odd numbers of thiophene rings. We intentionally performed calculations without nuclear-geometry relaxations when adding repeat units in order to observe purely the electronic localization independent of any lattice distortion. We performed additional calculations with nuclear relaxation when looking at bond length alternation (Figure 6.4).

atom type	x [Å]	y [Å]	z [Å]
C	5.65230	0.05154	5.00168
C	5.00000	1.23250	5.00000
H	6.73878	0.05646	5.00466
H	3.91366	1.23229	4.99703

Table 6.2: Position of atoms in the repeat unit of the tPA polymer.

atom type	x [Å]	y [Å]	z [Å]
C	9.78650	4.44954	8.36130
S	9.85070	1.25416	8.83650
C	9.76300	5.87687	8.36390
H	9.70500	3.85951	7.45640
H	9.66300	6.46822	7.46180
C	9.92300	3.90876	9.62660
C	10.00000	0.00000	10.00000
C	9.98130	2.50856	10.00200
C	9.88200	6.41670	9.63110
S	10.02300	5.16293	10.79570
C	10.14930	0.54054	11.26380
C	10.13860	1.96810	11.26490
H	10.24340	2.55868	12.16710
H	10.25727	-0.02888	12.11769

Table 6.3: Position of atoms in the repeat unit of the PT polymer.

Stochastic G_0W_0

Since the system size of the polymers of interest is prohibitively large for commonly used many body perturbation techniques we employed a stochastic formulation of G_0W_0 [38]. The key concept lies in the representing the complex self energy in the statistical sense, i.e. by using a set of random states to characterize the occupied subspace and to use random states to describe a propagator. For details of formulation, see Ref. [38]. We here report results for the IPs of thiophene polymers of large sizes, containing up to 962 valence electrons.

Our calculation used the Kohn-Sham potential and the charge density obtained from a DFT calculation [62] with the LDA exchange correlation functional [31] using Troullier-Martins norm conserving pseudopotentials [63]. The cut-off energy of 28 E_h and 0.5 a_0 regular real space mesh were found sufficient to provide the total energies and eigenvalues converged to within 0.03 eV. The number of real space points used in the calculation were converged with respect to the total energy and the eigenvalue energies, and the mesh sampled regions of at least 6 a_0 from the position of the terminal H atoms. The LDA results were then used to build the stochastic orbitals which are propagated in time to obtain the screened Coulomb potential. In contrast to the original formulation, we made direct use of the highest occupied orbital from the underlying DFT calculation, i.e. this orbital was not described through a stochastic state. By comparing results with different numbers of stochastic states we obtained results converged to better than 0.05 eV with 8 stochastic orbitals for the occupied subspace and 100 stochastic orbitals used to couple the quasiparticle propagator with the screened Coulomb potential (Eq. (9) in Ref. [38]). The stochastic evaluation of the self energy was obtained as a statistical average over more than 1500 iterations in each system studied.

6.4.2 Determination of ℓ_c, the critical length scale

Ionization potentials (IPs), expressed as the negative of the highest occupied orbital energy -ε_H, obtained with the LDA functional drop asymptotically linearly with $1/M$, where M is the number of repeat units , and can be fitted by the form:

$$-\varepsilon_H(M) = -\varepsilon_H(\infty) + \frac{\Delta\varepsilon}{M}, \tag{6.1}$$

where $-\varepsilon_H(\infty)$ is the IP for the infinite polymer and $\Delta\varepsilon$ is a slope parameter. Fit values for the calculated results are given in Table 6.4.

Due to size restrictions, we could not determine whether the B3LYP IPs continue to drop, like those of LDA linearly with $\frac{1}{M}$ or whether B3LYP localizes charge carriers (as e.g. BNL*) but on a considerably longer length scale. Assuming the linear dependence in Eq. (6.1) holds also for B3LYP, .we have fit our results for tPA and PT (Table 6.4).

The HF IPs converge quickly to the asymptotic value $-\varepsilon_H(\infty)$, but clearly in a nonlinear manner. We found that a good model for the energies is given by the following equation (see the dashed lines in Figure 6.1):

$$-\varepsilon_H(M) = -\varepsilon_H(\infty) + \Delta\varepsilon \exp\left(-\sqrt{M/M_0}\right). \tag{6.2}$$

The values of the model parameters, $-\varepsilon_H(\infty)$, $\Delta\varepsilon$, M_0 for which this model best reproduces the calculated $-\varepsilon_H(M)$ are given in Table 6.5. The critical

Functional	Polymer	$-\varepsilon_H(\infty)$/eV	$\Delta\varepsilon$/eV
LDA	tPA	4.4	3.4
	PT	4.6	0.3
B3LYP	tPA	4.6	4.0
	PT	4.9	0.4

Table 6.4: The ionization potentials model parameters (Eq. 6.1) for LDA and B3LYP functionals.

Functional	Polymer	$\varepsilon_H(\infty)$/eV	$\Delta\varepsilon$/eV	M_0	M_C	ℓ_c/nm	σ_∞/nm
HF	tPA	-6.12	11.01	0.91	20	4.9	0.8
	PT	-6.41	11.99	0.18	4	3.1	0.9
BNL*	tPA	-5.87	11.72	1.40	32	7.9	2.3
	PT	-6.69	14.57	0.22	5	4.3	1.4

Table 6.5: The IP model parameters (Eq. 6.2) and the resulting critical lengths beyond which the IP changes by less than $\Delta\varepsilon_{th} = 0.1$ eV. (Note: The critical lengths are given in terms of the number M_C of repeat units and in physical length $\ell_c = \ell_1 M_C$ where ℓ_1 is the length of a repeat unit). The estimated size of the hole σ_∞ in an infinite polymer is given as well (see Figure 6.3).

size M_C is chosen according to the criterion that for all $M > M_C$ the deviation $\varepsilon_H(M) - \varepsilon_H(\infty)$ as smaller than a predefined threshold $\Delta\varepsilon_{th}$ (taken as 0.1 eV):

$$M_C = \left(\log\left(\frac{\Delta\varepsilon_{th}}{\Delta\varepsilon}\right)\right)^2 M_0. \tag{6.3}$$

This parameter is also shown in Table 6.5 and we found $M_C^{tPA} = 20$ ($\ell_c^{tPA} = 4.9$ nm) for tPA and a much more localized hole $M_C^{PT} = 4$ ($\ell_c^{PT} = 3.1$ nm) for PT. The fact that the IPs converge to their asymptotic values in HF and BNL* calculations is illustrated also in Figure 6.5 where the derivative of $-d\varepsilon/d(M^{-1})$ (obtained by finite differences) is shown together with the analytical derivative of our model (Eq. 6.2).

We applied the same polymer size-dependence analysis to IPs calculated using BNL* with local correlation (shown in Figure 6.5). Following Eqs. (6.2) and (6.3) we find (see Table 6.5) a hole with $M_C^{tPA} = 20$ ($\ell_c^{tPA} = 7.9$ nm) for tPAand considerably more localized $M_C^{PT} = 5.5$ ($\ell_c^{TP} = 4.3$ nm) for PT. Additionally, we also employed gradient corrected correlation functionals (PBEc [64] and LYPc [65]) and found them to yield IP values lower by ∼0.4 eV but their dependence on M^{-1} has almost identical shape and the range separation parameters do not change significantly ($< 0.2\,\mathrm{nm}^{-1}$) when LYP/PBE correlation is used instead of LDA in the BNL* calculation.

6.4.3 Exciton Energy and Size

We calculated optical absorption spectra and fundamental gaps for selected tPA polymers using adiabatic LDA, BNL* and TDHF approaches. The fundamental (E_g) and optical gaps (E_{opt}) are reported in Table 6.6. We here provide a more detailed discussion of the LDA and TDHF results as the BNL* results are discussed in the paper itself.

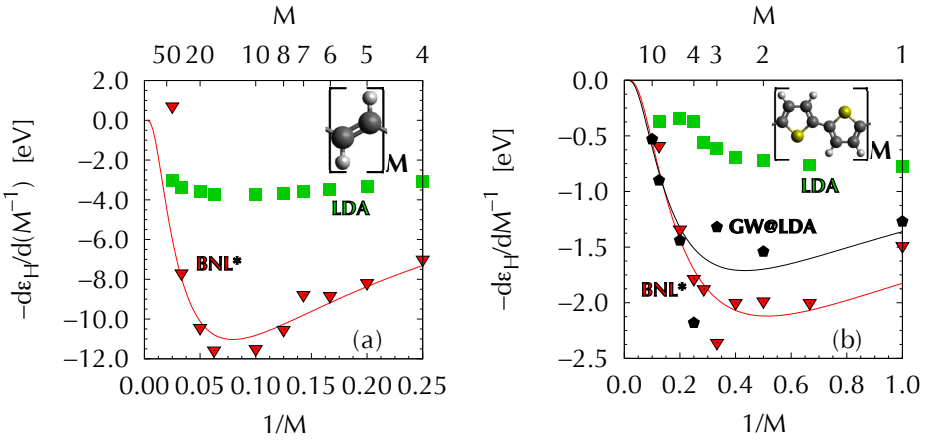

Figure 6.5: The derivative of the ionization potential for (a) tPA and (b) PT with respect to the inverse length of the polymer (given in the number of repeat units M) is shown for results of LDA, BNL* and GW@LDA in green squares, red triangles and black pentagons colors respectively. The analytical derivative of the model fit given in Eq. (6.2) is shown by full line in respective colors.

The ALDA optical gaps E_{opt}^{ALDA} are close to available experimental results [26–29] but consistently lower by 0.2-0.3 eV. Furthermore, E_{opt}^{LDA} are larger than the corresponding LDA fundamental gaps E_g^{LDA}, and hence $E_b^{LDA} = E_g^{LDA} - E_{opt}^{LDA}$, the exciton binding energy, is predicted to be negative in LDA. This corresponds to an unbound exciton (hole and electron do not attract and stay close together). Even for the infinite polymer length the binding energy does not become positive although $E_b^{LDA} \to 0$ in this limit (see the right panel of Figure 6.2). The infinite length asymptotic limit of the LDA optical gap can be obtained from fitting the results to the model of Eq. (6.2), leading to the result $E_{opt}^{LDA}(\infty) = 1.4$ eV. This is 0.5 eV lower than the experimental estimate of the infinite optical gap, $E_{opt}^{exp}(\infty) = 1.9$ eV [30].

The TDHF results exhibit peaks shifting to lower energies with increasing system size and in general very close to the experimental observations available for small polymers. Since HF does not allow for binding an extra electron in the system, i.e. the lowest unoccupied eigenvalue is larger than the vacuum level, fundamental gaps of HF thus coincide with the ionization potentials and the exciton is strongly bound. Extrapolating our results for long chains containing up to 40 repeat units, the TDHF exciton binding energy in an infinite polymer is significantly greater than 3 eV, with the maximum of the optical absorption being at 2.7 eV, based on the model fit using Eq. (6.2). This is however significantly larger than experiments, where the absorption maximum occurs at 1.9 eV [30].

M	BNL*		LDA		HF		Exp.
	E_{opt}	E_g	E_{opt}	E_g	E_{opt}	E_g	E_{opt}
1	7.74	11.02	7.81	5.59	7.49	10.12	7.65
2	5.95	9.48	5.60	3.85	5.98	8.68	5.92
3	4.92	8.41	4.52	2.99	5.11	7.95	4.95
5	3.82	6.65	3.37	2.16	4.55	7.48	4.02
8	3.03	5.38	2.51	1.63	4.16	7.18	-
10	2.72	4.87	2.17	1.44	3.51	6.69	-
16†	2.36	4.25	1.60	1.16	3.06	6.85	-
40†	1.97	3.77	1.03	0.92	2.77	5.99	-

Table 6.6: Fundamental (E_g) and optical gaps (E_{opt}) given in units of eV, for various tPA polymers containing M repeat units. The two longest polymers (M=16 and 40, indicated by a dagger) were calculated with the 3-21G basis set while the rest of the results were computed with the cc-pvTZ basis set.

Bibliography

[1] P. W. Anderson, Phys. Rev. **109**, 1492 (1958).

[2] N. F. Mott, Rev. Mod. Phys. **40**, 677 (1968).

[3] D. Basko, I. Aleiner, and B. Altshuler, Ann. Phys. **321**, 1126 (2006).

[4] R. H. Friend, R. W. Gymer, A. B. Holmes, J. H. Burroughes, R. N. Marks, C. Taliani, D. D. C. Bradley, D. A. Dos Santos, J. L. Bredas, M. Lögdlund, et al., Nature **397**, 121 (1999).

[5] T. Brandes and S. Kettemann, *Anderson Localization and Its Ramifications: Disorder, Phase Coherence, and Electron Correlations*, vol. 630 (Springer Science & Business Media, 2003).

[6] G. D. Scholes and G. Rumbles, Nat. Mater. **5**, 683 (2006).

[7] J. E. Johns, E. A. Muller, J. M. J. Frechet, and C. B. Harris, J. Am. Chem. Soc. **132**, 15720 (2010).

[8] D. P. McMahon and A. Troisi, ChemPhysChem **11**, 2067 (2010).

[9] M. Lannoo, *Point Defects in Semiconductors I: Theoretical Aspects*, vol. 22 (Springer Science & Business Media, 2012).

[10] R. Noriega, J. Rivnay, K. Vandewal, F. P. Koch, N. Stingelin, P. Smith, M. F. Toney, and A. Salleo, Nat. Mater. **12**, 1038 (2013).

[11] W. Kurlancheek, R. Lochan, K. Lawler, and M. Head-Gordon, J. Chem. Phys. **136**, 054113 (2012).

[12] U. Salzner, Wiley Interdiscip. Rev. Comput. Mol. Sci. **4**, 601 (2014).

[13] T. Körzdörfer and J.-L. Brédas, Acc. Chem. Res. **47**, 3284 (2014).

[14] A. Köhler and H. Bässler, *Electronic Processes in Organic Semiconductors: An Introduction* (John Wiley & Sons, 2015).

[15] N. Yao, C. Laumann, J. I. Cirac, M. Lukin, and J. Moore, arXiv preprint arXiv:1410.7407 (2014).

[16] W. De Roeck and F. Huveneers, Phys. Rev. B **90**, 165137 (2014).

[17] J. M. Hickey, S. Genway, and J. P. Garrahan, arXiv preprint arXiv:1405.5780 (2014).

[18] M. Schiulaz, A. Silva, and M. Müller, Phys. Rev. B **91**, 184202 (2015).

[19] T. Holstein, Ann. Phys. **8**, 325 (1959).

[20] P. Puschnig and C. Ambrosch-Draxl, Synth. Met. **135-136**, 415 (2003).

[21] I. H. Nayyar, E. R. Batista, S. Tretiak, A. Saxena, D. L. Smith, and R. L. Martin, J. Phys. Chem. Lett. **2**, 566 (2011).

[22] S. T. Hoffmann, F. Jaiser, A. Hayer, H. Bässler, T. Unger, S. Athanasopoulos, D. Neher, and A. Köhler, J. Am. Chem. Soc. **135**, 1772 (2013).

[23] D. Jones, M. Guerra, L. Favaretto, A. Modelli, M. Fabrizio, and G. Distefano, J. Phys. Chem. **94**, 5761 (1990).

[24] D. A. d. S. Filho, V. Coropceanu, D. Fichou, N. E. Gruhn, T. G. Bill, J. Gierschner, J. Cornil, and J.-L. Brédas, Philos. Trans. A. Math. Phys. Eng. Sci. **365**, 1435 (2007).

[25] M. Pinheiro, M. J. Caldas, P. Rinke, V. Blum, and M. Scheffler, Phys. Rev. B **92**, 195134 (2015).

[26] R. McDiarmid, J. Chem. Phys. **64**, 514 (1976).

[27] W. M. Flicker, O. A. Mosher, and A. Kuppermann, Chem. Phys. Lett. **45**, 492 (1977).

[28] K. L. D'Amico, C. Manos, and R. L. Christensen, J. Am. Chem. Soc. **102**, 1777 (1980).

[29] J. L. Bredas, R. Silbey, D. S. Boudreaux, and R. R. Chance, J. Am. Chem. Soc. **105**, 6555 (1983).

[30] A. Feldblum, J. H. Kaufman, S. Etemad, A. J. Heeger, T. C. Chung, and A. G. MacDiarmid, Phys. Rev. B **26**, 815 (1982).

[31] J. P. Perdew and Y. Wang, Phys. Rev. B **45**, 13244 (1992).

[32] R. Baer and D. Neuhauser, Phys. Rev. Lett. **94**, 043002 (2005).

[33] R. Baer, E. Livshits, and U. Salzner, Annu. Rev. Phys. Chem. **61**, 85 (2010).

[34] L. Kronik, T. Stein, S. Refaely-Abramson, and R. Baer, J. Chem. Theory Comput. **8**, 1515 (2012).

[35] A. Savin and H.-J. Flad, Int. J. Quantum Chem. **56**, 327 (1995).

[36] A. D. Becke, J. Chem. Phys. **98**, 5648 (1993).

[37] M. S. Hybertsen and S. G. Louie, Phys. Rev. B **34**, 5390 (1986).

[38] D. Neuhauser, Y. Gao, C. Arntsen, C. Karshenas, E. Rabani, and R. Baer, Phys. Rev. Lett. **113**, 076402 (2014).

[39] E. Livshits and R. Baer, Phys. Chem. Chem. Phys. **9**, 2932 (2007).

[40] G. Stefanucci and R. van Leeuwen, *Nonequilibrium Many-Body Theory of Quantum Systems: A Modern Introduction* (Cambridge University Press, 2013).

[41] U. Salzner, J. Phys. Chem. A **114**, 10997 (2010).

[42] U. Salzner and A. Aydin, J. Chem. Theory Comput. **7**, 2568 (2011).

[43] U. Salzner and R. Baer, J. Chem. Phys. **131**, 231101 (2009).

[44] T. Stein, J. Autschbach, N. Govind, L. Kronik, and R. Baer, J. Phys. Chem. Lett. **3**, 3740 (2012).

[45] P. Mori-Sánchez, A. J. Cohen, and W. Yang, Phys. Rev. Lett. **100** (2008).

[46] E. Livshits and R. Baer, J. Phys. Chem. A **112**, 12789 (2008).

[47] T. Stein, L. Kronik, and R. Baer, J. Am. Chem. Soc. **131**, 2818 (2009).

[48] G. Onida, L. Reining, and A. Rubio, Rev. Mod. Phys. **74**, 601 (2002).

[49] G. Leising, Phys. Rev. B **38**, 10313 (1988).

[50] M. Rohlfing and S. G. Louie, Phys. Rev. Lett. **82**, 1959 (1999).

[51] S. Rohra, E. Engel, and A. Görling, Phys. Rev. B **74**, 045119 (2006).

[52] A. Ferretti, G. Mallia, L. Martin-Samos, G. Bussi, A. Ruini, B. Montanari, and N. M. Harrison, Phys. Rev. B **85**, 235105 (2012).

[53] D. Neuhauser, E. Rabani, Y. Cytter, and R. Baer, ArXiv p. arXiv:1510.08519v1 (2015).

[54] F. Wang, G. Dukovic, L. E. Brus, and T. F. Heinz, Science **308**, 838 (2005).

[55] R. W. Godby and I. D. White, Phys. Rev. Lett. **80**, 3161 (1998).

[56] S. Öğüt, J. R. Chelikowsky, and S. G. Louie, Phys. Rev. Lett. **79**, 1770 (1997).

[57] V. Vlček, H. R. Eisenberg, G. Steinle-Neumann, L. Kronik, and R. Baer, J. Chem. Phys. **142**, 034107 (2015).

[58] T. Körzdörfer, J. S. Sears, C. Sutton, and J.-L. Brédas, J. Chem. Phys. **135**, 204107 (2011).

[59] L. Rodrigues-Monge and S. Larsson, J. Chem. Phys. **102**, 7106 (1995).

[60] C. S. Yannoni and T. C. Clarke, Phys. Rev. Lett. **51**, 1191 (1983).

[61] M. Valiev, E. Bylaska, N. Govind, K. Kowalski, T. Straatsma, H. Van Dam, D. Wang, J. Nieplocha, E. Apra, T. Windus, et al., Comput. Phys. Commun. **181**, 1477 (2010).

[62] Y. Zhou, Y. Saad, M. L. Tiago, and J. R. Chelikowsky, J. Comput. Phys. **219**, 172 (2006).

[63] N. Troullier and J. L. Martins, Phys. Rev. B **43**, 1993 (1991).

[64] J. P. Perdew, K. A. Jackson, M. R. Pederson, D. J. Singh, and C. Fiolhais, Phys. Rev. B **46**, 6671 (1992).

[65] C. Lee, W. Yang, and R. G. Parr, Phys. Rev. B **37**, 785 (1988).

Chapter 7

Stochastic GW calculations on large thiophene polymers

Vojtěch Vlček[1,2], Eran Rabani[3,4], Daniel Neuhauser[5], Roi Baer[1,6]

7.1 Abstract

We review in detail the stochastic formulation of the GW approximation and discuss the advantages of this formalism over common approaches. We employ stochastic GW for calculations on large thiophene polymers in 1D (as isolated chains) or 2D (as stacked polythiophene molecules), containing up to 1446 electrons. We demonstrate the practical calculations of the self-energies and show that with increasing system size the approach becomes effectively less expensive. leading to approximately linear scaling of the algorithm. For the 1D systems we confirm the presence of a recently discovered spontaneous quasiparticle localization, for the stacked polythiophene molecules the localization is not observed. This suggests that the spontaneous quasiparticle localization is either limited to 1D systems, or occurs on much larger lengthscales in higher dimensions.

[1]Fritz Haber Center for Molecular Dynamics, Institute of Chemistry, The Hebrew University of Jerusalem, Jerusalem 91904, Israel

[2]Bayerisches Geoinstitut, Universität Bayreuth, 95440 Bayreuth, Germany

[3]Department of Chemistry, University of California and Materials Science Division, Lawrence Berkeley National Laboratory, Berkeley, California 94720, U.S.A.

[4]The Sackler Center for Computational Molecular and Materials Science, Tel Aviv University, Tel Aviv 69978, Israel

[5]Department of Chemistry and Biochemistry, University of California, Los Angeles, California 90095, U.S.A.

[6]On sabbatical in the Department of Chemistry, University of California, Berkeley, California 94720, U.S.A.

7.2 Introduction

First principles calculations of electronic structure play central role in predicting and understanding behavior of matter at the nanoscale, and their development is one of the thriving fields in theoretical physics and chemistry. Highly accurate methods can be applied only to small systems with few electrons. Density functional theory (DFT) [1, 2] has proven to be a reliable tool for the prediction of ground state properties, and with the currently available numerical implementations and computational power, calculations for extremely large systems with thousands of electrons [3–5] are possible. Nevertheless, DFT is limited to the ground state and, in principle, cannot provide quasiparticle properties which are often required. The only exception is the lowest energy needed to remove an electron from the system (ionization potential) which it should predict exactly, in principle [6, 7]. Nevertheless, DFT falls short in terms of accuracy and yields ionization potential (IP) values with substantial deviation from experiment in many cases [8–12].

Quasiparticle energies are crucial not only from a theoretical perspective, but also for characterizing the possible excited states of systems under external influence; most notably for the prediction and analysis of photoemission spectra that directly characterize the electronic states within the system and ultimately help to design new (opto)electronic devices [13–18]. Theories beyond DFT, based on the many-body perturbation approach, are thus usually needed for the description of quasiparticle states. An established technique is the *GW* approximation [13, 19–23], which is the central point of this paper. Standard implementations of *GW* pose significant computational demands [24, 25] and are thus limited to relatively small systems with several tens of electrons. In this paper, we review in detail a recently developed stochastic formulation of *GW* [26] which overcomes many of the significant limitations and allows us to calculate systems of unprecedented sizes, as it scales approximately linearly with system size. We illustrate the technique on large thiophene polymers.

In a recent study [27] we have shown that in 1D strands of conjugated polymers the ionization potentials become independent of the system length and the associated quasiparticles (holes) spontaneously localize and break the periodicity of the underlying ionic lattice. Our finding has a significant bearing on the understanding of the formation of quasiparticles (QPs) in extended 1D systems and the theory of electronic structure in such systems: While the individual ground state electronic eigenstates span the whole polymer and ultimately correspond to the Bloch states in an infinite system, the QP size is finite and as such its properties depend solely on its immediate neighborhood. Such spontaneous charge localization can be a precursor of other phenomena, such as creation of self-trapped states [28–30], which subsequently lead to the formation of polarons, bipolarons or solitons [31–35] that were observed to be created by ionization on very short timescales [36]. Detailed understanding of these processes is thus necessary for further wide technological application of conjugated polymers in electronics [37–40].

In the present paper, we use the example of planar polythiophene (PT) chains with ideal periodic geometry within the polymer chain and investigate this phenomenon in 1D systems of increasing length. To determine whether this behavior may be observed in systems with higher spatial dimensions, we perform calculations on stacked PT molecules (containing up to 20 thiophene

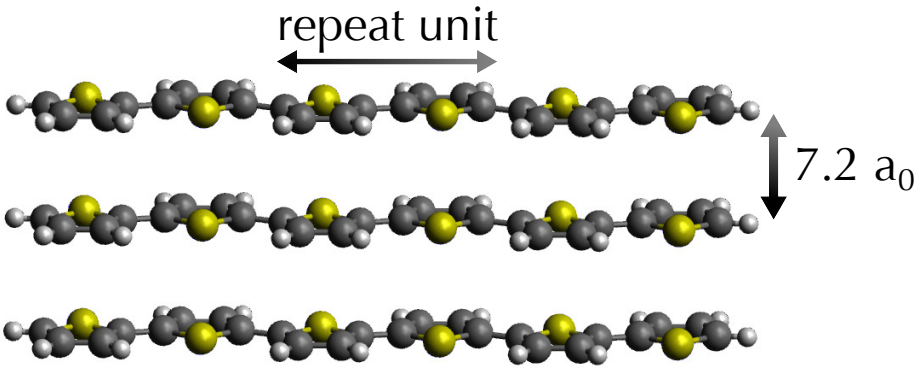

Figure 7.1: Example of a system with three parallel stacked molecules of PT with 3 repeat units in each layer (each containing 2 thiophene rings). Yellow spheres denote S, black C and white spheres H positions. The distance between two adjacent layers of PT is 7.2 a_0.

rings in three layers - see Figure 7.1). The stochastic formulation of the *GW* approximation [26] is used for systems which contain up to 1446 electrons. The paper is organized as follows: In Section 7.3 we provide a detailed description of the stochastic formulation of the *GW* approximation and emphasize its major merits. Next we show its computational performance together with the actual results for the PT polymers and a detailed discussion on the role of various contributions to the QP energy (Section 7.4). Our findings are summarized together with the implications for DFT in Section 7.5.

7.3 Stochastic formulation of the *GW* approximation

7.3.1 *GW* theory in the energy domain

From the perspective of many body theory, the dynamics of a quasiparticle introduced in the ground state of the system at point $\mathbf{r}$ and time $t = 0$ is described by a Green's function $G(\mathbf{r}, \mathbf{r}', t)$, from which the probability amplitude to propagate to point $\mathbf{r}'$ within time $t > 0$ (for quasielectrons) and $-t > 0$ (for quasiholes) is discerned. More accurately, the Green's function is defined by

$$iG(\mathbf{r}, \mathbf{r}', t) = \left\langle \Psi_0^N \left| T\left[\hat{\psi}(\mathbf{r}', t)\, \hat{\psi}^\dagger(\mathbf{r})\right] \right| \Psi_0^N \right\rangle. \tag{7.1}$$

The Fourier transform of the Green's function to frequency domain can be expressed in the Lehman representation as a sum of over poles (atomic units are used throughout the paper) as:

$$G(\mathbf{r}, \mathbf{r}', \omega) = \lim_{\eta \to 0^+} \hbar \sum_i \frac{\psi_i^{N\pm1*}(\mathbf{r}')\, \psi_i^{\mathrm{N}\pm1}(\mathbf{r})}{\hbar\omega - \varepsilon_i^{N\pm1} \pm i\eta}, \tag{7.2}$$

where ω is the frequency and η is a small real number shifting the pole of G along the imaginary frequency axis. The real poles of the function are the quasiparticle energies $\varepsilon_i^{N\pm1} = \mp\left(E_i^{N\pm1} - E_0^N\right)$ (the top/bottom sign corresponds

to electrons/holes) where formally E_i^N is the i^{th} energy eigenvalue of the many-body Hamiltonian for N electrons ($E_i^N \leq E_{i+1}^N$, $i = 0, 1, 2...$). The so-called Dyson orbitals in Eq. (7.2) are defined by

$$\psi_i^{N-1}(\mathbf{r}) = \left\langle \Psi_i^{N-1} \left| \hat{\psi}(\mathbf{r}) \right| \Psi_0^N \right\rangle \tag{7.3}$$

and

$$\psi_i^{N+1}(\mathbf{r}) = \left\langle \Psi_i^{N+1} \left| \hat{\psi}^\dagger(\mathbf{r}) \right| \Psi_0^N \right\rangle, \tag{7.4}$$

where Ψ_i^N is the i^{th} eigenstate of the many-body Hamiltonian for Nelectrons and $\hat{\psi}(\mathbf{r})$ /$\hat{\psi}^\dagger(\mathbf{r})$ are the annihilation/creation operators of an electron at space points $\mathbf{r}$.

It is possible to write a formal quasiparticle equation for these quantities:

$$-\frac{\hbar^2}{2m_e}\nabla^2\psi_i^{\mathrm{N}\pm1}(\mathbf{r}) + V_{ext}(\mathbf{r})\,\psi_i^{\mathrm{N}\pm1}(\mathbf{r}) + V_H(\mathbf{r})\,\psi_i^{\mathrm{N}\pm1}(\mathbf{r}) + \int \Sigma\left(\mathbf{r}, \mathbf{r}', \varepsilon_i^{N\pm1}\right)\psi_i^{\mathrm{N}\pm1}(\mathbf{r}')\,\mathrm{d}\mathbf{r}' = \varepsilon_i^{N\pm1}\psi_i^{\mathrm{N}\pm1}(\mathbf{r}), \tag{7.5}$$

which is similar to a Schrödinger equation, containing kinetic energy and potential energy terms, but having mean electrostatic interaction term, given by the Hartree potential energy

$$V_H(\mathbf{r}) = \int n(\mathbf{r}')\,v(|\mathbf{r}-\mathbf{r}'|)\,d\mathbf{r}', \tag{7.6}$$

where $n(\mathbf{r}) = \sum_i \left|\psi_i^{\mathrm{N}-1}(\mathbf{r})\right|^2$ is the ground-state density of the N electron system and $v(|\mathbf{r}-\mathbf{r}'|) = \frac{e^2}{4\pi\epsilon_0|\mathbf{r}-\mathbf{r}'|}$ is the bare Coulomb potential energy, while a non-local energy-dependent self-energy term $\Sigma(\mathbf{r}, \mathbf{r}', \omega)$ describes the many-body exchange and correlation effects. In actual applications, the self energy is approximated using Hedin's theory [19, 21–23]

$$\Sigma(\mathbf{r}, \mathbf{r}', \omega) = \lim_{\tau\to 0^+} i\int_{-\infty}^{\infty}\frac{d\omega'}{2\pi}G(\mathbf{r}, \mathbf{r}', \omega-\omega')\,W^{TO}(\mathbf{r}, \mathbf{r}', \omega')\,e^{-i\omega'\tau}. \tag{7.7}$$

$W^{TO}(\mathbf{r}, \mathbf{r}', \omega')$ is the time-ordered screened potential energy of an electron at $\mathbf{r}'$ due to a unit charge placed at position $\mathbf{r}$ which can be obtained from the retarded screened potential energy $W(\mathbf{r}, \mathbf{r}', \omega)$ by the following transform (omitting $\mathbf{r}, \mathbf{r}'$for brevity) [41]:

$$W^{TO}(\omega) = \mathrm{Re}W(\omega) + \mathrm{sign}(\omega)\,\mathrm{Im}W(\omega). \tag{7.8}$$

When the quasiparticle is added to the system, it polarizes the electrons of the system, creating a perturbation in electron density at point $\mathbf{r}''$ of magnitude $n_{ind}(\mathbf{r}|\,\mathbf{r}'', \omega)$. The screened potential energy $W(\mathbf{r}, \mathbf{r}', \omega)$ at point $\mathbf{r}'$ can then be expressed in terms of two contributions: the bare Coulomb potential energy $v(|\mathbf{r}-\mathbf{r}'|)$ from to the quasiparticle itself, and the potential energy due to the induced density perturbation $n_{ind}(\mathbf{r}|\,\mathbf{r}'', \omega)$, resulting in

$$W(\mathbf{r}, \mathbf{r}', \omega) = v(|\mathbf{r}-\mathbf{r}'|) + \int n_{ind}(\mathbf{r}|\,\mathbf{r}'', \omega)\,v(|\mathbf{r}''-\mathbf{r}'|)\,\mathrm{d}\mathbf{r}''. \tag{7.9}$$

Finally, the induced density can be calculated from linear response theory using the reducible polarizability $\chi(\mathbf{r},\mathbf{r}',\omega)$, i.e. the Fourier transform of the response function:

$$\chi(\mathbf{r},\mathbf{r}',\omega) = \frac{\delta n_{ind}(\mathbf{r}',\omega)}{\delta v_{ext}(\mathbf{r})}, \tag{7.10}$$

which describes the density perturbation $\delta n_{ind}(\mathbf{r}',\omega)$ at $\mathbf{r}'$ induced by an external potential perturbation $\delta v_{ext}(\mathbf{r})$. In our case $\delta v_{ext}(\mathbf{r})$ is the Coulomb potential of the added quasiparticle and thus equals to $v(|\mathbf{r}-\mathbf{r}'''|)$. This then yields the final expression for W:

$$\begin{aligned} W(\mathbf{r},\mathbf{r}',\omega) =& v(|\mathbf{r}-\mathbf{r}'|) + \\ & \iint v(|\mathbf{r}-\mathbf{r}'''|)\,\chi(\mathbf{r}''',\mathbf{r}'',\omega)\,v(|\mathbf{r}''-\mathbf{r}'|)\,\mathrm{d}\mathbf{r}''\mathrm{d}\mathbf{r}'''. \end{aligned} \tag{7.11}$$

It should be noted that the screened potential W, can be in principle obtained from the Green's function itself [13, 19, 21–23]. However, in our work we circumvent this as we will show below.

To summarize the above description, the GW approximation involves the following algorithm applied until self consistency is achieved:

GW **Algorithm**

1. Set iteration number $i = 0$ and a starting approximate self energy Σ_0.
2. Solve the single particle equations (Eq. 7.5) with Σ_i as the self energy and obtain the Dyson orbitals $\psi^{N\pm1}$ and energies $\varepsilon^{N\pm1}$.
3. Using $\psi^{N\pm1}$ and $\varepsilon^{N\pm1}$ within the Lehman representation of Eq. (7.2) obtain the Green's function for the i^{th} iteration, G_i.
4. Combining G_i and the screened potential energy W of Eq. (7.11), use Eq. (7.7) to obtain a new estimate for the self-energy Σ_{i+1}.
5. Increment $i \to i+1$ and repeat steps 2-4 until convergence.

7.3.2 The G_0W approach based on a Kohn-Sham reference

A numerical implementation of the full GW approach as described in the previous subsection is extremely demanding when large systems are treated. For this reason we follow Ref. [20] and take the Kohn-Sham (KS) system as a reference from which the starting self-energy Σ_0 (in the algorithm above) is taken and then the QP energies are computed through a first order perturbation approach avoiding the self-consistency cycle altogether. This method is commonly called the G_0W approximation.

In KS-DFT a system of non-interacting fermions trapped together in the so-called KS potential well $V_{KS}(\mathbf{r})$ is found, such that its ground state density is identical to that of the physical electronic system. Each of these fermions must be in a distinct eigenstate $\phi_i(\mathbf{r})$ of the KS Hamiltonian,

$$\hat{h}\phi_i(\mathbf{r}) = \varepsilon_i\phi_i(\mathbf{r}), \tag{7.12}$$

with $\hat{h} = -\frac{\hbar^2}{2m_e}\nabla^2 + V_{KS}(\mathbf{r})$. It is customary to order the KS eigenvalues of $\hat{h}$ such that $\varepsilon_i < \varepsilon_{i+1}$, $i = 1, 2, ...$ The first N eigenvalues are considered "occupied" while all other eigenstates are "unoccupied". Because the particles are non-interacting the KS states $\phi_{i\leq N}(\mathbf{r})$ are the quasihole Dyson orbitals of the non-interacting system. Similarly, $\phi_{i>N}(\mathbf{r})$, are the corresponding quasielectron Dyson orbitals. We will henceforth assume that the KS states are real. The common KS potential $V_{KS}(\mathbf{r})$ is given in terms of the external (nuclear) potential, the Hartree potential and a so-called exchange correlation potential $V_{XC}(\mathbf{r})$, which is usually a local or semilocal functional of the density:

$$V_{KS}(\mathbf{r}) = V_{ext}(\mathbf{r}) + V_H(\mathbf{r}) + V_{XC}(\mathbf{r}). \tag{7.13}$$

By inserting this expression for $V_{KS}(\mathbf{r})$ into Eq. (7.12) we find, upon comparison to Eq. (7.5), that the difference between the quasiparticle equation of the interacting particles and that of the non-interacting ones is the replacement of V_{XC} by Σ.

If the difference $\Sigma - V_{XC}$ is small in some sense, we can use perturbation theory to find a first order correction for the quasiparticle energy based on the KS calculation and write

$$\varepsilon_i^{N-1} - \varepsilon_{N-i} \approx \left\langle \phi_{N-i} \middle| \hat{\Sigma}_1\left(\hbar^{-1}\varepsilon_i^{N-1}\right) - \hat{V}_{XC} \middle| \phi_{N-i} \right\rangle \tag{7.14}$$

and

$$\varepsilon_i^{N+1} - \varepsilon_{N+1+i}^{KS} \approx \left\langle \phi_{N+i+1} \middle| \hat{\Sigma}_1\left(\hbar^{-1}\varepsilon_i^{N+1}\right) - \hat{V}_{XC} \middle| \phi_{N+i+1} \right\rangle, \tag{7.15}$$

where Σ_1 is calculated from Eq. (7.7) using G_0 instead of G, with

$$\begin{aligned} G_0(\mathbf{r}, \mathbf{r}', \omega) &= \lim_{\eta \to 0^+} \hbar \sum_i \phi_i(\mathbf{r}')\phi_i(\mathbf{r}) \\ &\times \left[\frac{f_i}{\hbar\omega - \varepsilon_i - i\eta} + \frac{1 - f_i}{\hbar\omega - \varepsilon_i + i\eta}\right]. \end{aligned} \tag{7.16}$$

Symbolically we therefore write: $\hat{\Sigma}_1 = G_0 W$, hence the name G_0W approximation, which in essence is the first SCF iteration in the GW algorithm. In Eq. (7.16) f_i is the orbital occupation, equal to 1 for occupied KS states and 0 for unoccupied states. One can also write f_i as the zero temperature Fermi-Dirac occupation $f_i = f(\mu - \varepsilon_i) = \lim_{\beta\to\infty} F_\beta(\mu - \varepsilon_i)$, where

$$F_\beta(\mu - \varepsilon) = \frac{1}{1 - e^{\beta(\varepsilon - \mu)}} \tag{7.17}$$

is the Fermi-Dirac function and $\mu = \frac{\varepsilon_{N+1} + \varepsilon_N}{2}$ is the zero temperature limit of the chemical potential. This choice of μ ensures that the number of occupied KS eigenstates is equal to the number of electrons: $\sum_i f_i = N$, as appropriate for non-interacting fermions.

The actual equation we solve for estimating for the lowest energy quasihole energy $\tilde{\varepsilon}_0^{N-1}$ is therefore

$$\tilde{\varepsilon}_0^{N-1} = \hbar\Omega\left(\tilde{\varepsilon}_0^{N-1}\right), \tag{7.18}$$

where [19, 20]

$$\hbar\Omega(\varepsilon) = \varepsilon_N^{\mathrm{KS}} + \left\langle \phi_N \middle| \hat{\Sigma}\left(\hbar^{-1}\varepsilon\right) - \hat{V}_{XC} \middle| \phi_N \right\rangle. \tag{7.19}$$

Summarizing, the G_0W approach involves the following procedure: First, a Kohn-Sham DFT calculation is performed on the system, determining the KS eigenstates and eigenvalues from which G_0 is defined. This is equivalent to steps 1-3 of the GW algorithm for the first iteration ($i = 0$). Next, the first cycle approximation to Σ_1 is used in a perturbative way to estimate the correction to the quasiparticle energy using Eqs (7.14) and (7.15).

7.3.3 GW in time domain

The G_0W approximation of the previous subsection, while considerably simplifying the full GW approach, is still a numerical challenge for systems of appreciable size. The numerical effort typically scales proportionally to N^4 or N^5 [24, 25]. We will now focus on the stochastic GW formulation [26] (sGW) which allows for a linear scaling G_0W and can hence be applied to very large electronic systems.

In order to develop a stochastic formulation of the G_0W method, we move from the frequency to the time domain, defining

$$G_0\left(\mathbf{r},\mathbf{r}',t\right) \equiv \int_{-\infty}^{\infty} G_0\left(\mathbf{r},\mathbf{r}',\omega\right) e^{-i\omega t} \frac{d\omega}{2\pi}. \tag{7.20}$$

Using Eq. (7.16) and the integral identity

$$\hbar \int_{-\infty}^{\infty} \frac{e^{-i\omega t}}{\hbar\omega - \varepsilon_i \mp i\eta} \frac{d\omega}{2\pi} = \pm i e^{-i\varepsilon_i t/\hbar} \theta\left(\mp t\right), \tag{7.21}$$

where $\theta\left(t\right)$ is the Heaviside function, we find:

$$iG_0\left(\mathbf{r},\mathbf{r}',t\right) = \lim_{\eta\to 0^+} \sum_i \phi_i\left(\mathbf{r}'\right)\phi_i\left(\mathbf{r}\right) e^{-i\varepsilon_i t/\hbar} \left[\left(1-f_i\right)\theta\left(t\right) - f_i\theta\left(-t\right)\right]. \tag{7.22}$$

Hence, the Green's function can be expressed as a matrix element of the Green's operator $G_0\left(\mathbf{r},\mathbf{r}',t\right) = \left\langle \mathbf{r}' \left| \hat{G}_0\left(t\right) \right| \mathbf{r} \right\rangle$, where

$$\hat{G}_0\left(t\right) = \hat{G}_0^{>}\left(t\right)\theta\left(t\right) - \hat{G}_0^{<}\left(t\right)\theta\left(-t\right) \tag{7.23}$$

is given in terms of the the greater/lesser evolution operators for the quasielectron/quasihole, namely

$$i\hat{G}_0^{<}\left(t\right) = e^{-i\hat{h}t/\hbar} f_\mu\left(\hat{h}\right) \tag{7.24}$$

and

$$i\hat{G}_0^{>}\left(t\right) = e^{-i\hat{h}t/\hbar}\left(1 - f_\mu\left(\hat{h}\right)\right). \tag{7.25}$$

We note that at time $t = 0$ the lesser Greens function gives the density matrix:

$$\left\langle \mathbf{r}' \left| iG_0^{<}\left(0\right) \right| \mathbf{r} \right\rangle = \left\langle \mathbf{r}' \left| f_\mu \right| \mathbf{r} \right\rangle = n\left(\mathbf{r},\mathbf{r}'\right). \tag{7.26}$$

In terms of the time domain Green's function the G_0W approximation for the self energy is

$$\Sigma(\mathbf{r},\mathbf{r}',t) = iG_0(\mathbf{r},\mathbf{r}',t)\,W^{TO}\left(\mathbf{r},\mathbf{r}',t^+\right), \tag{7.27}$$

where the symbol t^+ means that in cases where the ordering of times is important, the time in the expression for W^{TO} should be assumed infinitesimally later than t. $W^{TO}(\mathbf{r},\mathbf{r}',t)$ is the Fourier transform of $W^{TO}(\mathbf{r},\mathbf{r}',\omega)$ given in terms of the retarded screened potential $W(\mathbf{r},\mathbf{r}',\omega)$ (Eq. 7.8). The Fourier transform of $W(\mathbf{r},\mathbf{r}',\omega)$, can be written as:

$$W(\mathbf{r},\mathbf{r}',t) \quad = \quad v(|\mathbf{r}-\mathbf{r}'|)\,\delta(t) + W_P(\mathbf{r},\mathbf{r}',t). \tag{7.28}$$

The meaning of $W(\mathbf{r},\mathbf{r}',t)$ can be elucidated by considering the following problem: Suppose we add an external charge $n_1(\mathbf{r})$ to the system and remove it an infinitesimally small time $\delta\tau$ later, and then we monitor the change in potential energy of a "test-charge density" $n_2(\mathbf{r}')$ a time t later ($t \geq 0$). This energy is described by the screened potential energy as:

$$\delta E(t) = \delta\tau \iint n_1(\mathbf{r})\,W(\mathbf{r},\mathbf{r}',t)\,n_2(\mathbf{r}')\,d\mathbf{r}d\mathbf{r}'. \tag{7.29}$$

Immediately following the addition of the charge, the system's electrons have no time to react and the potential is given by

$$v_1(\mathbf{r}) = \int n_1(\mathbf{r}')\,v(|\mathbf{r}'-\mathbf{r}|)\,d\mathbf{r}'. \tag{7.30}$$

Hence, we may write

$$\delta E(t) = \delta(t)\int v_1(\mathbf{r})\,n_2(\mathbf{r})\,d\mathbf{r} + \delta E_P(t), \tag{7.31}$$

where the first term is the instantaneous bare interaction between the external potential and the test charge distributions $n_2(\mathbf{r})$. The second term,

$$\delta E_P(t) = \delta\tau \iint n_1(\mathbf{r})\,W_P(\mathbf{r},\mathbf{r}',t)\,n_2(\mathbf{r}')\,d\mathbf{r}d\mathbf{r}', \tag{7.32}$$

is a "polarization" energy, stemming from the interaction between the test charge density and the induced density change $\delta n^{ind}(\mathbf{r},t)$ in the system:

$$\delta E_P(t) \quad = \quad \iint \delta n^{ind}_{\delta\tau}(\mathbf{r},t)\,v(\mathbf{r},\mathbf{r}')\,n_2(\mathbf{r}')\,d\mathbf{r}d\mathbf{r}'. \tag{7.33}$$

We note that $\delta n^{ind}_1(\mathbf{r},t)$ can be described by the retarded reducible polarization function:

$$\delta n^{ind}_{\delta\tau}(\mathbf{r},t) = \delta\tau \int v_1(\mathbf{r}'')\,\chi(\mathbf{r}'',\mathbf{r},t)\,d\mathbf{r}''. \tag{7.34}$$

The self-energy of Eq. (7.27) can be written as a sum of an exchange at time (slightly less than) zero and a polarization self-energy $\Sigma_P(\mathbf{r},\mathbf{r}',t)$:

$$\Sigma(\mathbf{r},\mathbf{r}',t) = \Sigma_X(\mathbf{r},\mathbf{r}')\,\delta\left(t^+\right) + \Sigma_P(\mathbf{r},\mathbf{r}',t). \tag{7.35}$$

For the exchange energy we have to use $G(0^-) = -G_0^<(0)$, which follows from Eq. (7.23) and thus:

$$\Sigma_X(\mathbf{r},\mathbf{r}') = -n(\mathbf{r},\mathbf{r}')\, v(|\mathbf{r}-\mathbf{r}'|). \tag{7.36}$$

The polarization self-energy is:

$$\Sigma_P(\mathbf{r},\mathbf{r}',t) = iG_0(\mathbf{r},\mathbf{r}',t)\, W_P^{TO}(\mathbf{r},\mathbf{r}',t^+). \tag{7.37}$$

These exchange and polarization self energies are non-local operators. Application of these operators to a wave function leads to high algorithmic complexity which prevents the use of GW in large systems. As we now show, a stochastic formulation of the GW theory allows for an efficient evaluation even for large systems.

7.3.4 Stochastic representation of G_0 in real time

Application of the KS and GW methods require a representation of the single particle Hilbert space. We use a real space 3D Cartesian mesh of equally spaced grid points $\mathbf{r}_{ijk} = (i\hat{\mathbf{x}} + j\hat{\mathbf{y}} + k\hat{\mathbf{z}})\, d$, where $\hat{\mathbf{x}}$, $\hat{\mathbf{y}}$, and $\hat{\mathbf{z}}$ are unit vectors in the Cartesian x, y and z directions, i, j and k are integers and d is the grid spacing. For economy of notation we usually drop the ijk subscript. A mesh for systems of current interest usually consists of $10^5 - 10^7$ grid points. The Green's function $\hat{G}_0(t)$ thus becomes a huge matrix $G_0(\mathbf{r},\mathbf{r}',t)$, so a more economic representation is mandatory.

For this, we introduce a set of random states on the mesh:

$$\zeta(\mathbf{r}) \equiv \langle \mathbf{r}|\zeta\rangle = \frac{\exp[i\vartheta(\mathbf{r})]}{d^{\frac{3}{2}}}, \tag{7.38}$$

where $0 \le \vartheta(\mathbf{r}) < 2\pi$ is a *random phase variable* at each grid point $\mathbf{r}$. It is possible to show that the expectation value (expressed by an over-bar) of the projection $|\zeta\rangle\langle\zeta|$ is equal to the unit matrix,

$$\overline{|\zeta\rangle\langle\zeta|} = \hat{\mathbb{1}}(\mathbf{r},\mathbf{r}') = \delta_{\mathbf{r}\mathbf{r}'}, \tag{7.39}$$

giving a "stochastic resolution of identity" [42]. In practical calculations we estimate the expectation values using the average of a finite sample of N_ζ random states. According to the central limit theorem this average will converge to the expectation value as $N_\zeta \to \infty$ (for a discussion of convergence of the stochastic estimates see Section 7.4.1).

The fact that $|\zeta\rangle\langle\zeta|$ is the unit operator means we can insert it into any operator equation. For example, the projection operator on the occupied space $f_\mu\left(\hat{h}\right)$ can be written – using the stochastic resolution of the identity – as

$$f_\mu\left(\hat{h}\right) = f_\mu\left(\hat{h}\right)\overline{|\zeta\rangle\langle\zeta|} f_\mu\left(\hat{h}\right). \tag{7.40}$$

From this we obtain the stochastic representation of the lesser ($t \le 0$) Green's function:

$$G_0^<(\mathbf{r},\mathbf{r}',t) = \left\langle \mathbf{r}' \middle| \hat{G}_0^<(t) \middle| \mathbf{r} \right\rangle = \overline{\zeta^<(\mathbf{r}',t)\,\zeta^<(\mathbf{r})}, \tag{7.41}$$

where

$$\zeta^{<}(\mathbf{r}) = \langle \mathbf{r}| f_\mu\left(\hat{h}\right)|\zeta\rangle \tag{7.42}$$

and

$$\zeta^{<}(\mathbf{r}',t) = \theta(-t)\langle \mathbf{r}'| e^{-i\hat{h}t/\hbar}\left|\zeta^{<}\right\rangle. \tag{7.43}$$

A similar representation can be obtained for the greater Green's function:

$$i\hbar G_0^{>}(\mathbf{r},\mathbf{r}',t) = \overline{\zeta^{>}(\mathbf{r}',t)\,\zeta^{>}(\mathbf{r})}, \tag{7.44}$$

where

$$\zeta^{>}(\mathbf{r}',t) = \theta(t)\langle \mathbf{r}'| e^{-i\hat{h}t/\hbar}\left|\zeta-\zeta^{<}\right\rangle. \tag{7.45}$$

Note that $\zeta^{>}$ at $t=0$ is obtained from $\zeta-\zeta^{<}$. The final form of the Green's function is

$$G_0(\mathbf{r}',\mathbf{r},t) = \overline{\zeta^{>}(\mathbf{r}',t)\,\zeta^{>}(\mathbf{r})} - \overline{\zeta^{<}(\mathbf{r}',t)\,\zeta^{<}(\mathbf{r})}. \tag{7.46}$$

In practice, the stochastic wave function $\zeta^{<}$ in Eq. (7.42) can be represented as a series

$$\left|\zeta^{<}\right\rangle = \sum_{i=0}^{N_C} a_i(\mu)\left|\zeta^{i}\right\rangle, \tag{7.47}$$

where ζ^i are defined by the recursive iteration

$$\zeta^{i+1} = 2\hat{h}_N\zeta^i - \zeta^{i-1} \tag{7.48}$$

and $\zeta^0=\zeta$, $\zeta^1=\hat{h}_N\zeta$. $\hat{h}_N$ is the shifted-scaled Hamiltonian $\hat{h}_N=\frac{\hat{h}-\bar{E}}{\Delta E}$, designed such that its eigenvalues are in the interval $[-1,1]$, where $\bar{E}=\frac{E_{max}+E_{min}}{2}$ and $\Delta E=\frac{E_{max}-E_{min}}{2}$; E_{max} and E_{min} are the maximum and minimum eigenvalues of $\hat{h}$. The series is truncated to include only a finite number of terms N_C, which is governed by the size of the gap [43].

The series in Eq. (7.47) and the iteration scheme of Eq. (7.48) result from the Chebyshev expansion of the projection operator $f_\mu\left(\hat{h}\right)$ and allow a considerable simplification of the computational problem by embedding it in a Krylov subspace of much smaller size than the original Hilbert space.

7.3.5 Stochastic calculation of $\left\langle \phi_i\left|\hat{\Sigma}_X\right|\phi_i\right\rangle$

Using Eq. (7.26) we can express the density matrix as an average over a product of the occupied-projected stochastic states:

$$n(\mathbf{r},\mathbf{r}') = \overline{\zeta^{<}(\mathbf{r})\,\zeta^{<}(\mathbf{r}')}. \tag{7.49}$$

It is important to note that we never form the matrix $n(\mathbf{r},\mathbf{r}')$ and use the above expression instead. This leads to a simplified calculation of the expectation value of the exchange energy $\left\langle \phi_i\left|\hat{\Sigma}_X\right|\phi_i\right\rangle = -\iint \phi_i(\mathbf{r}')\,\phi_i(\mathbf{r})\,n(\mathbf{r},\mathbf{r}')\,v(|\mathbf{r}-\mathbf{r}'|)\,d\mathbf{r}d\mathbf{r}'$ in Eq. (7.36), where the 6-dimensional integral is calculated as an average of two 3 dimensional integrals, each of which scales linearly with system size.

The detailed procedure involves an auxiliary stochastic density $n_i(\mathbf{r}) = \phi_i(\mathbf{r})\zeta^<(\mathbf{r})$ and its Hartree potential, calculated as

$$V_i(\mathbf{r}) = -\int v(|\mathbf{r}-\mathbf{r}'|)\, n_i(\mathbf{r}')\, d\mathbf{r}', \tag{7.50}$$

with which the expectation value of the exchange energy is the average of the integral of the potential with the auxiliary density:

$$\left\langle \phi_i \left| \hat{\Sigma}_X \right| \phi_i \right\rangle = \overline{\int n_i(\mathbf{r})\, V_i(\mathbf{r})\, d\mathbf{r}}. \tag{7.51}$$

7.3.6 Stochastic calculation of $\left\langle \phi_i \left| \hat{\Sigma}_P \right| \phi_i \right\rangle$

Similar to Σ_X, we will evaluate $\left\langle \phi_i \left| \hat{\Sigma}_P(t) \right| \phi_i \right\rangle$ directly from Eq. (7.46) which for occupied KS states leads to

$$\left\langle \phi_i \left| \hat{\Sigma}_P(t) \right| \phi_i \right\rangle = -\overline{\iint \mathrm{d}\mathbf{r}\zeta^<(\mathbf{r})\,\phi_i(\mathbf{r})\, W_P^{TO}(\mathbf{r},\mathbf{r}',t)\,\phi_i(\mathbf{r}')\,\zeta^<(\mathbf{r}',t)\,\mathrm{d}\mathbf{r}'}. \tag{7.52}$$

We have two quantities that depend on time t, and using a stochastic orbital $\psi(\mathbf{r})$ (exploiting the identity $\overline{\psi(\mathbf{r}'')\psi(\mathbf{r}')} = \delta(\mathbf{r}''-\mathbf{r}')$) we separate them to form an average of a product of time-dependent functions:

$$\left\langle \phi_i \left| \hat{\Sigma}_P(t) \right| \phi_i \right\rangle = -\overline{\frac{\delta E_P^{TO}(t)}{\delta\tau} O(t)}, \tag{7.53}$$

where the overlap and energy components are

$$O(t) = \int \psi(\mathbf{r})\,\phi_i(\mathbf{r})\,\zeta^<(\mathbf{r},t)\,\mathrm{d}\mathbf{r} \tag{7.54}$$

and

$$\delta E_P^{TO}(t) = \delta\tau \iint \zeta^<(\mathbf{r})\,\phi_i(\mathbf{r})\, W_P^{TO}(\mathbf{r},\mathbf{r}',t)\,\psi(\mathbf{r}')\, d\mathbf{r}'\mathrm{d}\mathbf{r}, \tag{7.55}$$

respectively. $\delta\tau$ is a small time interval (see below).

Referring to Eq. (7.32) we see that the second term is the screened potential energy change when two stochastic charge distributions $n_1(\mathbf{r}) = \zeta^<(\mathbf{r})\,\phi_i(\mathbf{r})$ and $n_2(\mathbf{r}') = \psi(\mathbf{r}')$ interact in the presence of the system.

While the evaluation of $O(t)$ is straightforward, the calculation of $\delta E_P^{TO}(t)$ requires furtehr discussion. We first introduce the potential $v_1(\mathbf{r})$ of Eq. (7.30) as

$$v_1(\mathbf{r}) = \int \zeta^<(\mathbf{r}')\,\phi_i(\mathbf{r}')\, v(|\mathbf{r}'-\mathbf{r}|)\, d\mathbf{r}'. \tag{7.56}$$

We then calculate the *retarded* δE_P from Eq. (7.32), which in our present context becomes

$$\delta E_P(t) = \iint \delta n_{\delta\tau}^{ind}(\mathbf{r},t)\, v(|\mathbf{r}-\mathbf{r}'|)\,\psi(\mathbf{r}')\, d\mathbf{r}'\mathrm{d}\mathbf{r}. \tag{7.57}$$

This requires knowledge of the induced density $\delta n_{\delta\tau}^{ind}(\mathbf{r},t)$, defined in Eq. (7.34), and is estimated using time dependent (TD) DFT [44, 45]. We expose the system to an impulse potential $v_1(\mathbf{r})$ for an infinitesimal duration $\delta\tau$. Then,

$\delta n_{\delta\tau}^{ind}(\mathbf{r},t)$ is expressed as the difference between the time propagated density and the ground-state density of the system:

$$\delta n_{\delta\tau}^{ind}(\mathbf{r},t)=\sum_{n=1}^{N}\left|\phi_n(\mathbf{r},t)\right|^2-n(\mathbf{r}), \tag{7.58}$$

where $\phi_n(\mathbf{r},t)$ $(n=1,2,\ldots,N)$ are the time-dependent KS orbitals. The effect of the impulsive potential is achieved by perturbing each state $\phi_n(\mathbf{r},t)$ at time $t=0$:

$$\phi_n(\mathbf{r},t=0)=e^{-\frac{i}{\hbar}v_1(\mathbf{r})\delta\tau}\phi_n(\mathbf{r}). \tag{7.59}$$

For $t>0$ we evolve $\phi_n(\mathbf{r},t)$ according to the time-dependent Hartree (TDH) equations:

$$i\hbar\frac{\partial}{\partial t}\phi(\mathbf{r},t)=\left(\hat{h}+\int\delta n_{\delta\tau}(\mathbf{r}',t)\,v(|\mathbf{r}-\mathbf{r}'|)\,d\mathbf{r}'\right)\phi(\mathbf{r},t). \tag{7.60}$$

This procedure involves an $O\left(N^2\right)$ effort. If we want to use the full set of occupied KS orbitals, this will lead us right back to a high scaling algorithm which we wanted to avoid. Therefore, in Eq. (7.60) we use the stochastic representation of the time dependent density,

$$\delta n_{\delta\tau}(\mathbf{r},t)=\overline{\left|\xi_{\delta\tau}^{<}(\mathbf{r},t)\right|^2-\left|\xi_{\delta\tau=0}^{<}(\mathbf{r},t)\right|^2}, \tag{7.61}$$

where $\xi_{\delta\tau}^{<}(\mathbf{r},t)$ is propagated by the *stochastic* TDH equations,

$$i\hbar\frac{\partial}{\partial t}\xi_{\delta\tau}^{<}(\mathbf{r},t)=\left(\hat{h}+\int\left(\overline{\left|\xi_{\delta\tau}^{<}(\mathbf{r}',t)\right|^2}-\overline{\left|\xi_{\delta\tau}^{<}(\mathbf{r}',0)\right|^2}\right)v(|\mathbf{r}-\mathbf{r}'|)\,d\mathbf{r}'\right)\xi_{\delta\tau}^{<}(\mathbf{r},t), \tag{7.62}$$

starting from the perturbed ($\delta\tau>0$) or unperturbed ($\delta\tau=0$) occupied-projected stochastic orbitals:

$$\xi_{\delta\tau}^{<}(\mathbf{r},0)=e^{-\frac{i}{\hbar}v_1(\mathbf{r})\delta\tau}\xi^{<}(\mathbf{r}). \tag{7.63}$$

Note that the even without a perturbation, namely when $\delta\tau=0$, the stochastic orbitals are not stationary since they do not start as the eigenstates of the KS Hamiltonian $\hat{h}_{KS}$. The induced density is thus given as

$$\delta n_{\delta\tau}^{ind}(\mathbf{r},t)=\delta n_{\delta\tau>0}(\mathbf{r},t)-\delta n_{\delta\tau=0}(\mathbf{r},t). \tag{7.64}$$

Using this equation we evaluate Eq. (7.57) and obtain $\delta E_P(t)$. Note that the induced density in Eq. (7.64) and the resulting screened potential energy change are retarded (causal) quantities, but the GW formalism requires use of time-ordered ones. As mentioned earlier the difference between the time-ordered and retarded quantities is clearly observed in the frequency domain (Eq. 7.8). The behavior of the time-ordered screened potential W^{TO} in the complex frequency plane is governed by χ^{TO} – in the same way as W is related to χ in Eq. (7.11) –, which has poles at the excitation energies of the system. While the retarded function is holomorphic in either upper or lower half-plane, the time ordered function exhibits poles for both positive and negative complex frequencies. This can be viewed as a consequence of Eq. (7.21), in which the imaginary parts of the denominator in the frequency domain change its sign for

positive and negative times in the time domain. We can thus transform the retarded potential into the time-ordered one by requesting these properties to hold through Eq. (7.8). Since the properties of $\delta E_P(t)$ are governed by W, we can employ the same type of transformation here. We first multiply $\delta E_P(t)$ by a regularization function $\exp\left(-\gamma^2 t^2/2\right)$ and perform the Fourier transform to the frequency domain, obtaining $\delta E_P(\omega)$. Here we choose γ such that the range of the Fourier transfom is finite. We select the maximum time of propagation τ, employed in the evaluation of δn^{ind} (Eq. 7.57), such that $\tau = 3/\gamma$. The time ordered screened potential energy is then obtained as

$$\delta E_P^{TO}(\omega) = \text{Re}\delta E_P(\omega) + \text{sign}(\omega)\,\text{Im}\delta E_P(\omega), \tag{7.65}$$

which is transformed back to time domain, yielding $\delta E_P^{TO}(t)$. Finally we can evaluate the expectation value of the polarization part of the self energy by Eq. (7.53).

7.3.7 Algorithm for sGW

In the two preceding subsections, we have shown how the expectation values of the exchange and polarization part of the self energy are obtained in principle; here, the practical implementation will be summarized. The evaluation of Σ_X is straightforward and is performed with several $\zeta^<$ (for actual numbers see the section on convergence of the sGW algorithm). The polarization part Σ_P requires closer inspection. The crucial aspect of the evaluation of Σ_P is the description of the induced density (Eq. 7.64) which requires substantially more stochastic states to average over in comparison to the Green's function (Eq. 7.46).

Since the evaluation of the exchange and polarization part of the self energy is independent of each other, we have the freedom to use the stochastic states for different purposes in each computational step. In practice, the expectation value of the self-energy – applied to the eigenstate ϕ_i of the KS Hamiltonian – is obtained by performing the following steps:

1. We take N_ζ stochastic states ζ which are used to calculate the expectation value of Σ_X (Eq. 7.51) via the auxiliary potential (Eq. 7.50).

2. We take *again* the same stochastic states ζ (sic!), which are now used to describe the *induced density* (Eq. 7.64).

3. We take a single random state ξ to characterize the occupied/unoccupied subspace $\xi^</\xi^>$ and propagate it as in Eq. (7.43) to yield the Green's function.

4. For each choice of ξ, we pick a new set of N_ψ stochastic states ψ to describe the resolution of identity (Eq. 7.53).

5. Using the KS state ϕ and the random states ψ and ξ we calculate N_ψ overlaps $O(t)$, defined in Eq. (7.54) as $O(t) = \int \psi(\mathbf{r}')\,\phi_i(\mathbf{r}')\,\xi^<(\mathbf{r}', t)\,\mathrm{d}\mathbf{r}'$.

6. Using the KS state ϕ and the random states ψ, ξ we calculate the N_ψ retarded potential energy $\delta E_P(t)$ defined in Eq. (7.57).

7. We perform the time-ordering transformation given in Eq. (7.65) on each of the N_ψ functions $\delta E_P(t)$.
8. We combine the results of steps 2-7 and obtain the expectation value of Σ_P via Eq. (7.53).
9. We combine Σ_X with the Fourier transform of Σ_P to the frequency domain and calculate the quasiparticle shift via Eq. (7.19).
10. Steps 1-9 are repeated till the quasiparticle shift is converged.

Note that the whole algorithm is repeated many times. A single state ξ in each iteration was found to be fully sufficient as the convergence is driven by how accurately δn^{ind} is obtained at each step. To clarify we illustrate the algorithm in Figure 7.3.7.

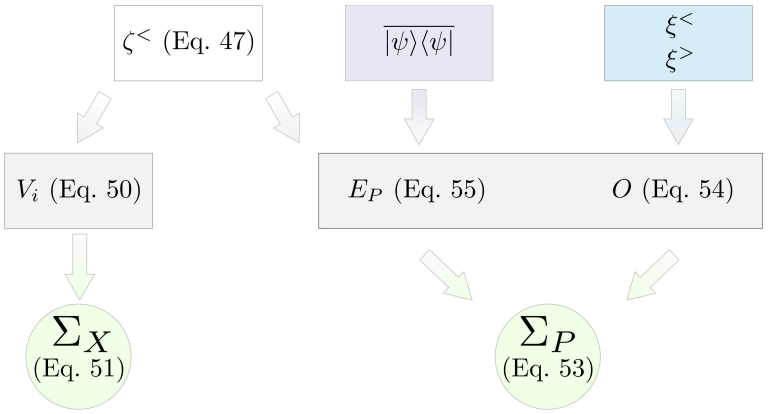

Figure 7.2: A schematic representation of the evaluation of the self energy components Σ_X and Σ_P through the stochastic GW formalism. The figure depicts a single iteration and is repeated N times; the resulting self energy is averaged over N iterations and the procedure is repeated till a desired accuracy in Σ is reached. The random states generated at the beginning of each iteration are shown in the top row. The auxiliary quantities which are derived in Section 7.3 are shown in gray rectangles in the middle and are combined to calculate the individual contributions to the self energy shown in green circles.

7.3.8 Discussion of the computational aspects of stochastic GW

The conventional methods construct $G_0(\mathbf{r}, \mathbf{r}', t)$ and $W(\mathbf{r}, \mathbf{r}', t)$ from the KS eigenstates and the self energy is obtained as a 6-dimensional integral over space

(i.e. all real-space points on the regular grid). This represents a computationally demanding task and inhibits the use of such methods for large systems. In the stochastic approach, we are able to decouple the integration to obtain 3-dimensional integrals. This is shown in the preceding sections for both Σ_X and Σ_P. Hence, the complexity of the calculation reduces significantly and scales approximately linearly with system size, allowing us to treat systems of unprecedented sizes.

Furthermore, note that the stochastic approach reduces the workload by using the Chebyshev projection: The conventional approaches construct the Green's function, polarizability and the screened potential directly from the KS eigenstates, yet again such computations are demanding as the eigenstates have to be stored and form a bottleneck limiting the maximum size of the system which can be treated with current computational resources. This has already been mentioned in the preceding section when the evaluation of the induced density was discussed. The Chebyshev expansion of the Fermi-Dirac occupation function (Eq. 7.47) allows us to obtain the occupied subspace from the stochastic states. This represents a considerable simplification and translates the problem to a Krylov subspace of much smaller size than the original Hilbert space. In practice, we employ the projection to obtain: (i) the auxiliary potential (Eq. 7.50) used to calculate Σ_X; (ii) the Green's function for the polarization part of the self energy; and (iii) the induced density which is used to calculate the polarization potential.

Finally, note that in the conventional GW approaches the polarization potential is calculated via an explicit evaluation of the inverse dielectric function ϵ^{-1}. While it can be obtained directly from the reducible polarizability as mentioned above (Eq. 7.11), it is more common to first evaluate the dielectric function ϵ (via the irreducible polarizability constructed from the Green's function [19, 21–23]) and then invert it to obtain ϵ^{-1}. While this method is consistent with the original formulation of Hedin's equations and allows for their iterative solution to self-consistency, it is actually applied even when a G_0W approach is used. Given that the dielectric function is evaluated for a large number of frequencies, and for each given frequency it represents a matrix that depends on two coordinates $\mathbf{r}$ and $\mathbf{r}'$, inversion of ϵ represents another limiting factor that effectively determines the maximum size of the system that is computationally accessible.

Aside from exceptions [46], the dielectric function usually employs the evaluation of the polarizability via the Adler-Wiser relation [47, 48] which requires explicit sums over a large number of unoccupied states. This significantly increases the size of the dielectric matrix at given frequency and – due to the computationally demanding matrix inversion – makes such GW calculation expensive. As mentioned earlied, in our approach, the explicit evaluation of ϵ^{-1} is avoided (though it is possible in principle), and we directly evaluate the screened potential via TDH or TDDFT equations. The former approach has been applied here and is equivalent to the commonly used random phase approximation (RPA). Note that in Eq. (7.60) we can readily go beyond the RPA approach, i.e. we include not only the induced Hartree potential, but also the term describing change in the exchange and correlation potential. In such an approach, the screened potential will also include the mutual quasiparticle interactions [13], and this will be examined further in future studies.

7.4 Results and Discussion

7.4.1 Convergence of the sGW calculations

In the following, we model the PT polymers as planar chains with M identical repeat units which contain two thiophene rings (length $\ell_1^{PT} = 0.782$ nm, cf. Ref. [27]). Moreover, we construct 2D systems formed by stacking three individual PT chains with a distance of $7.2\,a_0$ as illustrated in Figure 7.1.

For our starting DFT calculations we use the Chebyshev filtering approach [49] with an local density approximation (LDA) XC functional [50] using Troullier-Martins norm-conserving pseudopotentials [51]. A cut-off energy of 28 E_h and a 0.5 a_0 regular real space mesh are found sufficient to converge the total energies and eigenvalues to within 1 mE_h. The number of real-space points used in the calculation is converged with respect to the total energy and the eigenvalue energies, and the mesh samples regions at least 6 a_0 from the position of the terminal H atoms.

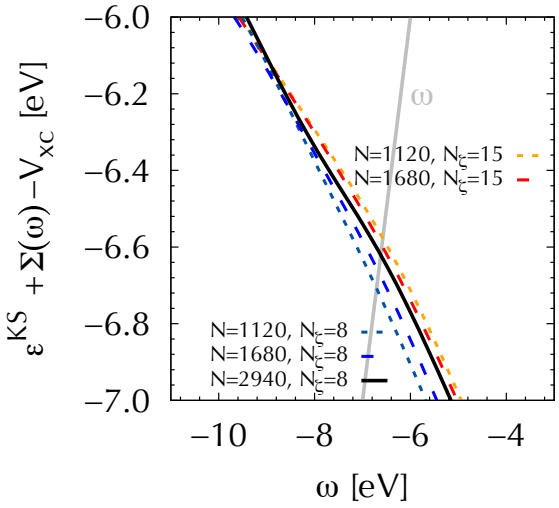

Figure 7.3: Convergence of the QP energy with respect to the number of iterations N and number of stochastic orbtials N_ζ. Shown are results for PT with 8 thiophene rings ($M = 4$), containing $N_e = 194$ valence electrons. The QP energy is the intersection of the grey line (frequency ω) with $\varepsilon^{KS} + \Sigma(\omega) - V_{xc}^{\mathrm{KS}}$ (given at the ordinate). The converged result is shown by the curve for $N_\zeta = 8$ and $N = 2940$, and the QP energy does not change if N is further increased. We note that for $N_\zeta = 8$ and $N = 1680$ the resulting QP energy is converged to better than 0.05 eV. The figure also shows that for $N_\zeta = 15$ increasing N reaches the same limit, but converges to the asymptotic value much faster.

We then use the KS results, namely the highest occupied eigenstate ϕ_H and its energy ε_H for evaluating the expectation values of the GW self-energies (Eqs. 7.14 and 7.15). Many parameters control the calculation and should be sufficiently converged towards their asymptotic value: the Chebyshev expansion length N_C, the strength of the perturbation $\delta\tau$, the temporal grid spacing δt, the temporal damping factor γ, the number of iterations N and the number of random orbitals ψ and ζ in each iteration (N_ψ and N_ζ). The actual values

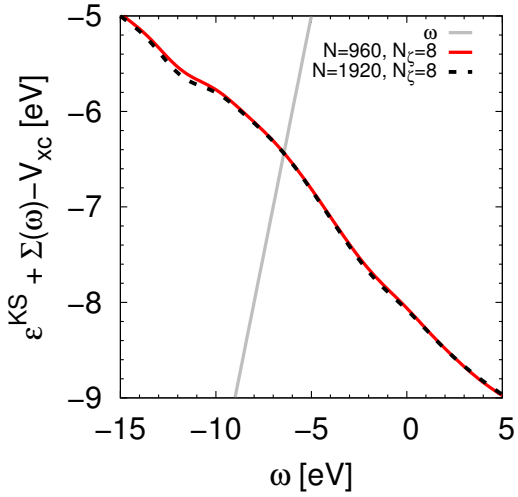

Figure 7.4: Results for PT with 16 thiophene rings (M=8), containing 386 valence electrons, obtained with $N_\zeta = 8$ stochastic orbitals. The $\varepsilon^{KS} + \Sigma(\omega) - V_{xc}^{\mathrm{KS}}$ lines are obviously well behaved and converge over wide range of energies when the number of iterations is $N = 960$. The QP energy is the intersection of the gray line (frequency ω) with $\varepsilon^{KS} + \Sigma(\omega) - V_{xc}^{\mathrm{KS}}$ (given at the ordinate). The difference between QP energy obtained for $N = 960$ and $N = 1920$ is < 0.01 eV.

selected for these parameters must be checked carefully in order to achieve the desired accuracy and optimal performance. Some of the parameters have small influence on the outcome of the calculation: the temporal grid spacing $\delta t = 0.05$ *a.u.* (used in Eqs. (7.43), (7.45) and (7.60)) and the strength of the perturbation $\delta\tau = 0.001$ *a.u.* used to calculate the reducible polarizability (Eq. 7.59). We use $N_\psi = 100$ for the resolution of identity (step 3 of the algorithm) and found that the final quasiparticle energy was rather insensitive to the precise value of N_ψ. It is also worth noting that the value of $N_\psi$has little influence on the overall computational cost. We use $N_C = 50,000$ for the Chebyshev expansion (Eq. 7.47), corresponding to a value of the inverse temperature $\beta = 200\ E_h^{-1}$.

The accuracy and stability of the stochastic approach is mainly governed by the states propagated in time to describe the induced density. A finite number of stochastic orbitals can be propagated only for a limited time as the response to an external impulse (Eq. 7.59) gets amplified with increasing time leading to an instability [52]. As mentioned, the maximum time of propagation is governed by the damping factor γ used to perform the Fourier transform. In our case a factor of $\gamma = 0.04$ a.u.$^{-1}$ was found optimal if the number stochastic states ζ used to describe the induced density δn^{ind} is $N_\zeta = 8$. While the parameter γ can be further reduced when higher values of N_ζ are used, this is not deemed necessary since we find that the estimated value of the quasiparticle energies is sufficiently converged (see Figure 7.4.1).

Finally, besides the above mentioned parameters, the whole sGW algorithm outlined in Section 7.3 and illustrated in Figure 7.3.7 is evaluated in N iterations,

i.e. the self energy $\Sigma(\mathbf{r}', \mathbf{r}, \omega)$ in Eq. (7.19) is averaged N times. The QP energies are converged with respect to the number of stochastic orbitals (N_ζ) and iterations (N); converged results are obtained for $N_\zeta = 8$ and $N > 1800$. If a larger value of N_ζ is selected (e.g. $N_\zeta = 15$) the number of iterations needed for convergence is in fact lower. This is illustrated in Figure 7.4.1 for PT with 8 thiopehene rings, where the fully converged result is shown by a black line for $N_\zeta = 8$ and $N = 2940$. For comparison, a result with $N_\zeta = 8$ and $N = 1680$ is shown, for which the QP energy deviates from the asymptotic value by < 0.05 eV. For the same number of iterations ($N = 1680$), but higher number of stochastic states ($N_\zeta = 15$), we observe faster convergence of the QP energies and the deviation is < 0.2 eV. Furthermore, with increasing system size, the number of iterations N required to reach a given level of accuracy decreases. This is illustrated in Figure 7.4.1, where results for PT with 16 thiopehene rings are shown. Using $N_\zeta = 8$, we find that the QP energies obtained with $N = 960$ are practically indistinguishable from the result for $N = 1920$, their difference is < 0.1 eV. The fact that the number of iterations decreases rapidly with system size is one of the reasons for the overall linear scaling of the stochastic *GW* approach as discussed previously [26].

7.4.2 Ionization potentials of the PT chains

In DFT, the ionization potential is taken as a negative of the highest occupied eigenvalue $-\varepsilon_H$. However, calculations with (semi)local density functionals suffer from delocalization error, which also leads to spreading of the hole density over the whole system preventing localization [27]. As a consequence the LDA results for ε_H not only severely underestimate the IPs of the polythiophene chains with respect to experiments, but for large polymers the ionization potential shows a dependence of $1/L$. For comparison, we also show calculations with optimally tuned range-separated hybrid functional (BNL*) [45, 56–58] in which the delocalization error is minimized by enforcing the IP theorem [10, 59], $E^{N-1} - E^N = \varepsilon_H$, where E^N is the total energy of N-particle system. The ionization potentials obtained with BNL* show a completely different behavior from the LDA results, and for large systems the IPs become independent of system size.

We emphasize that the localization of the hole inherently captures the response of the system to the excess charge. The density of the hole in the system is thus given as

$$\Delta n(\mathbf{r}) = n^N(\mathbf{r}) - n^{N-1}(\mathbf{r}), \tag{7.66}$$

where the superscripts N and $N-1$ denote the density evaluated for the neutral system and a cation. $\Delta n(\mathbf{r})$ thus does not correspond to the density of the highest occuppied eigenstate $|\phi_H|^2$ which is *not* necessarily localized [27]. We use the LDA results in which ϕ_H spans the whole system and calculated the quasiparticle correction from Eq. (7.19) for the highest occupied KS eigenstate ε_H. The *GW* estimates of the IPs are shown in Figure 7.4.2. The QP energy is shifted substantially towards better agreement with experimental data available and becomes independent of the system size, consistent with the BNL* results.

Our results can be fitted by

$$I(M) = I_\infty - \Delta \times e^{-\alpha\sqrt{M/M_0}}, \tag{7.67}$$

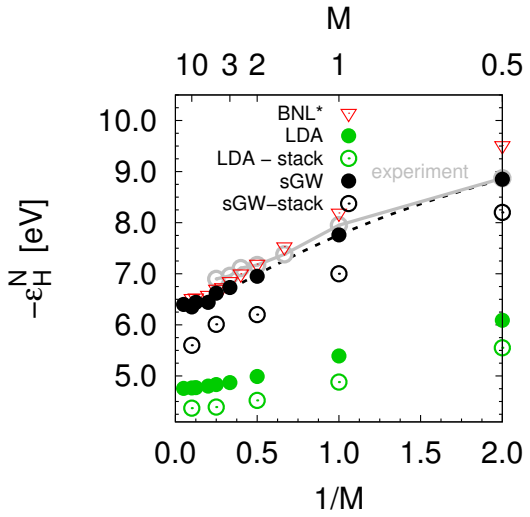

Figure 7.5: Results for PT containing between 1 and 20 thiophene rings (M=0.5 - 10). The full green circles represent the underlying LDA calculations for single PT strands while open green circles show results for the stacked molecules (illustrated in Figure 7.1). The quasiparticle energies calculated with the one-shot stochastic *GW* method on top of the LDA starting point are shown by full and open black circles for the single PT strands and three stacked layers of PT, respectively. DFT results obtained with optimally-tuned range-separated hybrid functional (BNL*) from Ref. [27] are shown for comparison in open red triangles. Experimental data shown in gray circles were taken from Refs. [53–55].

shown by dashed lines in Figure 7.4.2. The values of $I_\infty = 6.4$ eV, $\Delta = 10.1$ eV, $M_0 = 0.25$ reproduce the calculated IPs best. The critical size M_C is chosen such that for $M > M_C$ the difference $I(M) - I_\infty$ is smaller than 0.1 eV:

$$M_C = \left[\log\left(\frac{0.1}{\Delta}\right)\right]^2 \times M_0. \tag{7.68}$$

From the results we estimate that the hole energy becomes independent of the polymer size for M > 5.5 repeat units, i.e. 11 thiophene rings. This corresponds to a length of 4.2 nm, in close agreement with BNL*. This not only validates our DFT results on spontaneous hole localization in the sytems considered, but also strengthens the optimal tuning procedure employed with the BNL* functional. Note that in LDA $v_{XC}(\mathbf{r})$ is local and cannot provide an eigenstate energy independent of system size if ϕ_H is delocalized. Nevertheless, if LDA is used as a starting point for (even single shot) *GW*, the QP corrections calculated through Eq. (7.19) lead to qualitative change in the description of the charge removal.

To investigate this further, we evaluated Eqs. (7.36) and (7.37) independently and the individual contributions to the QP shift are shown in Figure 7.4.2. The polarization part of the self energy Σ_P is relatively small (~ 0.5 eV) and decreases slightly with system size. Our results for single polythiophene strands do

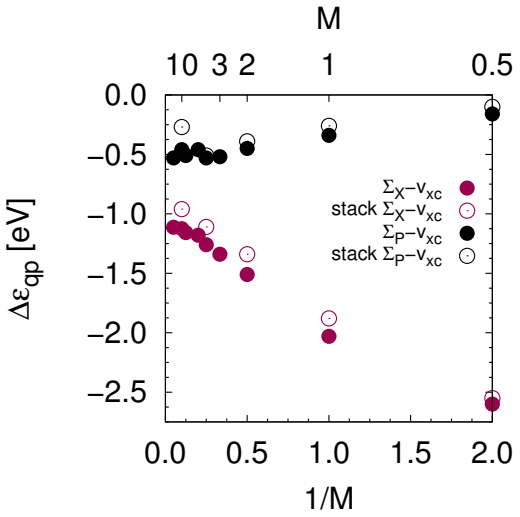

Figure 7.6: Contributions to the quasiparticle corrections for PT containing between 1 and 40 thiophene rings (M=0.5 - 20), with up to 962 valence electrons, for the single PT chains and between 1 and 20 rings in each layer for the stacked chains. The purple circles show the contribution stemming purely from the exchange part of the self energy Σ_X given in Eq. (7.36). The contribution solely from Σ_P (Eq. 7.37) is shown in black circles. The filled circles stand for calculations with a single PT strand while open circles represent the results for the stacked systems.

not indicate a significant change in the behavior of Σ_P for long polymer chains. On the other hand, the magnitude of the Σ_X contribution to the QP correction dominates: For small systems it is large (-2.6 eV for the single thiophene molecule) and it decreases significantly with polymer size. For large systems however, it becomes constant with $\Sigma_X \sim -1.1$ eV.

The results for the IP of the stacked PT molecules are also shown in Figure 7.4.2 where the length of the system is defined as the number of repeat units in a single layer. The LDA results show energies that are lower than the estimates for a single polymer strand and IP values further decrease with increasing length of the system. The quasiparticle correction shifts the values towards higher energies, similar to the single PT strands, but the magnitude of this correction is smaller. The individual contributions to the quasiparticle corrections are shown in Figure 7.4.2 such that they can be compared to the results for single PT strands (like in Figure 7.4.2, the length is expressed by a number of repeat units in a single layer). The major difference between the single and mutiple layer systems is in the behavior of the exchange part of the self energy, which keeps decreasing as a function of M, even for large systems.

For small systems the general behavior of the ionization potential (aside from the shift to lower energies) is almost identical for a single strand of PT and stacked system. For systems containing more than 3 repeat units in each layer (i.e. 6 PT rings), however, the behavior differs and the rapid stabilization of the ionization potential with increasing system size, associated with the local-

ization of the quasihole in the chains, is not observed. We cannot infer whether the quasiparticle will localize if the system size if further increased, or if the localization phenomenon occurs at much larger lengthscales. It is also possible that for the large stacked system, the starting point dependence becomes more crucial. Clearly, further investigations are necessary.

7.5 Summary and Conclusions

In summary, we have reviewed the foundations of the *GW* approach and showed that the quasiparticle dynamics can be efficiently described in the time domain by use of stochastic orbitals. This represents a major step towards applying many-body perturbation theory to extremely large systems, since the current method overcomes many bottlenecks of the conventional formulation. We demonstrate the major points of improvement over the common approaches, outlook for future development and illustrate the performance of the stochastic *GW* method with calculations on extremely large polythiophene (PT) polymer chains.

In the present paper, we investigate PT polymers with ideal geometry in order to further study spontaneous charge localization which was recently described. The results confirm our previous finding that the energies of positive quasiparticles (holes), which localize spontaneously in large 1D polymer chains, stabilize for polymer length larger than 4.2 nm. However, this energy stabilization was not observed in systems of higher dimensionality, namely for three planar PT chains stacked in parallel with distance 7.2 a_0.

From an analysis of the contributions to the quasiparticle energy we conclude that the non-locality of the exchange part of the self-energy plays the critical role, unlike the frequency dependence of Σ_P. This agrees with our previous finding that the hole localization in PT is driven by non-local exchange and cannot be explained in terms of classical electrostatics. For all systems studied the Σ_X contribution to the quasiparticle energy significantly dominates and for the 1D systems it reaches a constant of ~ -1.1 eV. When increasing the dimensionality of the system, i.e. for systems containing three stacked molecules, the exchange part of the self energy keeps changing and further decreases in magnitude, in agreement with the fact that the localization of the quasihole energy is not observed even for the largest system with three stacked PT chains.

The fact that the (non-local) exchange contribution to the self energy remains dominant even in large systems indicates the importance of inclusion of non-local exchange in the DFT calculations. From the fact that the IP stabilization is not observed in the stacked (2D) systems of the sizes considered here, we conclude that either the localization phenomenon is limited to 1D, or the size of the localized quasiparticle may be much smaller than in 1D and with increasing dimensionality the localization occurs on much larger lengthscales. Further investigations regarding this issue are ongoing.

Bibliography

[1] P. Hohenberg and W. Kohn, Phys. Rev. **136**, 864 (1964).

[2] W. Kohn and L. J. Sham, Phys. Rev. **140**, A1133 (1965).

[3] J. VandeVondele, U. Borstnik, and J. r. Hutter, J. Chem. Theory Comput. **8**, 3565 (2012).

[4] R. Baer, D. Neuhauser, and E. Rabani, Phys. Rev. Lett. **111**, 106402 (2013).

[5] W. Hu, L. Lin, and C. Yang, The Journal of chemical physics **143**, 124110 (2015).

[6] J. Katriel and E. R. Davidson, Proc. Natl. Acad. Sci. USA **77**, 4403 (1980).

[7] C.-O. Almbladh and U. Von Barth, Phys. Rev. B **31**, 3231 (1985).

[8] P. Mori-Sanchez, A. J. Cohen, and W. T. Yang, J. Chem. Phys. **125**, 201102 (2006).

[9] A. J. Cohen, P. Mori-Sánchez, and W. Yang, Science **321**, 792 (2008).

[10] P. Mori-Sánchez, A. J. Cohen, and W. Yang, Phys. Rev. Lett. **100** (2008).

[11] L. Kronik, T. Stein, S. Refaely-Abramson, and R. Baer, J. Chem. Theory Comput. **8**, 1515 (2012).

[12] V. Vlček, H. R. Eisenberg, G. Steinle-Neumann, L. Kronik, and R. Baer, J. Chem. Phys. **142**, 034107 (2015).

[13] G. Onida, L. Reining, and A. Rubio, Rev. Mod. Phys. **74**, 601 (2002).

[14] A. Damascelli, Z. Hussain, and Z.-X. Shen, Rev. Mod. Phys. **75**, 473 (2003).

[15] F. Reinert and S. Hüfner, New J. Phys. **7**, 97 (2005).

[16] Y. Ping, D. Rocca, and G. Galli, Chem. Soc. Rev. **42**, 2437 (2013).

[17] S. Hüfner, *Photoelectron Spectroscopy: Principles and Applications* (Springer Science & Business Media, 2013).

[18] C. Di Valentin, S. Botti, and M. Cococcioni, *First Principles Approaches to Spectroscopic Properties of Complex Materials*, vol. 347 (Springer, 2014).

[19] L. Hedin, Phys. Rev. **139**, A796 (1965).

[20] M. S. Hybertsen and S. G. Louie, Phys. Rev. B **34**, 5390 (1986).

[21] F. Aryasetiawan and O. Gunnarsson, Reports Prog. Phys. **61**, 237 (1998).

[22] L. Hedin, J. Phys.: Condens. Matter **11**, R489 (1999).

[23] C. Friedrich and A. Schindlmayr, NIC Series **31**, 335 (2006).

[24] H.-V. Nguyen, T. A. Pham, D. Rocca, and G. Galli, Phys. Rev. B **85**, 081101 (2012).

[25] J. Deslippe, G. Samsonidze, D. A. Strubbe, M. Jain, M. L. Cohen, and S. G. Louie, Comput. Phys. Commun. **183**, 1269 (2012).

[26] D. Neuhauser, Y. Gao, C. Arntsen, C. Karshenas, E. Rabani, and R. Baer, Phys. Rev. Lett. **113**, 076402 (2014).

[27] V. Vlček, H. R. Eisenberg, G. Steinle-Neumann, and R. Baer, ArXiv p. arXiv:1509.05222v2 (2015).

[28] T. Holstein, Ann. Phys. **8**, 325 (1959).

[29] A. J. Heeger, S. Kivelson, J. Schrieffer, and W.-P. Su, Rev. Mod. Phys. **60**, 781 (1988).

[30] A. Köhler and H. Bässler, *Electronic Processes in Organic Semiconductors: An Introduction* (John Wiley & Sons, 2015).

[31] R. H. Friend, R. W. Gymer, A. B. Holmes, J. H. Burroughes, R. N. Marks, C. Taliani, D. D. C. Bradley, D. A. Dos Santos, J. L. Bredas, M. Lögdlund, et al., Nature **397**, 121 (1999).

[32] U. Salzner, Wiley Interdiscip. Rev. Comput. Mol. Sci. **4**, 601 (2014).

[33] P. Puschnig and C. Ambrosch-Draxl, Synth. Met. **135-136**, 415 (2003).

[34] I. H. Nayyar, E. R. Batista, S. Tretiak, A. Saxena, D. L. Smith, and R. L. Martin, J. Chem. Theory Comput. **9**, 1144 (2013).

[35] S. T. Hoffmann, F. Jaiser, A. Hayer, H. Bässler, T. Unger, S. Athanasopoulos, D. Neher, and A. Köhler, J. Am. Chem. Soc. **135**, 1772 (2013).

[36] P. B. Miranda, D. Moses, and A. J. Heeger, Phys. Rev. B **64**, 081201 (2001).

[37] A. O. Patil, A. J. Heeger, and F. Wudl, Chem. Rev. **88**, 183 (1988).

[38] G. D. Scholes and G. Rumbles, Nat. Mater. **5**, 683 (2006).

[39] R. Fitzner, C. Elschner, M. Weil, C. Uhrich, C. Körner, M. Riede, K. Leo, M. Pfeiffer, E. Reinold, E. Mena-Osteritz, et al., Adv. Mater. **24**, 675 (2012).

[40] A. Mishra and P. Bäuerle, Angew. Chem. Int. Ed. **51**, 2020 (2012).

[41] A. L. Fetter and J. D. Walecka, *Quantum Theory of Many-Particle Systems* (Dover Publications, 2003).

[42] M. F. Hutchinson, Commun. Stat. Simul. Comput. **19**, 433 (1990).

[43] R. Baer and M. Head-Gordon, J. Chem. Phys. **107**, 10003 (1997).

[44] R. Baer and D. Neuhauser, J. Chem. Phys. **121**, 9803 (2004).

[45] R. Baer and D. Neuhauser, Phys. Rev. Lett. **94**, 043002 (2005).

[46] M. Govoni and G. Galli, J. Chem. Theory Comput. **11**, 2680 (2015).

[47] S. L. Adler, Phys. Rev. **126**, 413 (1962).

[48] N. Wiser, Phys. Rev. **129**, 62 (1963).

[49] Y. Zhou, Y. Saad, M. L. Tiago, and J. R. Chelikowsky, J. Comput. Phys. **219**, 172 (2006).

[50] J. P. Perdew and Y. Wang, Phys. Rev. B **45**, 13244 (1992).

[51] N. Troullier and J. L. Martins, Phys. Rev. B **43**, 1993 (1991).

[52] E. Rabani, R. Baer, and D. Neuhauser, Phys. Rev. B **91**, 235302 (2015).

[53] D. Jones, M. Guerra, L. Favaretto, A. Modelli, M. Fabrizio, and G. Distefano, J. Phys. Chem. **94**, 5761 (1990).

[54] D. A. d. S. Filho, V. Coropceanu, D. Fichou, N. E. Gruhn, T. G. Bill, J. Gierschner, J. Cornil, and J.-L. Brédas, Philos. Trans. A. Math. Phys. Eng. Sci. **365**, 1435 (2007).

[55] M. Pinheiro Jr, M. J. Caldas, P. Rinke, V. Blum, and M. Scheffler, Phys. Rev. B **92**, 195134 (2015).

[56] R. Baer, E. Livshits, and U. Salzner, Annu. Rev. Phys. Chem. **61**, 85 (2010).

[57] E. Livshits and R. Baer, J. Phys. Chem. A **112**, 12789 (2008).

[58] T. Stein, J. Autschbach, N. Govind, L. Kronik, and R. Baer, J. Phys. Chem. Lett. **3**, 3740 (2012).

[59] J. P. Perdew, R. G. Parr, M. Levy, and J. L. Balduz, Phys. Rev. Lett. **49**, 1691 (1982).

Erklärung

Hiermit erkläre ich, dass ich die vorliegende Arbeit selbstständig verfasst und keine anderen als die angegebenen Quellen und Hilfsmittel verwendet habe.

Die Arbeit wurde weder in gleicher noch in ähnlicher Form bei anderen Prüfungsbehörden zur Erlangung eines akademischen Grades vorgelegt.

Weiterhin erkläre ich, dass ich keine Hilfe von gewerblichen Promotionsberatern bzw. -vermittlern oder ähnlichen Dienstleistern in Anspruch genommen habe und auch nicht beabsichtige diese zukünftig in Anspruch zu nehmen.

Weiterhin erkläre ich, dass ich bisher keinen anderweitigen Promotionsversuch unternommen habe.

Bayreuth, den 19. April 2016 Vojtěch Vlček